NIK/MAP3K14 IS A BIOENERGETIC STRESS SENSOR AND PROMOTER OF OXIDATIVE PHOSPHORYLATION

A Dissertation

by

MICHAEL KAMRADT

Submitted to the Office of Graduate and Professional Studies of
Texas A&M University
in partial fulfillment of the requirements for the degree of

DOCTOR OF PHILOSOPHY

Chair of Committee,	Raquel Sitcheran
Co-Chair of Committee,	Andrew Philip West
Committee Members,	David W. Threadgill
	Carl Gregory
Head of Department,	Carol Vargas

May 2021

Major Subject: Medical Sciences

ABSTRACT

The control of cell metabolism is intimately linked to the size and shape of mitochondria, which varies significantly across cell types. Mitochondria can elongate (fuse) with other nearby mitochondria, or they can fragment and become smaller (fission). These alterations in mitochondrial dynamics allows cells to respond rapidly to changes in the source and quantity of sugars being used, reactive oxygen species, as well as removal of damaged mitochondria through mitophagy. Imbalances in mitochondrial dynamics underlies many human diseases, including cancer. Our lab recently demonstrated that NF-κB Inducing Kinase (NIK) associates with mitochondria and promotes fission. Here, we investigate our hypothesis that NIK regulates other mitochondrial processes, such as mitochondria metabolism (OXPHOS), which is often de-regulated in cancer cells. We establish that mitochondria of human brain cancer cell lines exhibit fissioned mitochondria upon acute metabolic switch from glycolytic (glucose; high sugar) to OXPHOS-promoting (galactose) media. We further demonstrate that the metabolic stress sensor, AMP-activated protein kinase (AMPK) is consistently upregulated in $NIK^{-/-}$ GBM cells. Critically, we show that NIK relocates to the mitochondria under conditions of metabolic stress and that NIK-deficient glioma cells die upon nutrient switching from high glucose to galactose media. Furthermore, we present data that highlights the altered metabolic status and energy consumption of NIK-deficient cancers through LC-MS metabolomics as we mitochondrial metabolism and glycolysis assays.

DEDICATION

I would like to dedicate this dissertation to my family for all of their care and support throughout my life and my education. I'd also like to dedicate this dissertation to my dog Blackjack.

ACKNOWLEDGEMENTS

I would like to thank my committee chair and advisor, Dr. Raquel Sitcheran, my co-chair, Dr. Andrew West, and my committee members, Dr. Carl Gregory and Dr. David Threadgill for their guidance and support over the course of my Ph.D.

Thanks also to my friends and colleagues at Texas A&M for making pursuing my doctorate here a great experience.

I would also like to thank my Mom, Dad, and sister for their encouragement, support, and love over the course of the past six years. Without them, a career in research would have be impossible for me to pursue.

CONTRIBUTORS AND FUNDING SOURCES

Contributors

This work was supervised by a thesis committee consisting of Dr. Raquel Sitcheran (advisor/chair of the committee), Dr. Andrew Philip West (co-chair), and Dr. Carl Gregory (committee member) of the Department of Cell and Molecular Medicine. This work was also supervised by Dr. David W Threadgill (Department of Nutrition and Food Science).

The data in figure 5d was performed by Victor Fanniel, graduate student (Interdisciplinary Program in Genetics). Figure 5e-i and figure 7a-c quantification was performed by Jiung Jung, Ph.D. Figure 7 a-c microscopy imaging and Figure 10 were contributed by Kathryn Pflug, graduate student (Interdisciplinary Program in Genetics). Figure 17b and 22b were contributed by Dr. Dong W Lee, Ph.D. Figure 30 model was modified from a schematic made by Dr. Raquel Sitcheran, Ph.D. Model slides and schematics were made with Biorender (Biorender.com).

All other work conducted for the dissertation was completed by the student independently.

Funding Sources

This work was supported by grants from the NIH (2R01NS082554-04A1 to R.S.) and The Cancer Prevention and Research Institute of Texas (RP160842 to R.S.), as well as a seed grant from the Texas Brain and Spine Institute.

NOMENCLATURE

ADP	Adenosine diphosphate
AMP	Adenosine monophosphate
AMPK	AMP-activated protein kinase
ATP	Adenosine triphosphate
cIAP	Cellular inhibitor of apoptosis
Drp1	Dynamin-related protein 1
ECM	Extracellular matrix
ER	Endoplasmic reticulum
ETC	Electron transport chain
FADH2	Flavin adenine dinucleotide
Fis1	Mitochondrial fission 1 protein
Fn14	Fibroblast growth factor-inducible 14
GBM	Glioblastoma multiforme
GFP	Green fluorescent protein
HGG	High Grade Glioma
IKKα/β	I kappa B kinase α/β
IMM	Inner mitochondria membrane
IκB	I kappa B
LIR	LC3-interacting region
LTβR	Lymphotoxin-β receptor

MAM	Mitochondria-associated membrane
Mff	Mitochondria fission factor
Mfn1	Mitofusin 1
Mfn2	Mitofusin 2
MID49	Mitochondrial dynamics protein of 49 kDa
MID51	Mitochondrial dynamics protein of 51 kDa
MMP9	Matrix Metallopeptidase 9
mtDNA	Mitochondrial DNA
NADH	Nicotinamide adenine dinucleotide
NEMO	Nuclear factor κB essential modulator
NF-κB	Nuclear Factor-kappa B
NIK	NF-κB inducing kinase
OMM	Outer mitochondria membrane
OPA1	Optic Atrophy 1
OXPHOS	Oxidative phosphorylation
RHD	Rel homology domain
ROI	Regions of interest
ROS	Reactive oxygen species
SDS	Sodium dodecyl sulfate
SRC	Spare respiratory capacity
TAK1	Transforming growth factor ß activated kinase
TLR	Toll-like receptor

TNF	Tumor necrosis factor
TNFR	Tumor necrosis factor receptor
TRAF	TNF receptor-associated factor
UPR	Unfolded protein response

TABLE OF CONTENTS

Page

LIST OF FIGURES

Page

I. INTRODUCTION AND LITERATURE REVIEW

1.1 Nuclear Factor Kappa B (NF-κB)

1.1.1 Canonical vs non-canonical signaling pathways

NF-κB was discovered in 1986 in the laboratory of Dr. David Baltimore while searching for transcription factors in B lymphocytes that could bind to the light chain κ enhancer (Zhang et al., 2017). Among the factors they discovered, they found one that specifically bound to the light chain κ enhancer and had a consensus DNA sequence—later referred to as a κB binding site (Brignall et al., 2019). They termed this protein "NF-κB" because it was a nuclear factor that bound to the light chain κ enhance in B lymphocytes(Baltimore, 2009). To test the specificity of this protein to regulate light chain κ gene expression, they treated a pre-B cell leukemia cell line with undetectable NF-κB expression (70Z/3 cells) with lipopolysaccharide (LPS)—which was known to stimulate light chain κ expression. When LPS was delivered to the cells, NF-κB rapidly appeared in the nucleus, and investigators recognized that NF-κB's rapid appearance occurred even in the absence new protein synthesis (Sen and Baltimore, 1986). This finding strongly suggested that NF-κB was already present in some form in the cell and that it was likely inhibited from executing its function when not activated by LPS. In 1988, Baltimore and his team discovered that the inactive form of NF-κB was found in the cytoplasm and they were able to purify the inhibitor that sequestered it and named it "inhibitor of κB" (IκB).

In the years and decades that followed, five proteins became recognized as core NF-κB family members: NF-κB1, NF-κB2, RelA, RelB, and c-Rel (Oeckinghaus and Ghosh, 2009). All five family members contain a conserved 300 amino acid sequence termed a Rel homology domain (RHD). Sequences within this domain are essential for DNA binding, dimerization, and nuclear translocation (Ghosh et al., 1998).

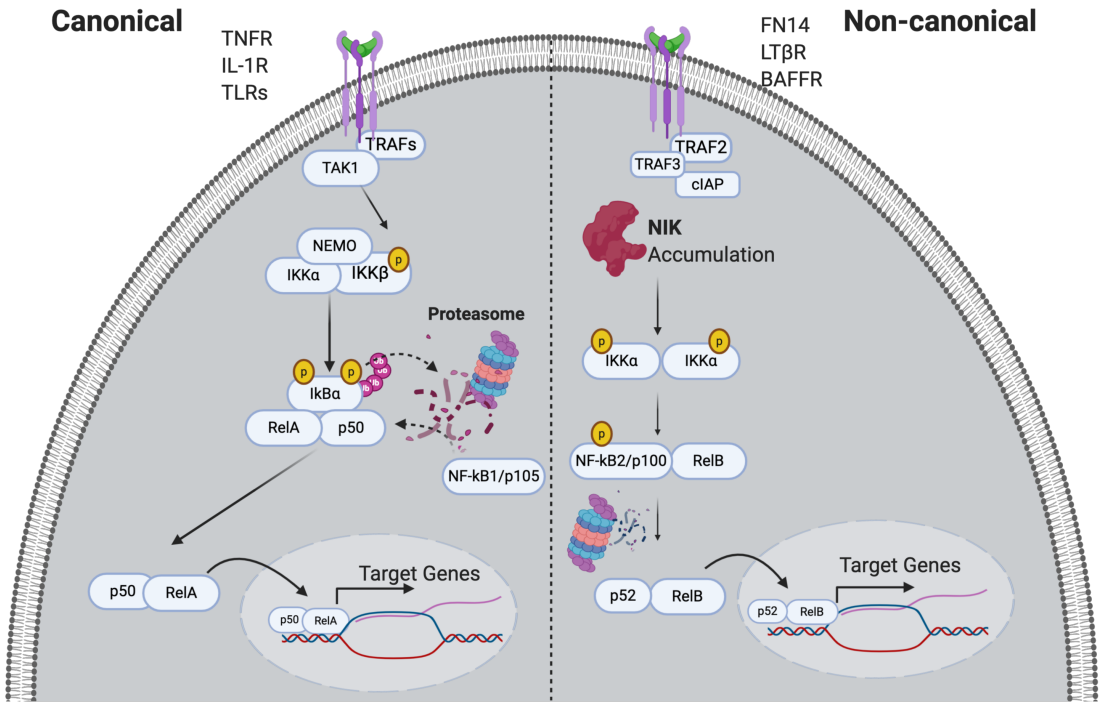

Figure 1. Canonical vs non-canonical NF-κB signaling
NF-κB signaling is activated through two distinct pathways: the canonical signaling pathway (left) and non-canonical signaling pathway (right). The pathways differ in the receptors which activate them but both share IKKa as well as require the proteasome for activation.

Canonical NF-κB signaling begins with stimulation of a receptor that then recruits transforming growth factor ß activated kinase (TAK1). TAK1 phosphorylates/activates IKKß of the IκB kinase complex (NF-κB essential modulator (NEMO or IKKγ), IKKα, and IKKß). IKKß proceeds to phosphorylate IκBα at serines

32 and 36, which then target IκBα for degradation by the proteasome. Once IκBα is destroyed, RelA/p50 heterodimers that were previously sequestered by IκBα are free to translocate to the nucleus to serve as transcription factors (Figure 1) that regulate a vast network of genes involved in cell survival, growth, inflammation and immunity (Zhang et al., 2017).

In 1994, the story of NF-κB continued to broaden when a mouse line was characterized that was defective in both humoral and cell-mediated immune functions and were extremely susceptible to infections. Alymphoplasia (*aly/aly*) mice harbored a mutation that caused defects in lymph nodes, B cell maturation, and splenic tissue organization (Miyawaki et al., 1994). This *aly* phenotype was traced a point mutation encoding NF-κB-inducing kinase (NIK/MAP3K14) (Shinkura et al., 1999), a serine/threonine kinase that propagated the NF-κB signaling cascade. The discovery that NIK promoted a distinct alternative (non-canonical) NF-κB pathway did not occur until 2001, when research into p100 processing to NF-κB2 (p52) revealed that its degradation is inducible by NF-κB inducing Kinase. Furthermore, NIK mutant cell lines that had functional canonical NF-κB signaling could not compensate for defects in NIK activity and could not sufficiently process p100 to p52 (Xiao et al., 2001).

NIK is a MAP3 kinase that contains four main domains: an N-terminal domain that binds TNF receptor associated factor (TRAF) proteins associated with the activating receptor, a negative regulatory domain necessary for E3 ligase binding, a kinase domain, and a C-terminal domain responsible for binding IKKα (Liao et al., 2004; Xiao and Sun, 2000). The crystal structure of the kinase domain of NIK suggests a

constitutively active conformation (de Leon-Boenig et al., 2012) which is stabilized through a salt bridge linking Lys429 to Glu440 (Tao and Ghosh, 2012). Furthermore, although NIK can autophosphorylate, phosphorylation of NIK is not required for its activity (Liu et al., 2012).

Regulation of NIK occurs primarily at the post-translational level. Under unstimulated conditions, NIK is actively targeted for proteasomal degradation by a cIAP-TRAF2-TRAF3 complex. While both TRAF2 and TRAF3 are E3 ubiquitin ligases, neither protein is able to ubiquitinate NIK at lysine 48—the most prominent proteasome targeting signal (He et al., 2006; Liao et al., 2004; Wallach and Kovalenko, 2008). In order to accomplish this, TRAF3 recruits the E3 ubiquitin ligase cIAP and acts as a bridge that allows NIK to be ubiquitinated by cIAP at lysine 48 (Yang and Sun, 2015).

When non-canonical NF-κB signaling is stimulated, NIK is released from the TRAF degradation complex and accumulates in the cytosol where it is free to phosphorylate IKKα homodimers at Ser 176 (Figure 1). Phosphorylated IKKα then phosphorylates NF-κB2 precursor protein p100, which then is partially degraded to p52 (NF-κB2). After proteolysis to p52, the RelB/p52 heterodimer in the cytoplasm is then free to enter the nucleus to transcribe non-canonical NF-κB target genes (Sun, 2011, 2017; Tegowski and Baldwin, 2018). The predominant function for NIK/MAP3K14 is to phosphorylate IKKα and stimulate the non-canonical NF-κB pathway, however if NIK is highly expressed or overly stabilized it may exhibit crosstalk with and activate the canonical signaling cascade as well (Odqvist et al., 2013).

1.1.2 NF-κB as a driving force in cancer progression

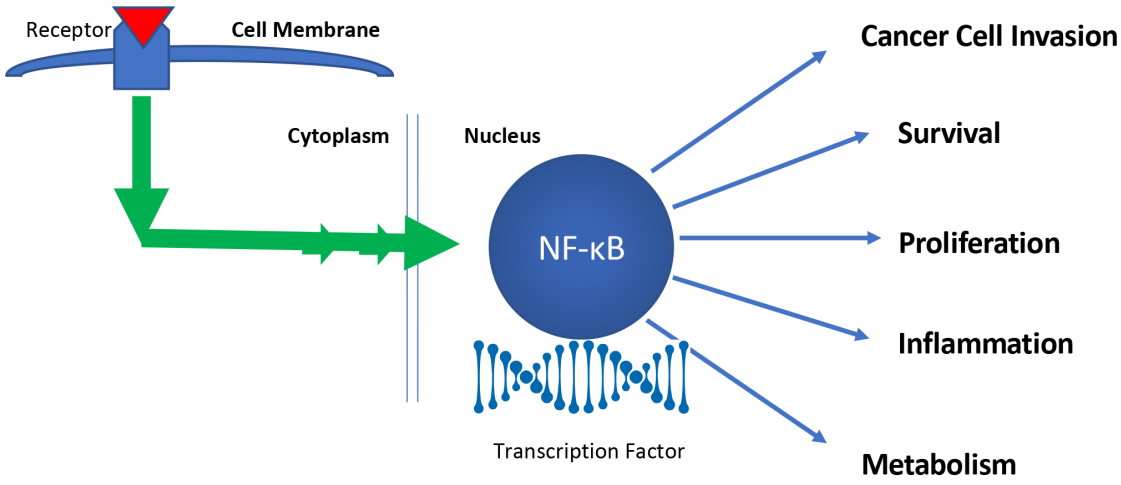

Figure 2. NF-κB controls the hallmarks of cancer
Above: NF-κB signal transduction starts at the membrane through binding of a ligand with its receptor. Once the receptor is activated, it engages a signal transduction pathway that results in NF-κB translocating to the nucleus to act as a transcription factor and regulates many of the hallmarks of cancer. These hallmarks include cancer cell invasion, survival, proliferation, inflammation, and cancer metabolism.

While there have been a multitude of oncogenes that have been studied for their roles in driving cancer development and progression, few have garnered the attention that NF-κB has. NF-κB can control virtually all of the hallmarks of cancer (Figure 2) (Karin, 2006). Hyperactivation of NF-κB results in the transcription of genes associated with multiple aspects of tumorigenesis—including evading apoptosis, promoting angiogenesis, uncontrolled proliferation, rewiring metabolism, and increasing invasiveness and metastatic potential (Baldwin, 2001; Mauro et al., 2011; Prasad et al., 2010).

While NIK indisputably has critical roles in adaptive immunity, it has become

increasingly clear that NIK has a wide range of functions in human diseases ranging from bone and autoimmune disorders to cancer. Aberrant NIK signaling has been associated with multiple myeloma, B and T-cell lymphomas, melanoma, lung cancer, ovarian cancer, prostate cancer, and glioma (Demchenko and Kuehl, 2010; Duran et al., 2016; Keats et al., 2007; Pham et al., 2011; Saitoh et al., 2010; Uno et al., 2014). This list of non-canonical NF-κB dysregulated cancers is not exhaustive and continues to grow.

Although the transcriptional targets of p52/RelB may vary depending on the cancer type, non-canonical NF-κB upregulation generally promotes tumor cell survival and invasion. NIK/non-canonical NF-κB driven tumor invasion is primarily accomplished through expression of matrix metalloprotease 9 (MMP9) and membrane type 1 matrix metalloproteinase (MT1-MMP) (Duran et al., 2016; Rangaswami et al., 2006). Increased stability and accumulation of NIK protein also drives the formation of pseudopodia and invadopodia which promote invasiveness (Duran et al., 2016). Furthermore, RelB was demonstrated to drive cancer proliferation through increasing expression of Cyclin D1 and genes critical for G1/S cell cycle transition in patient tumor samples (Ge et al., 2016). However, not all functions of NIK are p52/RelB dependent (Boutaffala et al., 2015), as NIK has also been shown to regulate tumor survival through Beta-catenin-dependent expression of surviving in cancer (Thu and Richmond, 2010).

1.2 Glioblastoma

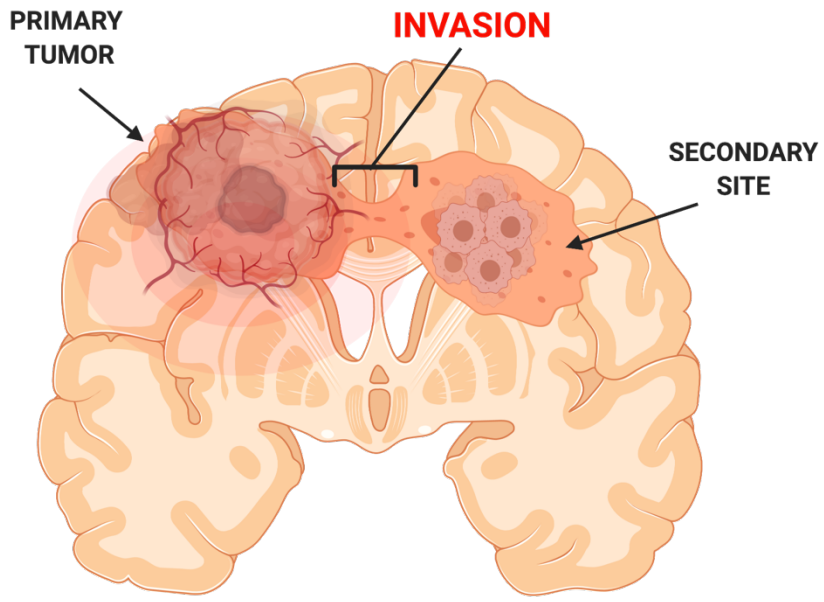

Figure 3. Glioblastoma multiforme
Above: Schematic of a coronal section of human brain with glioblastoma multiforme (GBM). GBM is a particularly pernicious disease not because of the primary tumor but because of the motility of the tumor cells through the parenchyma of the brain (invasion). These invasive cells seed into new areas of the brain where they form new tumors.

Glioma is the most common tumor of the Central Nervous System (CNS) and is prevalent among the general population regardless of age. This cancer originates form the supportive cells (astrocytes) of the neurons in the brain and spinal cord. While normal, non-malignant glial cells are helpful for the nervous system, gliomas are destructive toward neurons as they grow and invade surrounding healthy brain tissue.

The World Health Organization (WHO) grades adult brain tumors 2 to 4 based on how malignant they are. In general gliomas are graded 2 if the tumor cells are well-differentiated and are less likely to invade surrounding tissue of the CNS. Grade 2

gliomas are termed low grade gliomas and have good prognosis. Grade 3 and 4 are high grade gliomas (HGG) and are highly dangerous and malignant tumors of the CNS (Vigneswaran et al., 2015). Grade 3 malignant gliomas often recur as grade 4 glioblastoma, and glioblastoma that arises from grade 3 glioma is termed "secondary glioblastoma" and occurs roughly 10% of the time. Primary glioblastoma, *de novo*, is much more common (approximately 90% of glioblastomas) and arise without any pre-existing disease.

In an attempt to understand the tumor heterogeneity common in this disease (Fedele et al., 2014) and to attempt to personalize medical care based on individual patients, grade 4 glioblastoma multiforme (GBM) is further subdivided into three subtypes based on the molecular profiles: classical, proneural, and mesenchymal (Behnan et al., 2019; Phillips et al., 2006; Verhaak et al., 2010). The classical subtype often has inactivation of the retinoblastoma tumor suppressor (pRB) as well as overexpression of epidermal growth factor receptor (EGFR) and also tends to be enriched in pathways associated with metabolism—such as fatty acid activation with CoA to form fatty acyl CoA (Zhang et al., 2020). Gene mutations in p53, platelet-derived growth factor receptor A (PDGFR-A), and isocitrate dehydrogenase 1 (IDH1) are characteristics of the proneural subtype. The mesenchymal subtype is characterized by extensive necrosis, inflammation, angiogenesis, deletion of tumor suppressor genes p53, neurofibromatosis type 1 (NF1), and phosphate and tensin homolog (PTEN) as well as high expression of genes in the NF-κB pathway (Behnan et al., 2019; Zanotto-Filho et al., 2017).

Despite the insights provided by these classifications, glioblastoma multiforme, the most aggressive subtype of glioma, remains elusive for cancer treatments due to its often subtle and cryptic symptoms during onset and due to its high invasive potential (Figure 3). The gold-standard of treatment is surgical resection followed by radiation and adjuvant therapy with Temozolomide. Yet despite this treatment, and despite the years of research into glioblastoma, it remains one of the most lethal of all cancers, with a median survival time of only 12 months and a 5-year survival rate of 5% (Delgado-López and Corrales-García, 2016). Furthermore, glioblastoma treatment and indeed targeting brain tumors in general have the additional hurdle of finding drugs that can cross the blood-brain barrier.

Due to glioblastoma's nearly uniformly fatal rate, in addition to the lack of progress in changing its lethal prognosis, as well as difficulty in pinpointing precise germline genetic mutations or environmental factors, clinicians and researchers have begun to reexamine the paradigm for its treatment. Drugs targeting cancer metabolism have gained acceptance for tumor treatment, although glioma still is relatively an unproven cancer for this approach. Instead, research has primarily been focused on finding druggable targets that reduce the invasive potential of GBM and make complete tumor resection more feasible.

1.3 Cancer Metabolism

1.3.1 Historical Perspectives and Warburg Effect

In the early 1920s in Germany, a scientist named Otto Heinrich Warburg made a peculiar discovery. Building off of his research on the metabolism of fertilized sea urchin eggs in Italy, he turned his attention toward tumor metabolism. He predicted that, like the developing sea urchin, tumor cells rapidly proliferated and should exhibit similar metabolic characteristics—namely that they should exhibit a preference for oxidative phosphorylation over lactic acid production in the presence of oxygen. However, the reverse observation held true. Warburg noticed that when supplemented with glucose in the presence of oxygen, the media he used turned color—indicating an acidification of the media used (Otto, 2016). He postulated, that this increase in tumor glycolysis was due to damaged mitochondria respiration. Furthermore, altered metabolism toward aerobic glycolysis, he proposed, was a principle driving force in tumorigenesis. This phenomenon of glycolysis even in aerobic conditions became known as the "Warburg effect" (Pavlova and Thompson, 2016).

After Warburg died in 1970, and growing evidence supported that mutations in DNA led to the inactivation of genes important for tumor repression (tumor suppressors) or aberrant activation of genes important for cell cycle regulation or growth (oncogenes) (Bister, 2015), the Warburg effect (aerobic glycolysis) and belief that cancer was driven by metabolic reprogramming was relegated to an odd footnote in the history of cancer research. Opinions shifted yet again however, as evidence emerged that mutations in

many tumor suppressors and oncogenes can indeed alter the metabolism of cells (Jones and Thompson, 2009). When the flux of glucose into a tumor is disrupted, the proliferation of cancer cells are often stunted (Pavlova and Thompson, 2016). Metabolic reprogramming did in fact coincide with tumorigenesis and cancer progression and actually was proposed to benefit cancer cells in the following ways.

First, glucose is one of the most abundant and universal circulating nutrients in the body and as such it provides an advantage to the cancer cell to preferentially utilize it since it would hardly be in short supply. Second, the glycolytic pathway does not utilize oxygen, and as a tumor cell metastasizes and needs to promote angiogenesis to link itself to a supply of oxygenated blood, it is beneficial to rely on an anaerobic mode of metabolism to aid the cell during the process (Lu, 2019). Third, the breakdown of glucose results in metabolic intermediates that can be used in branching metabolic pathways—such as the use of glucose-6-phosphate in the pentose phosphate pathway—which is needed for nucleotide synthesis and tumor growth (Liberti and Locasale, 2016; Newsholme et al., 1985). Fourth, glycolysis requires far fewer enzymes than oxidative phosphorylation, and in chaotic and mutation-prone cancer cells it is possible the simplest solution to energy production is the best (Occam's razor).

The addiction of cancer cells toward glucose consumption has led researchers over the years to debate what role, if any, oxidative metabolism and the mitochondria have in regard to tumorigenesis. However, while there are cancers that do have damage to their capacity to conduct oxidative metabolism, and there are cancers that exhibit the Warburg effect and are sensitive to glucose deprivation—there are some notable

exceptions. Gliomas, for example, have great capacity to perform mitochondrial respiration and can switch between modes of oxidative phosphorylation (OXPHOS) and glycolysis (Marie and Shinjo, 2011). These observations have led researchers to re-examine the role of the mitochondria in cancer.

1.3.2 Roles for oxidative phosphorylation in cancer

The mitochondria is formed of roughly 1,500 proteins (McCormick et al., 2018). Most of these mitochondrial proteins are encoded from the nucleus, but a very important subset is expressed in the mitochondria DNA (mtDNA) genome. Encoded in the mitochondria DNA are the instructions to produce the core mitochondrial membrane bound components of OXPHOS: complexes I, III, IV, and V.

The OXPHOS metabolic pathway produces ATP through the transport of electrons through a series of five complexes embedded in the inner mitochondria membrane. The electrons, provided by biochemical intermediaries in the citric acid cycle in the mitochondrial matrix, pass through electron transport chain complexes I-IV. The energy provided by this transfer of electrons drives the pumping of protons through complex I, III, and IV into the intermembrane space of the mitochondria (Zhao et al., 2019). As OXPHOS proceeds, these complexes create a high proton gradient/membrane potential and the protons pass from the intermembrane space back into the matrix through ATP Synthase (complex V). Oxygen accepts the final electron at complex IV and is consumed during the process.

During OXPHOS, misappropriation of electrons to oxygen can create dangerous superoxide radicals (reactive oxygen species, ROS) that must be eliminated. If free radical scavenging molecules, such as superoxide dismutase (SOD), cannot alleviate this oxidative stress the cell will be damaged and will ultimately die (Zhao et al., 2019). ROS can also function as a signaling molecule, and so while ROS in high excess can prove fatal for the cell, some moderate amount of reactive oxygen species is useful for cellular processes. In fact, mitochondrial metabolism and mitochondrial reactive oxygen species have been demonstrated to be essential for some cancers(Liou and Storz, 2010).

There is a broad spectrum of metabolic preferences in cancers. Some cancers are highly reliant on OXPHOS, have increased mitochondrial DNA (mtDNA), and inhibition of mitochondria complexes has been shown to decrease tumor cell survival of these cancers both *in vitro* and *in vivo*. Tumors often contain regions of low oxygen, termed hypoxia, and it has been demonstrated that hypoxic tumor cells are resistant to cancer therapies. Interestingly, inhibition of OXPHOS can alleviate hypoxic tumor microenvironment in some cancers and can thereby improve treatment outcomes (Ashton et al., 2018).

Other cancers have strong preference for aerobic glycolysis—as Warburg predicted—and do have impaired mitochondria. To make matters more complicated, some studies have indicated that tumors exhibit metabolic heterogeneity (Kim and DeBerardinis, 2019). Cancer stem cells may be more heavily reliant on OXPHOS (Chae and Kim, 2018) whereas differentiated cancer cells may rely more heavily on glycolysis. This metabolic heterogeneity may allow the tumor to maintain plasticity—allowing the

tumor cell to respond to what mode of metabolism is required inside of its microenvironment.

1.3.3 Energy Homeostasis and response to energetic demands and stress

Cells require a mechanism by which to respond to changing energetic demands in the environment. One can envision that the tracking of ATP, the metabolic currency of the cell, would be beneficial for a cell since it can give a snapshot of the energetic wealth a cell has available. Having a system responsive to ADP is intuitive as well, since it would indicate an energy deficient state for the cell. However, a system in which proteins respond to AMP is multiple fold more sensitive to that of ADP (Hardie, 2011; Hardie and Hawley, 2001), and there are proteins critical for homeostasis that have evolved to respond to this metabolite.

AMP-activated protein kinase (AMPK) is a critical nutrient sensor that is activated during nutrient deprivation. AMPK is a heterotrimeric protein complex that consists of an α, β, and γ subunit. Activity of AMPK is driven through binding of AMP on the γ subunit and phosphorylation of Thr172 on the α subunit by the LKB1/STRAD/MO25 complex (Hawley et al., 2003). Alternate pathways for AMPK activation also exist and depend on the activity of calmodulin-dependent protein kinase kinase 2 (CAMKK2) or by mitochondrial ROS (Rabinovitch et al., 2017; Racioppi and Means, 2012). Regardless, once activated AMPK directs the cell to increase a number of catabolic pathways such as beta-oxidation of fatty acids, lipolysis, glycolysis,

autophagy, and oxidative metabolism to restore energy to the cell to prevent starvation (Herzig and Shaw, 2018).

Upon activation, AMPK also can slow cell proliferation and protein synthesis. This is accomplished primarily through its direct phosphorylation and inhibition of the regulatory associated protein of mTOR (RAPTOR) which then results in the inactivation of mammalian target of Rapamycin (mTOR) signaling (Gwinn et al., 2008). mTOR is a serine/threonine protein kinase that acts as a catalytic subunit for two protein complexes: mTOR complex 1 (mTORC1) and mTOR complex 2 (mTORC2) (Liu and Sabatini, 2020). Through these two complexes, mTOR acts as a central engine of the cell and responds to amino acids and conditions of energy abundance to drive anabolic reactions in order to promote growth and proliferation. In order for AMPK to execute its functions properly, mTOR must be inhibited.

If AMPK could not halt the functions of mTOR, the cell would engage in a metabolic treadmill: anabolic reactions and catabolic reactions would engage simultaneously, and energy would be expended purposelessly. Because of this inhibition of the mTOR complex, specifically mTORC1, AMPK activation is detrimental for many cancers (Li et al., 2015). However, the role of AMPK in cancer is context specific. Evidence suggests that in lung cancers and in GBM, AMPK is essential for tumor growth (Chhipa et al., 2018; Eichner et al., 2019). This may due to the role of AMPK in reducing endoplasmic reticulum stress (ER stress) and also through driving autophagy—an ancient and conserved nutrient recycling mechanism protein degradation by delivery

of damaged cell structures in cargo vesicles, termed autophagosomes, to the lysosome (Liu et al., 2018; Tian et al., 2015).

Autophagy is critical for the survival of some cancer cells experiencing a nutrient crisis (Bhutia et al., 2013). However, the benefits that autophagy bestows on a cancer cell can come at some risk as well. If properly regulated, autophagy can clear damaged organelles—such as mitochondria (mitophagy)—as well as providing a steady pool of amino acids for the cell to use. But if autophagy is deregulated and persistently increased, the cancer cell risks eating itself to death (White and DiPaola, 2009). AMPK and mTOR's control over autophagy hinges on Unc-51 like autophagy activating kinase 1 (ULK1), an important regulator of autophagosome formation. Under conditions of nutrient stress, AMPK activates ULK1 through phosphorylation on serine 555 while under conditions of nutrient excess mTOR inhibits it. Once activated, ULK1 triggers the formation of the autophagosome. The autophagosome then incorporates autophagy-related protein 8 (ATG8/LC3-II) into its membrane. Autophagosomes can then bind to cargo receptor proteins—containing LC3-interacting regions in their amino acid sequence (LC3 interacting motif)—and cargo (proteins, damaged organelles) and direct the autophagosome to the lysosome for destruction (Parzych and Klionsky, 2014).

1.4. Mitochondria Dynamics

1.4.1 Mitochondria fission, fusion, and key regulators of the process

Mitochondria are not static structures inside of the cell. Each mitochondrion can break apart (fission) or join with neighboring mitochondria (fuse). Mitochondria can also

traffic along microtubules to areas of the cell in need of high energy—which is particularly evident in the brain along the axons of neurons (Schwarz, 2013). The processes of fission and fusion of mitochondria are rapid and the balance between the processes are regulated by several core proteins that are critical to the processes.

Fusion of two mitochondria requires two membrane fusion events of the outer mitochondria membrane (OMM) and the inner mitochondria membrane (IMM) and is regulated by multiple large GTPases. The outer mitochondria membrane fusion is controlled by mitofusin 1 and 2 and optic atrophy protein 1 (OPA1) is found in and controls the IMM fusion (Tilokani et al., 2018). In non-pathological contexts, mitochondria fusion has been demonstrated in response to glucose deprivation and offers protection from mitophagy (Rambold et al., 2011).

Mitochondria fission on the other hand is centrally regulated by the small GTPase dynamin related protein 1 (DRP1). Fission is controlled by post-translational modifications of DRP1—primarily through the phosphorylation of DRP1 serine 616 (Kashatus et al., 2015). Once phosphorylated at serine 616, DRP1 shuttles from the cytoplasm to the mitochondria where it binds to one of four receptors on the OMM: Fis1, mitochondria fission factor (MFF), MiD49, and MiD51(Losón et al., 2013). At these receptors, DRP1 oligomerizes around mitochondria as a contractile ring and fissions mitochondria.

These events are not completely random. Fission has a higher probability at occurring at mitochondria/ER contact points where ER tubules cross over and wrap around mitochondria (Friedman et al., 2011). Furthermore, mitochondria undergo

fragmentation during S and M phase of the cell cycle (Scott and Youle, 2010) to help ensure an equal segregation of mitochondria among daughter cells. Increased ROS, crashes in mitochondria membrane potential, increased calcium influx into mitochondria from the ER, and hypoxia can all trigger mitochondria fragmentation (Willems et al., 2015). Mitochondria depolarization and subsequent fragmentation is also an important step in the intrinsic apoptosis pathway because it promotes the release of cytochrome c from the intermembrane space of mitochondria (Sheridan et al., 2008). Conversely to mitochondria fusion in glucose deprivation, mitochondria fission has been observed in conditions of glucose excess (Mishra and Chan, 2016). However, there is significant debate over whether these observations of fusion in nutrient deprivation and fission in nutrient excess applies across all contexts and disease states.

Interestingly, mitochondria dynamics play an important role in cancer progression as well. There are multiple research studies have demonstrated that the leading (invasive) edge of a cancer is comprised of cells with a highly fragmented mitochondria network (Ferreira-da-Silva et al., 2015; Zhao et al., 2013). Furthermore, restoration of a fused mitochondria phenotype through DRP1 knockdown or overexpression of mitofusin proteins hindered cancer cell growth (Rehman et al., 2012; Xie et al., 2015).

1.5 NF-κB at the mitochondria

1.5.1 Canonical and Non-canonical signaling proteins are recruited to mitochondria

Many proteins of the canonical NF-κB pathway have been found to be recruited to the mitochondria. IκBα, RelA (p65) and p50 have all been found in the mitochondria matrix (Albensi, 2019). RelA and p50 subunits have been also found bound to mitochondria DNA where they regulate mitochondria gene expression (Johnson et al., 2011). TNFα and IKKα have been shown to increase mitochondria fusion through regulation of OPA1 (Laforge et al., 2016). Furthermore, IκBα has also been demonstrated to localize to the outer mitochondria membrane where it interacts with a voltage dependent anion channel (VDAC) and hexokinase 2 to prevent cytochrome c release and subsequent apoptosis (Pazarentzos et al., 2014).

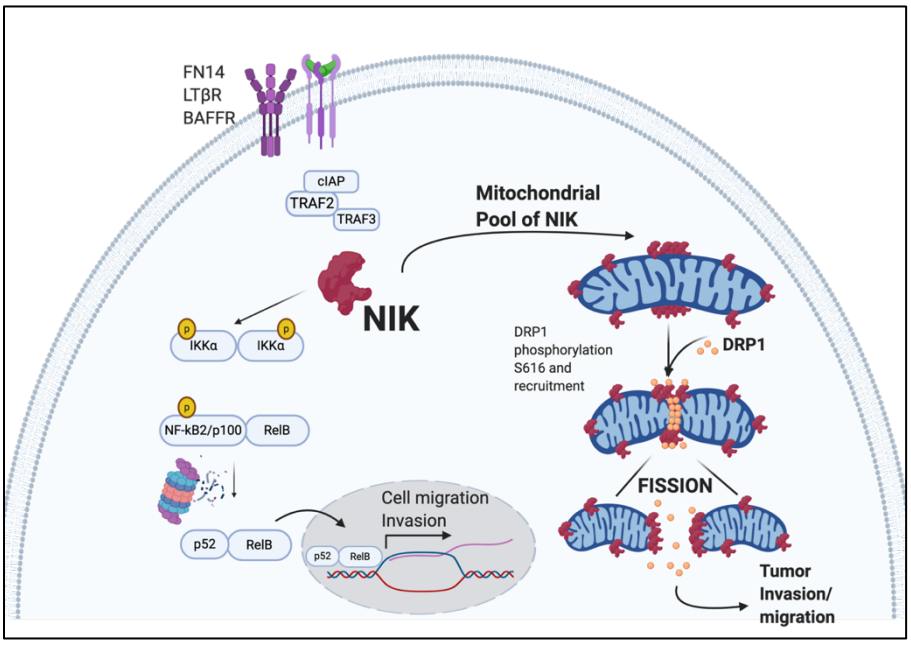

Figure 4. A pool of NIK resides at the mitochondria in steady-state conditions
Above: NIK/MAP3K14 was initially thought to be a strictly cytosolic protein where it initiates the non-canonical NF-κB signaling cascade. However, NIK also is recruited to the mitochondria where it promotes fission. Both processes (non-canonical signaling and increased mitochondria fission) can increase tumor cell invasion and migration.

The non-canonical NF-κB pathway proteins have also been implicated in metabolic functions. RelB, for example, has demonstrated importance in regulation of metabolism in skeletal muscle (Shintaku et al., 2016), while NIK has been demonstrated to promote glucagon activity and increase production of glucose in the liver (Sheng et al., 2012). However, there has been significantly less work investigating non-canonical NF-κB signaling in metabolism when compared to the canonical signaling pathway.

In 2016 our lab discovered that a pool of NIK/MAP3K14 is recruited to the mitochondria (Figure 4) where it promotes the recruitment and phosphorylation of DRP1(Jung et al., 2016). Our lab's primary focus is NF-κB Inducing Kinase (NIK; MAP3K14), the principal kinase in the non-canonical NF-κB signaling cascade. Upregulation of NIK is associated with increased invasion in many cancers due in part to increased transcription and translation of matrix metallopeptidase 9 (MMP-9), a critical protein involved in the breakdown of type IV collagen in the extracellular matrix (Li et al., 2009). Therefore, attenuation of NIK signaling can have profound effects on a tumor cell's ability to invade (Raychaudhuri et al., 2007). Our lab discovered this NIK-dependent invasion is also due in part to its interaction with DRP1 at the mitochondria, as DRP1 KO cells that overexpress NIK have diminished invasive capacity (Jung et al., 2016).

1.6 Summary

In summary, there are two distinct branches of NF-κB signaling. While the canonical NF-κB is stimulated by LPS, TNF-α, and IL-1, non-canonical NF-κB signaling has a distinct set of activating ligands, receptors, downstream signaling kinases and transcription factors. Both NF-κB1 and NF-κB2 exist in the cytosol as inactive forms—p105 and p100 respectively. Both precursors are activated through IKK phosphorylation and proteolytic processing to their active form, where they bind a Rel protein as a heterodimer and translocate to the nucleus and serve as transcription factors(Ghosh and Hayden, 2012). Furthermore, though the canonical NF-κB signaling cascade is known as the chief regulator of inflammatory signals and innate immunity, the non-canonical pathway was initially recognized in knockout mice as being critical for adaptive immunity.

While initially thought to possess a role specific for B lymphocyte differentiation, it has become apparent that NF-κB executes critical processes in a variety of cell types and contributes to a multitude of cellular activities and diseases, including cancer. NF-κB can be activated by a wide range of stimuli, including cytokines such as TNF- α and IL-1ß, bacterial and viral components such as LPS and dsRNA, DNA damage and reactive oxygen species (ROS) (Gloire et al., 2006; McCool and Miyamoto, 2012; Oeckinghaus and Ghosh, 2009; Zamanian-Daryoush et al., 2000). While the canonical NF-κB pathway responds to a large repertoire of receptors such as the tumor necrosis factor-α receptor (TNFR), interleukin-1 (IL1) receptor-1 (ILR1), and all members the toll-like receptor family (TLRs) (Wertz and Dixit, 2010), the non-

canonical pathway is only activated by a small subset of receptors. These receptors include the CD30 ligand (CD30L), CD40 ligand (CD40L), lymphotoxin ß receptor, B-cell activating factor receptor (BAFF-R), as well as the fibroblast growth factor-inducible 14 (Fn14) receptor (Sun, 2011).

Like NIK, AMPK also maintains a cytoplasmic, nuclear, and mitochondria localized pool (Kodiha et al., 2007; Park et al., 2006; Toyama et al., 2016). Indeed, upon nutrient deprivation and subsequent activation, AMPK localizes with the DRP1 outer membrane receptor mitochondrial fission factor (MFF) where it helps drive mitochondrial fission (Toyama et al., 2016). This AMPK-mediated mitochondria fission has been proposed to be an important driver in autophagy through phosphorylation and activation of Unc-51 like autophagy activating kinase 1 (ULK1) while simultaneously inhibiting the mTORC1 complex (Zhang and Lin, 2016).

Recognizing metabolic vulnerabilities of gliomas will aid in the development of novel treatments to starve and destroy glioma tumor cells and extend patient lifespan. This project seeks to ascertain whether NF-κB Inducing Kinase (NIK; MAP3K14) drives metabolic reprogramming in glioma, identify the molecular mechanism by which it occurs, and establish whether NIK-dependent metabolic rewiring is important for glioma cell survival *in vivo*.

II. METHODS

Materials and Methods

2.1 Cell culture. BT25 and BT114 patient-derived cells were obtained as previously described (Kelly et al., 2009). Cells were maintained as spheroids in Neural Stem Cell (NSC) medium containing Advanced DMEM/F-12, 1X B-27 supplement minus Vitamin A, 1X Glutamax, 25 ng/ml EGF, 25 ng/ml bFGF and 1X Pen/Strep (Life Technologies). Tumor spheres were not cultured beyond ~100uM. 293T and COS-7 cells were obtained from ATCC and cultured in DMEM medium with 10 % FBS and 1X Pen/Strep. All cells were cultured at 37 °C with 95 % humidity and 5 % CO_2. All cell lines are routinely tested for mycoplasma and authenticated by STR fingerprinting.

2.2 Immunofluorescence staining. 2 x 10^4 cells were seeded in collagen-coated (40-50 ug/ml) 8 well chamber slides (Ibidi, #80827, Munich, Germany) or on coverslips in the presence of 1% FBS and allowed to adhere overnight. Cells were fixed with 4 % paraformaldehyde, permeabilized for 20 minutes with 0.3 % Triton X-100 in PBS and blocked 30 min at room temperature with 5 % serum corresponding to secondary antibody host. Cells were incubated overnight in 0.1 % Triton X-100, 1 % BSA in PBS at 4 °C with either the primary antibody phospho-DRP1 S616 (Cell Signaling Technology, 4494), Tim50 (Santa Cruz, sc-393678), Rab7 (Cell Signaling Technology, 9367) or Tom20-AF488 (Abcam, ab205486). Cells were then incubated in 1 % BSA for

1 h at room temperature with secondary antibodies Alexa Fluor 488 or Alexa Fluor 594 from Life Technologies.

2.3 Live cell imaging. BT25 cells and COS-7 cells were plated on 8 well chamber slides with a glass bottom (Ibidi) and then were transfected with Lipofectamine 3000 (Invitrogen) with constructs expressing GFP-NIK, mCherry-Drp1, and mito-BFP. After 18 hours, time-lapse images were acquired every 5 seconds for 3 minutes on a Nikon TI A1R inverted confocal microscope with 60x Plan-Apochromat lenses and Stage-top incubator system. Random fields of mitochondria were imaged (n > 19 cells each) and analyzed using NIS-Elements imaging software (Nikon, Japan). The diffuse cytosolic images were threshold-adjusted by subtracting background signal in the cytosol. For analysis of COS-7 cells under metabolic switching conditions, cells were seeded at a density of 50,000 cells into a collagen coated (50μg/mL), 8 chamber slide (Ibidi) with 1% FBS. 24hrs later, cells were transfected with GFP-NIK, mCherry-DRP1, Mito-BFP (40ng each) using lipofectamine (Lipofectamine 3000, Invitrogen). 24-48hrs after transfection, cell media was either switched to media containing 25 mM galactose (without glucose) or media containing 25mM glucose. Cells were live imaged as described above. Correlation analysis was done on RBG images using NIS Elements software. Mander's correlation coefficient of the pixel overlap was measured in individual frames from enhanced video.

2.4 Subcellular fractionation. Subcellular fractionation was performed as previously described (Otera et al., 2010). In brief, cultured cells were washed twice with ice-cold PBS and scraped in 2 ml of ice-cold PBS. After removing supernatants following centrifugation at 800 xg for 5 min, pellets were resuspended and homogenized in homogenization buffer (10 mM HEPES-KOH, pH 7.5, 0.25 M sucrose) by passing a 27-gauge needle 10 times. Post-nuclear supernatants were collected by centrifugation at 1,000 xg for 10 min and then, heavy membrane fraction was separated from the resultant supernatant by centrifugation at 8,000 xg for 10 min at 4 ˚C. The pellets of heavy membrane fraction, mitochondria-enriched fraction were washed with buffer and solubilized in 100 μl of solubilization buffer (50 mM Tris-HCI [pH 8.8], 5 mM EDTA, 1 % SDS). The remaining supernatants as cytosol fraction were centrifuged again at 16,000 xg for 10 min at 4 ˚C to remove any remaining insoluble membranes.

2.5 Immunoblot assays. Cells were lysed in RIPA lysis buffer (Pierce, #89900, Rockford, lL) with protease/phosphatase inhibitor cocktail (Thermo Scientific). Equal amounts of protein were mixed with NuPage 4X LDS sample buffer (Invitrogen, NP0008) containing reducing agent and denatured at 100 ˚C for 7 min. Proteins were separated on 8 % - 12 % SDS-PAGE and transferred to nitrocellulose membranes (Bio-Rad, #162-0115). The membranes were blocked for 1 h with 5 % non-fat dry milk in 0.1 % Tween-20/TBS (TBST) or Odyssey blocking buffer (LI-COR Biosciences, 927-40000) and incubated with primary antibodies for either IKKα (EMD Millipore, OP133), phospho IKKα/β (Ser176/180) (Cell Signaling Technology, 2697S), NIK (Cell Signaling

Technology, 4994S), HA-tag (Cell Signaling Technology, 3724S), V5-tag (Cell Signaling Technology, 13202S), GST (Santa Cruz Biotechnology, sc-138), NFKB2 (Cell Signaling Technology, 4882S), GAPDH (Santa Cruz Biotechnology, sc-365062), β-actin (Santa Cruz Biotechnology, sc-69870), Tom20 (Cell Signaling Technology, 52406S), TOM70 (Santa Cruz Biotechnology, sc-390545), HSP60 (Cell Signaling Technology, 12165S), OPA1 (Cell Signaling Technology, 80471S), DRP1 (Cell Signaling Technology, 8570S), phospho-DRP1 S616 (Cell Signaling Technology, 4494S) diluted in blocking buffer at 4 °C overnight. After washing in TBST, membranes were incubated with goat anti-rabbit IRDye800CW (LI-COR Biosciences), goat anti-mouse IRDye680 (LI-COR Biosciences) or goat anti-rabbit HRP conjugate (Thermo Scientific) diluted in blocking buffer and incubated for 1 hour at room temperature. The blots were washed with TBST and developed using Chemiluminescent HRP Substrate (EMD Millipore, WBKLS0100) for detection of HRP or an Odyssey Infrared Imaging system (LI-COR Biosciences) for detection of IRDye fluorescent dyes.

2.6 MTS Proliferation/ Propidium Iodide Cell Survival Assay. BT25 cells were transitioned to low glucose using the following protocol. Cells were initially cultured for 5-7 days in NSC media as previously described. Cells were then dissociated and seeded at a density of 5 x 10^5 cells in DMEM/F12 media (US Biological Life Sciences, D9807-02, Salem, MA) containing 18 mM D-Glucose with 1 mg/L Insulin (Gibco, 12585014). Cells were then dissociated and seeded the same density in DMEM/F12 media containing 5 mM D-Glucose with 1 mg/L Insulin and expanded for 5-7 days.

Cells were then dissociated again and seeded in the same media containing 18 mM D-Galactose, 2 mM D-Glucose, 1 mg/L Insulin for 7 days. Cells were then seeded at a density of 1 x 10^4 cells in triplicate on collagen coated 96-well plate into media containing either DMEM/F12 containing 18 mM D-Glucose or 18 mM D-Galactose and 1% FBS. MTS (Cell Titer AQ_{ueous} One Solution Cell Proliferation Assay, G3581, Promega) readings were then taken on the day the cells were seeded (day 0) and every 24 hours thereafter for 5 days using the Victor X3 microplate reader at 490 nm. The measurements normalized to day 0. For propidium iodide (PI) cell death flow cytometry analysis, cells were transitioned to galactose in the same manner as in the MTS proliferation assay, except they were left to grow as suspension cells for 48 hrs in either DMEM/F12 NSC media containing 18 mM glucose or 18 mM galactose. At the 48 hr time point cells were dissociated with Accutase and stained with propidium iodide (ThermoFisher Scientific, Alexa Fluor 488 Annexin V Dead Cell Apoptosis kit, V13241) as described by manufacturer's instructions. The Fortessa X-20 flow cytometer was then utilized to detect percentage of dead cells per condition and cell death was measured as fold change % dead cells in galactose/% dead cells in glucose n=3-4 replicates per condition.

2.7 Plasmids. For NIK overexpression, mouse (mNIK) cDNA was cloned into pLenti6-V5-DEST (Addgene, Cambridge, MA) using the GATE-WAY™ Cloning System (Invitrogen). Luciferase (Promega) coding sequences were subcloned into pLenti6-v5-DEST (Invitrogen) and served as a control vector for NIK overexpression. For GFP-

NIK construct GFP was fused to N-terminal of full-length human NIK (modified from addgene plasmid #27554). EGFP-LC3 was a gift from Karla Kirkegaard (addgene plasmid # 11546). For DRP1-S616E overexpression. DRP1 616E was created by point mutagenesis using Q5™ Site Directed Mutagenesis Kit (NEB) and the following oligos: DRP1 616E up: TATGCCAGCCGCTCCACAAAAAG. DRP1 616E dn: ATTGGAATGGGTTTTGATTTTTC. The mutated construct was then cloned into pLenti6-V5-DEST (Addgene, Cambridge, MA) using the GATE-WAY™ Cloning System (Invitrogen). For DRP1 616A construct, which additionally harbors a 637 E mutation, we utilized the same strategy as with 616E but used the following oligos: DRP1 616SA up TATGCCAGCCGAGCCACAAAAAG DRP1 S616SA dn ATTGGAATGGGTTTTGATTTTTC. DRP1 S637SE up ACGAAAACTAgctGCTCGGGAAC. DRP1S637SE dn GCAACAGGAACTGGCACATC.

2.8 CRISPR-Cas 9 gene knockout. BT25 cells were transduced with a mixture of Lenti-CrispR-v2 carrying 3 gRNAs for each target. The gRNA sequences for human NIK and DRP1 are previously described (Bayless et al., 2009; Jung et al., 2016). The sequences for IKKα are: gIKKa1 ACAGACGUUCCCGAAGCCGC, gIKKa2 ACGUCUGUCUGUACCAGCAU, gIKKa3 UUCUGGAGGAGAUCUCCGAA. The sequences for IKKβ are: gIKKb1 GAUUUGGAAAUGUCAUCCGA, gIKKb2 UCAGCCCCCGGAACCGAGAG, gIKKb3 CCUUCCGGAGAUCUCCUCCU. Loss of NIK, Drp1, IKKα, and IKKβ expression was confirmed by immunoblot, qPCR and/or

immunofluorescence microscopy analysis of puromycin-resistant cells. For BT25-NIK$^{-/-}$, DRP1$^{-/-}$, IKKα/β$^{-/-}$ cells and single colony cells were isolated by serial dilution. All experiments were repeated with at least two knockdown clones.

2.9 Lentivirus production. Twenty-four μg of lentiviral plasmids and 72 μg of polyethyleneimine were used to transfect 293T cells. After 3 days of transfection, viral supernatant was harvested and filtered through a 0.45 μM syringe filter. After filtration, viral particles were concentrated 20-fold to 500 μl using Lenti-X Concentrator (Clontech, #631231, Mountain View, CA), and 100 μl of concentrated virus were used to infect cells. Stably transduced cells were selected for 72 h in medium containing 0.6 μg/ml puromycin or 3 μg/ml blasticidin (Invitrogen).

2.10 Seahorse analysis. Metabolic shifting strategy: BT25 cells to be measured in 18 mM glucose by the Seahorse XF96e analyzer were grown in NSC media containing Advanced DMEM/F12 were and were then plated on collagen coated Seahorse XFe96 microplates. BT25 cells to be measured in 18 mM Galactose were first passaged from Advanced DMEM/F12 NSC media to DMEM/F12 media containing 5 mM D-Glucose with 1 mg/L Insulin and expanded for 5 days. Cells were then dissociated and plated on collagen coated Seahorse XFe96 microplates in the same media containing 18 mM D-Galactose, 2 mM D-Glucose, 1 mg/L Insulin overnight. Thirty thousand cells per well were plated in the Agilent Seahorse XFe96 microplates and left to settle overnight before analysis with the FluxPak kits according to company standards. Each experiment with 3-

4 replicates per sample was repeated ≥ 3 independent times. Mitochondrial Stress Tests were conducted following Seahorse guidelines (Agilent Technologies). For the assay base, media was supplemented with either 18 mM glucose (Sigma, G7021, St. Louis, MO) or 18 mM galactose (Sigma, G0750, St. Louis, MO), 2 mM Glutamine (Sigma, G85420, St. Louis, MO), and 1 mM pyruvate (Gibco). Inhibitors were used at the following concentrations: 1 μM Oligomycin A (Sigma, 75351, St. Louis, MO), 1 μM FCCP (Sigma, C2920, St. Louis, MO), and mixture of 0.5 μM rotenone (Enzo Life Sciences, Farmingdale, NY, ALX-350-360)/.5 μM antimycin A (Sigma, A8674, St. Louis, MO). Normalization was performed by quantifying DNA content with DRAQ5 (Thermo Fisher Scientific, 50-712-282) and analyzed with an Odyssey scanner. The DRAQ5 RFU values were entered into Wave software. Analyses were conducted using Wave software and XF Report Generators (Agilent Technologies) and statistical analysis were conducted in PRISM. Mitochondrial ATP production was quantified by taking the initial O2 consumption measurements (in absence of oligomycin) for each cell type and comparing that to the corresponding initial O2 measurement upon addition of oligomycin. The difference in O2 consumption between these two points is the mitochondria-dependent ATP production. Spare respiratory was calculated by taking the initial O2 consumption measurements (in absence of oligomycin) for each cell type and comparing that to the corresponding initial O2 measurement upon addition of FCCP. The difference in O2 consumption between these two points is the spare respiratory capacity of the cell. For glycolysis stress tests, cells were initially plated on collagen coated Seahorse XFe96 plates overnight in 18 mM galactose +2 mM glucose and then

starved for one hour in Seahorse DMEM base media before the experiment began. 5 mM glucose was injected in port A and delivered to the cells. Glycolysis is defined as the change in ECAR from baseline readings to the first point after glucose injection. The seahorse assay and analysis were performed in the Texas A&M College of Medicine Cell Analysis Facility (COM-CAF). For the mitostress plots, the same BT25 control 18 mM glucose and 18 mM galactose data points were used as references between figures 6, 11, 13 and 16.

2.11 Single organelle analysis of mitochondria by flow cytometry. BT25 NIK$^{-/-}$ +mNIK-v5 cells were plated in 6 cm dishes in Advanced DMEM/F12 complete NSC media with 1% FBS and grown to roughly 85-90% confluence before being switched 18 mM Glucose DMEM/F12 with B27 supplement, EGF, bFGF, 10 mg/L Insulin and 1% FBS. For galactose condition, the appropriate plates were switched to 18 mM galactose DMEM/F12 with B27 supplement, EGF, bFGF, 10 mg/L Insulin and 1% FBS for 6 hours. Heavy membrane organelles were isolated, fixed in 4% PFA on ice for 20 minutes, and stained with Tom20-AF488 (Abcam, ab205486, 1:200), and V5-AF647 (Invitrogen 451098 1:200) diluted in Perm/Wash buffer (BD Biosciences, 554723). The fractions were resuspended in 1:5 homogenization buffer:PBS and analyzed on Fortessa X-20. For DRP1 recruitment by single organelle analysis, BT25 control, NIK$^{-/-}$, and DRP1$^{-/-}$ cells were plated, metabolically switched to glucose or galactose for 3 or 6 hours, stained for 20 minutes with 2.5 μM Mitosox^{TM} Red (Thermo Fisher Scientific, M36008) at 37°C and fractionated as described above. The heavy membrane was then

fixed with 4% PFA on ice for 20 minutes and then labeled with DRP1 (CST 8570S) conjugated to Alexa Fluor™ 488 (Invitrogen Zip AF488 Label Kit, Z11233). The DRP1-AF488/ Mitosox™ Red labeled heavy membrane from the control, $NIK^{-/-}$, and $DRP1^{-/-}$ cells were then analyzed on the Fortessa X-20. DRP1 mitochondria coverage was determined using FlowJo Overton % Positive subtraction of DRP1-$AF488^{+}$ signal between the control and $NIK^{-/-}$ Mitosox™ Red^{+} organelles compared to the $DRP1^{-/-}$ (negative control) signal. For protease protection assay, cells were first stained for 20 minutes with 2.5 μM Mitosox™ Red at 37°C. The cells were then fractionated, and either treated with proteinase K for 30 minutes on ice or kept in SEM buffer without proteinase K. Proteinase K treated heavy membrane fractions were then treated with PMSF, fixed for 20 minutes with 4% PFA then stained with V5-AF647 and Tom20-AF488 before being analyzed with the Fortessa X-20. To detect V5-AF647 mitochondria the heavy membrane was first gated based on Mitosox Red^{+} organelles, then gated to detect Tom20-AF488 positive and V5-AF647 positive membranes. Single stained and unstained controls were used for all single organelle analysis experiments to determine spillover between channels. Mitochondria size measurements were established by calibrating the Fortessa with 1 μM, 2 μM and 4 μM beads (Molecular Probes, F-13838, Oregon). Mitochondria analyses by flow cytometry were repeated in at least 3 independent experiments and ≥10,000 individual mitochondria events were collected for each experiment.

2.12 Mouse Xenograft Assay. All animal experiments were done in compliance with IACUC, AAALAC and Texas A&M Health Science Center Biosafety guidelines using an IACUC-approved Animal Use (Protocol # 2018-0483 and 2015-0330). For orthotopic tumor inoculations, 0.5-1x10^6 cells were injected into the right striatum of 4 - 6 week old CD-1 nude mice. Mice were imaged injected with luciferin and imaged for luminescence weekly post tumor inoculation on the IVIS Spectrum In Vivo Imaging System (Perkin Elmer). Tumor cells were either stably expressing luciferase or were labeled using a DiD Cytoplasmic Membrane dye (Biotium, abs/ em=644/665). For each cell type, ≥3 - 4 animals were injected.

2.13 Histology and Tumor Imaging. Mice were euthanized and brains were dissected and fixed in 10% Neutral Buffered Formalin. The fixed brains were sucrose cryoprotected and sectioned on a cryostat (10 µm sections) and H&E stained and were imaged on a VS120 Virtual Slide Microscope (Olympus).

2.14 Protease Protection Assay—Immunoblot Blot Analysis. Protease protection assay was performed as previously described (PMID: 17095012). The heavy membrane fraction was mixed with 100 µl ice-cold SEM buffer (10 mM MOPS/KOH [pH 7.2], 250 mM sucrose, 1 mM EDTA) at a concentration of 5µg/µl. One aliquot of Swell buffer treated heavy membrane fraction and one aliquot of SEM buffer treated heavy membrane fraction were treated with 5.26µl Proteinase K (1mg/ml in SEM buffer) and incubated on ice for 30 min. Protease activities were inhibited in all samples adding

5.26µl of Phenylmethylsulfonyl Fluoride (PMSF) (200mM in Isopropanol) to each sample. Protein was precipitated from solution with 72% Trichloroacetic Acid (TCA) overnight on ice. Precipitate was collected by centrifugation at 28,000 xg for 30 min at 4 ˚C and washed two times with ice-cold PBS to remove any remaining supernatant.

2.15 3D invasion assay. Invasion assays were performed as described previously [24,25]. In brief, Type I collagen extracted from rat tail tendons was diluted to 2 mg/ml in DMEM/F12 (1× Pen/Strep) and matrices polymerized in 96-well plates. 40,000 cells per well were seeded in 100 µl DMEM/F12 (1× Pen/Strep, 1× Glutamax) without growth factors or serum. Cells were fixed with 3% glutaraldehyde solution after 48 h of invasion and stained with 0.1% toluidine blue. Invasion density was quantified by counting cells below the plane of the monolayer by bright-field light microscopy using a 10 × 10 ocular grid at 20× magnification corresponding to a .25 mm^2 field. Numbers in equivalent fields were counted (n = 3 wells).

2.16 Measurement of mitochondria superoxide. BT25 control GBM cells were grown in Advanced DMEM/F12 media with 1% FBS to approximately 85% confluency. The cells were then switched to media containing DMEM/F12 media (US Biological) with either 18 mM glucose or 18 mM Galactose as described earlier with 1% FBS for 1 hr, 3 hr, or 6 hr. Accutase was used to detach the cells from the plates and they were incubated with 1 µM MitoSox Red™ for 30 minutes at 37 degrees C. The cells were then analyzed by flow cytometry with the Fortessa X-20. n=10,000 cells per condition.

2.17 RNA extraction, cDNA synthesis, and RT-PCR. RNA was extracted from BT25 cells with the Purelink™ RNA Mini Kit (Life Technologies). cDNA was synthesized from 1 μg total RNA using iScript reverse transcription supermix (Bio-Rad, Hercules, CA) following the manufacturer's protocol. Quantitative RT-PCR was performed using iTaq Universal SYBR Green Supermix (Bio-Rad) with StepOnePlus Real-Time PCR System (Applied Biosystems, Foster City, CA). The primers used for CHOP were as follows: CHOP-Forward—CCTGCTTCTCTGGCTTGG, CHOP-Reverse—CTTGGTCTTCCTCCTCTTCC

2.18 LC-MS Untargeted Metabolomics. BT25 control, $NIK^{-/-}$, $DRP1^{-/-}$, and $NIK^{-/-}$ +mNIK-v5 cells were grown in suspension for 5 days in advanced DMEM/F12 NSC media as described earlier. The cells were pelleted and weighed to ensure 100 milligrams of pelleted cell mass per condition and snap frozen in liquid nitrogen. Samples were then extracted with methanol: chloroform and subjected to positive phase LC-MS preparation and analysis by the IMAC lab at Texas A&M.

2.19 Identification of NIK binding partners by mass spectroscopy. BT25 control and $NIK^{-/-}$ +mNIK-v5 cells were grown to 85-90% confluence on a 15 cm dish which included advanced DMEM/F12 NSC media + 1% FBS. When the proper cell density was reached, the cells were switched to DMEM/F12 NSC media containing either 18 mM glucose or 18 mM galactose + 1% FBS for 3 hours. The cells were rinsed with

PBS, scraped from the plates, and homogenized as described earlier. However, the solubilization buffer normally used for homogenization experiments was instead exchanged for RIPA buffer. 1 mg of protein was used to immunoprecipitated on to V5 tagged dynabeads (MBL, M215-11). The protein was released from the dynabeads with 5% SDS solution containing no reducing reagents. The protein was digested with trypsin and purified using S-trap columns (Protifi, Huntington, NY). The protein was then sent for mass spec analysis at the TAMU protein chemistry lab and the results were viewed on Scaffold software.

2.20 Quantification and statistical analysis. Statistical analysis was carried out using GRAPHPAD PRISM software, and details of the statistical analysis can be found in the figure legends where applicable. The data presented here was considered statistically significant if $p<.05$. Tukey post-hoc tests were used for one-way and two-way ANOVA. For ANOVA each group sample is from a normally distributed population, all samples are independent of each other and have a common variance.

III. RESULTS: PART I

3.1 NIK is an outer mitochondrial membrane protein that co-localizes with DRP1 at mitochondrial fission sites *in vivo*.

We previously reported that a subset of NIK protein localizes to mitochondria and is required for maximal mitochondrial recruitment of Drp1. Here we sought to determine topology of NIK at the mitochondria through use of the protease protection assay combined with single organelle analysis (Schneider et al., 2019). BT25 $NIK^{-/-}$ cancer cells overexpressing full length murine NIK tagged with V5 were first labeled with Mitosox red™ — a mitochondria superoxide sensitive dye that accumulates in the mitochondria matrix — and fractionated in a sucrose gradient (Fig 5a). The heavy membrane fraction was resuspended in an isotonic buffer either containing proteinase K or withheld from proteinase K treatment. After protease treatment the heavy membrane was labeled with Alexa Fluor 647 (AF647) conjugated V5 antibody and AF488 conjugated Tom20 antibody and then analyzed on the Fortessa X20 flow cytometer. The results indicated that NIK follows a similar pattern for protease treatment as Tom20 (Figure 5b, 1c). However, unlike Tom20, which is housekeeping mitochondrial protein with ubiquitous expression, NIK tended to localize to larger mitochondria membranes as indicated by the higher levels of forward scatter (Figure 5b).

To further confirm that NIK resides at the outer mitochondria membrane, we performed an additional protease protection assay and analyzed by western blot (Figure 5d). For this assay we utilized Tom 70 as a marker for the outer mitochondria membrane, OPA1 as a marker for the inner mitochondria membrane, and HSP60 as a as

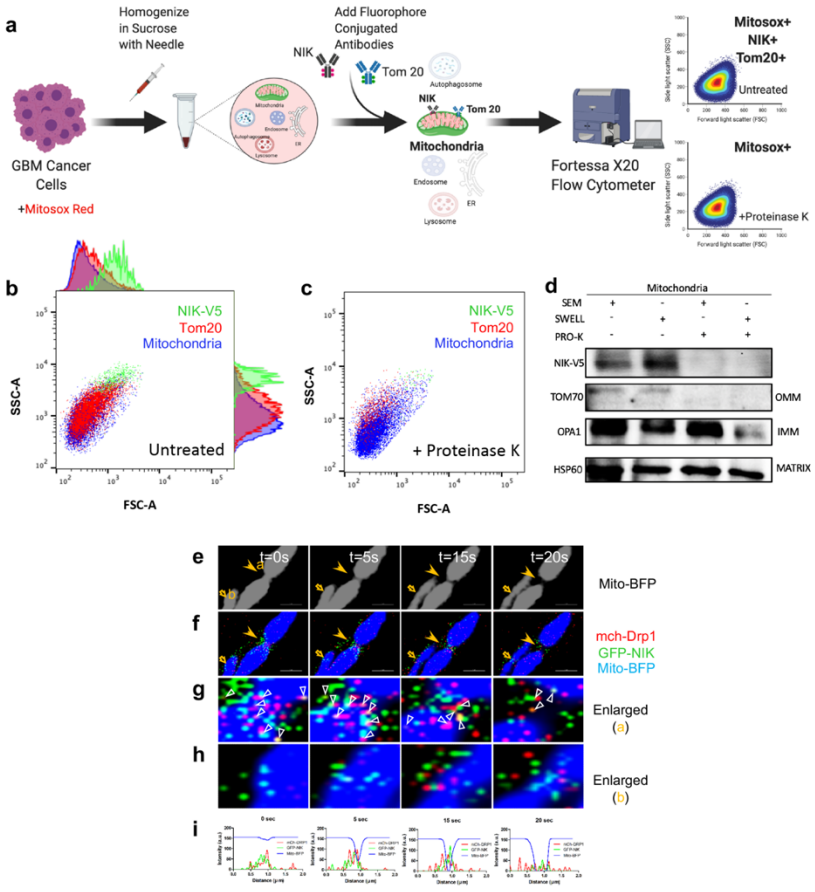

Figure 5. A pool of NIK resides at the outer membrane of mitochondria and co-localizes with DRP1 at mitochondria fission sites.

a, Schematic showing single cell organelle analysis strategy for determining NIK localization at the mitochondria membrane. **b-c,** Representative protease protection assay was performed using single organelle flow cytometry analysis of untreated **(b)** and Proteinase K-treated mitochondria **(c)** isolated from BT25 cells expressing V5-tagged NIK (NIK-V5) and stained with AF647-conjugated V5 antibody (pseudocolored green), Tom20-AF488 conjugated antibody (pseudocolored red) and MitoSOX™ (pseudocolored blue). NIK-V5, Tom-20, and MitoSOX™ positive organelles were analyzed by forward scatter (FSC-A) and side scatter (SSC-A) to evaluate mitochondrial size and complexity. **d**, Representative western blot showing protease protection assay with indicated antibodies. **e,** Grayscale images show mito-BFP fluorescence with filled arrow indicating fission site and open arrow indicating a constriction site. **f,** mch-DRP1 (red) and GFP-NIK (green) is shown merged with mito-BFP (blue). Scale bar, 2µm. **g,** Enlargement of the mitochondrial fission site indicated by the closed arrow (a) in 1e shows co-localization of mch-DRP1 with GFP-NIK. Open arrowheads indicate colocalization of mch-DRP1 and GFP-NIK. **h,** Enlargement of the mitochondrial constriction site indicated by the open arrow (b) in 1f shows NIK (green) and DRP1 (red) recruitment to mitochondria. **i,** Line-scan analysis of mean fluorescence intensity shows highest GFP-NIK and mch-DRP1 localization at the mitochondrial fission site (lowest mito-BFP signal). Images were threshold-adjusted by subtracting background GFP or mcherry signal in the cytosol, followed by deconvolution. The images shown are a representative of live cell imaging of mitochondria (n>5), respectively.

a representative protein of the mitochondria matrix. We found that NIK was degraded

upon addition of proteinase K in an isotonic buffer (SEM) but not inner membrane protein OPA1. Only when the heavy membrane was first incubated in a hypotonic swelling buffer (SWELL), which disrupts the mitochondria outer membrane, was the inner mitochondria membrane accessible to proteinase K and both NIK and OPA1 were degraded (Figure 1d). Taken together, the single organelle protease protection assay and the immunoblot protease protection assay demonstrate that NIK associates with the outer mitochondria membrane where it preferentially localizes to large mitochondria.

We next used live cell confocal imaging to address whether NIK binds mitochondria *in vivo*. We first transfected BT25 GBM cells with mito-BFP, a plasmid that encodes a blue fluorescent protein targeted to the mitochondrial matrix. We further co-transfected the cells with a green fluorescent NIK fusion protein (GFP-NIK) and an mCherry tagged DRP1 (mch-DRP1). Time-lapse confocal microscopy of mitochondria undergoing fission (Figure 5e) revealed that NIK and DRP1 are both recruited to mitochondria fission sites (Figure 5f). We evaluated the recruitment of GFP-NIK and mch-DRP1 to mitochondria constriction sites (Figure 5f-1i). The mitochondria labeled "a" (early mitochondria fission at t=0s) and "b" (middle of constriction at t=0s) (Figure 5e) are shown enlarged in Figures 5g and 5h respectively. These time lapse images reveal that NIK and DRP1 co-localize at the outer surface of future constriction sites (closed arrowhead "a" and open arrow head "b", Figure 5e). Fluorescence intensity plots (Figure 5i) verified GFP-NIK and mch-DRP1 colocalization—with strongest colocalization occurring at fission sites where mito-BFP was the lowest. While there is undoubtedly co-localization between NIK and DRP1 at the mitochondria fission sites

(open arrows Figure 5g), there are still GFP-NIK signal that is not colocalized with mch-DRP1 (Figure 5g). DRP1 is known to assemble on the mitochondria outer membrane via membrane receptors, so the reason may be that not all DRP1 adjacent to the mitochondria is bound to NIK. Furthermore, the interaction of a kinase and its binding partner has rapid on/off rates and the fact that not all NIK is colocalized to DRP1 may be indicative of a transient interaction between these two proteins.

3.2 Metabolic shift from glycolysis to OXPHOS triggers NIK-dependent mitochondrial fission.

Mitochondrial morphology constantly changes and is influenced by metabolic stimuli. In order to force GBM cells to utilize oxidative phosphorylation instead of glycolysis, we used media in which the glucose was substituted for galactose while holding the amount of sugar constant (18 mM glucose vs 18 mM galactose). This strategy to force OXPHOS in cell lines has been used extensively and has been used to reveal metabolic defects in mitochondria metabolism (Arroyo et al., 2016). In high glucose (18 mM glucose) media, cancer cells primarily utilize glycolysis over oxidative phosphorylation for energy production. Glucose provided by the media is broken down into intermediates which generates a net of 2 ATP in the process. Pyruvate generated by glycolysis and supplemented in the media can enter the mitochondria and feed into the citric acid cycle (Figure 6). However, since the cells are primed for glycolysis—and since there is such an excess of glucose—pyruvate may overwhelm the mitochondria pyruvate transporters and lactate may build up instead (Figure 6a, Top).

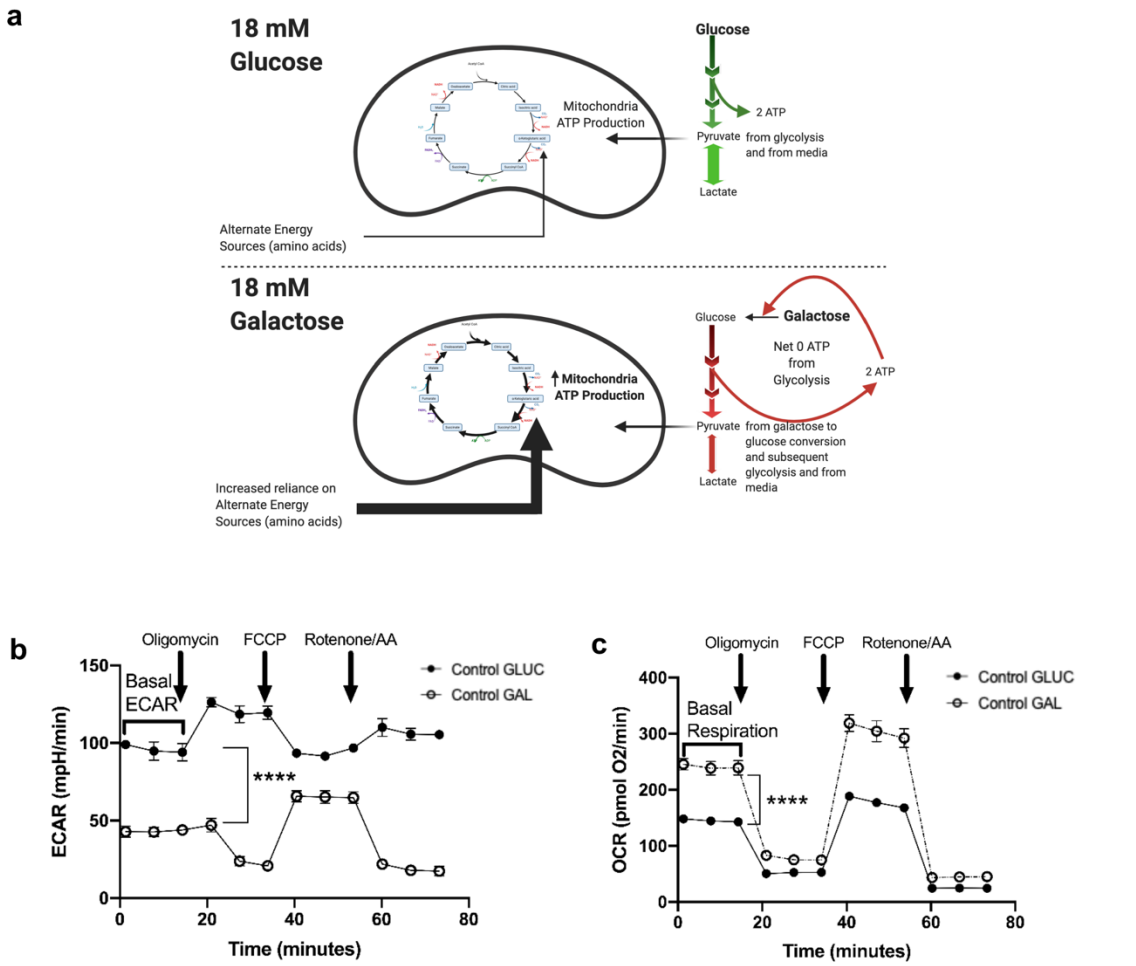

Figure 6. Use of galactose media forces switch in GBM cells from glycolytic ATP production to mitochondrial ATP production.
a, Schematic of metabolic changes when cells are transitioned from media containing 18 mM glucose (GLUC, top) to 18 mM Galactose (GAL, bottom). **b,** Representative Seahorse XF Cell Mito Stress test showing extracellular acidification rate (ECAR) of BT25 control cell in glucose and galactose media. Bracket indicates significance between basal ECAR between the conditions. Student's t test (paired, two tailed) $p<.0001$. **c,** Change in O_2 consumption rate (OCR) plotted as pmol O_2 per minute. Brackets indicate significantly different basal respiration. Student's t test (paired, two-tailed) $p<.0001$

In galactose media (18 mM galactose), galactose is converted to glucose, but ATP is utilized in the process. The net ATP produced from galactose being used in glycolysis is zero. Galactose use in glycolysis therefore represents a futile cycle in which the ATP produced from glycolysis is cycled back into conversion of galactose to glucose (Figure 6a, bottom). One can argue that this strategy is still better than simply

starving the cells of glucose completely. Although no net ATP is produced from glycolysis in this scenario, glucose 6-phosphate still can be a useful intermediate for the pentose phosphate pathway and synthesize nucleotides that are critical for cell growth.

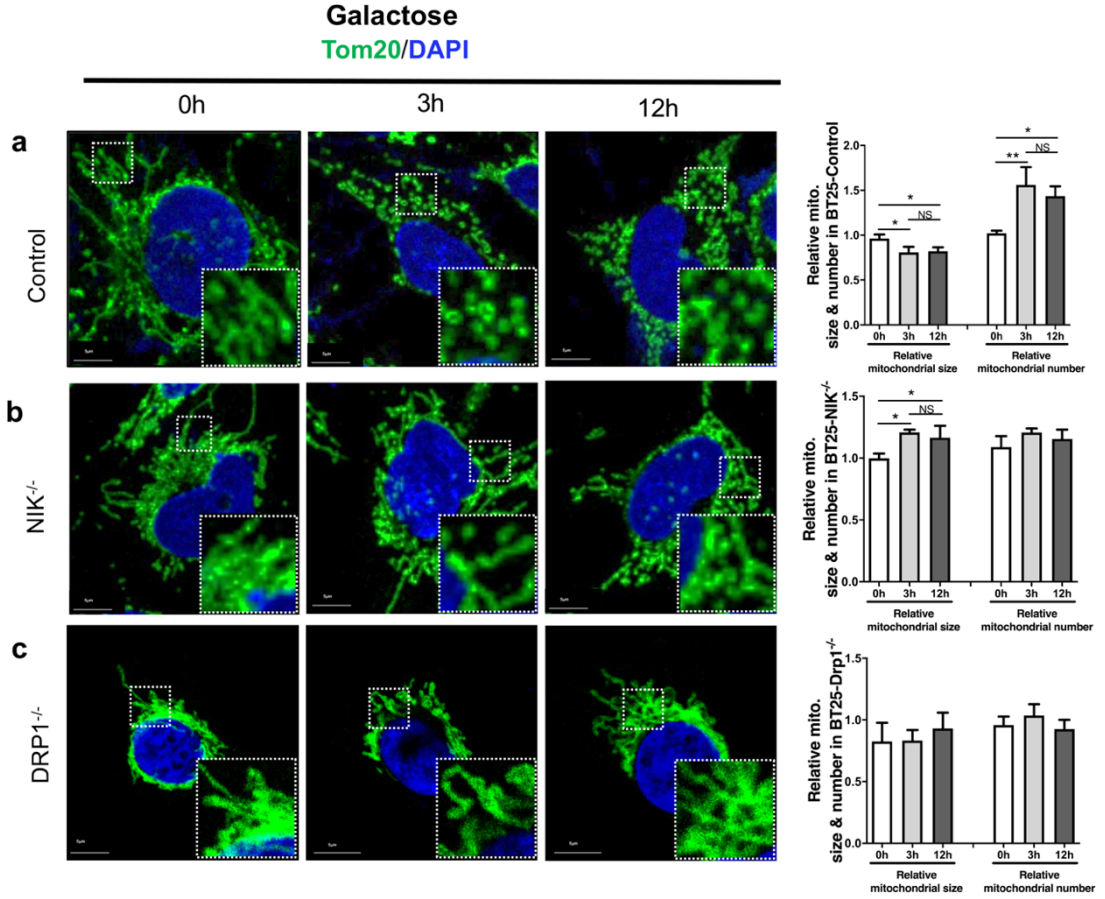

Figure 7. Metabolic shift toward OXPHOS triggers NIK-dependent mitochondria fission.
a-c, Representative confocal images of BT25 control, NIK$^{-/-}$ and DRP1$^{-/-}$ cells grown in 18mM glucose and shifted to 18mM galactose for the indicated time points and immunostained with a Tom20-FITC conjugated antibody. Areas marked with white squares are amplified and shown in the insert. Scale bar, 5 μm. Quantification of mitochondria size and number of control, NIK$^{-/-}$ and DRP1$^{-/-}$ cells pictured to the right of each image respectively. Mitochondria was quantified using Image J and significance was determined by One-Way ANOVA followed by Tukey post hoc analysis (n≥30 cells per cell condition). * $p < 0.05$, ** $p < 0.01$, ns: not significant.

In the absence of energy produced from glycolysis, the cell must rely on alternative energy sources such as pyruvate and amino acids, particularly glutamine, in the media. These alternative fuels drive ATP production in the mitochondria.

In order to ensure that BT25 control GBM cells remodel their metabolism to promote OXPHOS when switched from GLUC (18 mM glucose) to GAL (18 mM GAL) media we utilized the Seahorse XFe96 analyzer from Agilent labs. When GBM cells were glucose starved and shifted to galactose as a carbon source, they exhibit an increased utilization of the OXPHOS metabolic pathways. This was observable from the decrease in extracellular acidification rate (ECAR) (Figure 6b) as well as the increase in basal mitochondrial oxygen consumption rate (OCR) (figure 6c). We observed that GBM control cells that were forced to rely on OXPHOS due to the GAL media exhibited fragmented mitochondria. This mitochondria fragmentation was observable at 3 hours and persisted through 12 hours of GAL treatment (Figure 7a). Importantly, this fragmentation was NIK and DRP1 dependent, as $NIK^{-/-}$ and $DRP1^{-/-}$ GBM cells did not demonstrate significant mitochondria fragmentation over the course of 12 hours (Figure 7b and 7c). In fact, in the case of the $NIK^{-/-}$ GBM cells the mitochondria were significantly lengthened in GAL media compared to the corresponding GLUC condition (Figure 7b quantification). These results reveal that nutrient stress in GBM cells triggers NIK/DRP1-dependent mitochondria fission.

3.3 Forced reliance on OXPHOS increases mitochondrial accumulation of NIK.

Strikingly, we observed that forcing GBM cells to rely on mitochondrial metabolism by switching from glucose to galactose media increases accumulation of

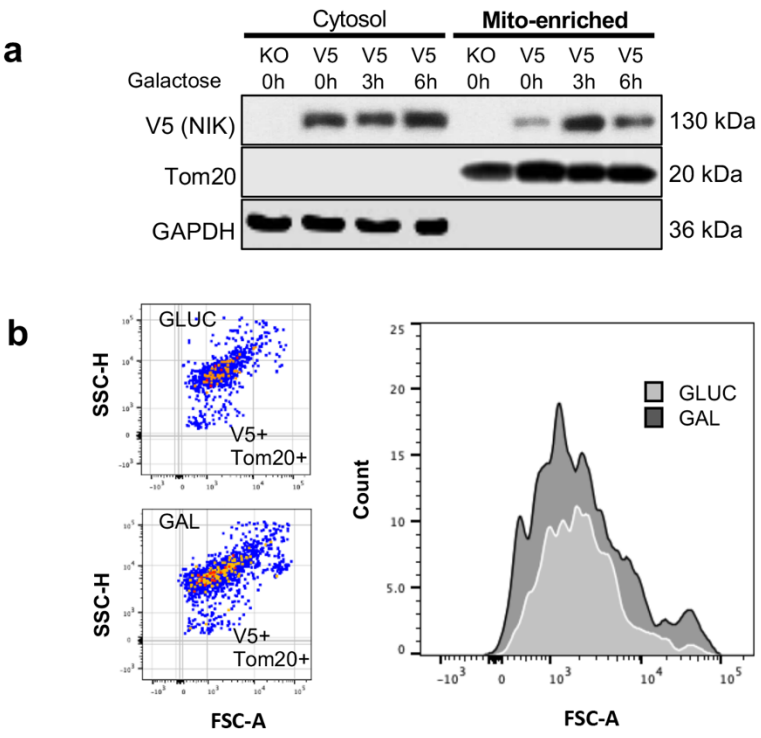

Figure 8. Forced reliance on OXPHOS triggers NIK accumulation at the mitochondria in GBM cells

a, Representative immunoblot analysis of cytosolic and mitochondrial subcellular fractions in BT25 NIK$^{-/-}$ cells reconstituted with NIK conjugated to V5 tag (NIK-V5) after metabolic switch from glucose to galactose media was performed with indicated antibodies. **b,** Representative single organelle flow cytometry analysis was performed on BT25 NIK-V5 cells cultured in 18mM glucose (top left) or 18mM galactose (bottom left) for 6 hours and immunostaining with mitochondrial Tom20 (AF488) and V5 (AF647). (Right) histogram demonstrating the increase in NIK-V5+ mitochondria upon switch to 18mM galactose media. Individual mitochondria analyzed for glucose conditions n=20,268 and individual mitochondria for galactose conditions, n=20,242.

NIK at mitochondria within 3 hours and persisted through 6 hours (Figure 8a). Single cell-organelle analysis of NIK$^{-/-}$ + mNIK GBM cells further revealed that NIK is recruited upon forced metabolic shift to OXPHOS (Figure 8b, histogram) by roughly 2-fold. Additionally, DRP1 levels decreased in the cytosol and increased in the mitochondria-enriched heavy membrane fraction at 3 hours in control GBM cells (Figure 8a). However, in cells lacking NIK the opposite trend was observed. At 3 hours

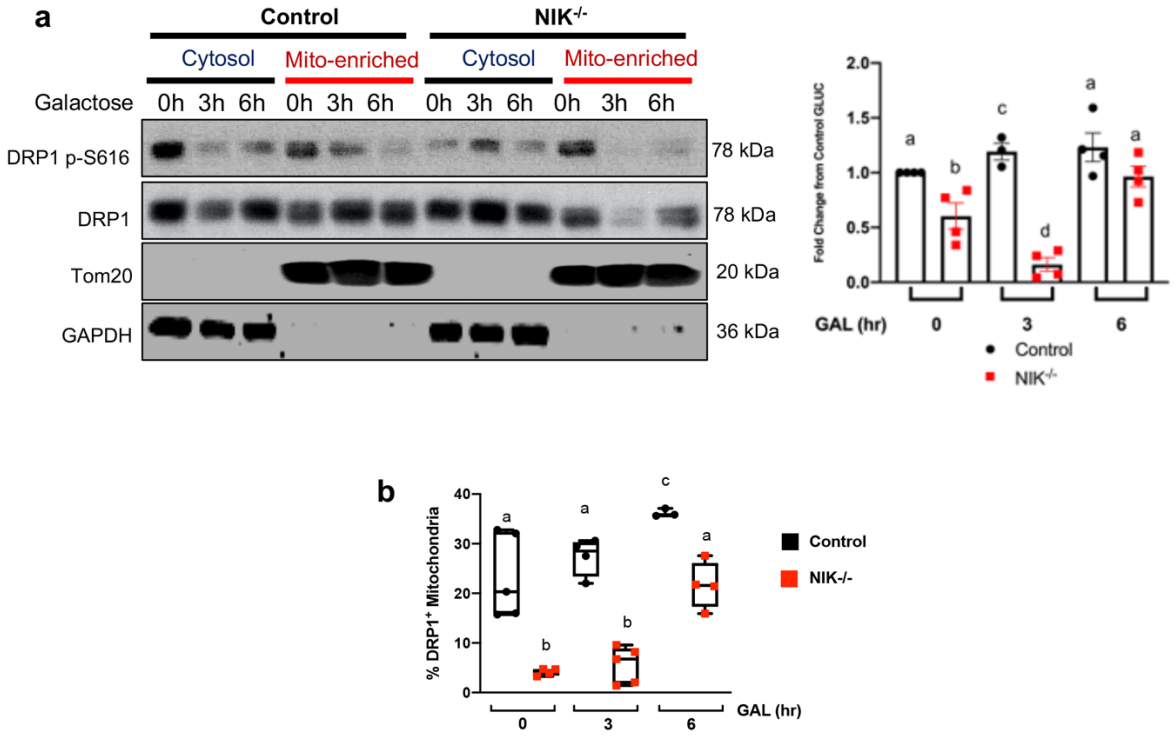

Figure 9. Forced shift toward OXPHOS triggers NIK-dependent DRP1 retention at mitochondria

a, Immunoblot analysis was performed with indicated antibodies using cytosolic and mitochondrial subcellular fractions from BT25 control and NIK$^{-/-}$ cells shifted from glucose to galactose at the indicated times (left). Quantification of n=3-4 independent biological replicates of total DRP1 western blot shown in (**b**). Individual student's t tests were performed between conditions. Different letters indicate statistically significant differences. "a v b," "a v c," "b v c" and "b v d" $p<.05$. "a v d" $p<.001$ and "c v d" $p<.0001$. **c,** Single organelle flow cytometry analysis of DRP1-AF488 recruitment at MitoSox™ Red+ mitochondria. Each cell/condition was compared to DRP1$^{-/-}$ as a negative control to determine level of mitochondria enrichment. Individual student's t tests were performed between conditions. Different letters indicate statistically significant differences. "a v b" and "b v c" $p<.0001$, "a v c" $p<.01$.

galactose, compared to 0 hours glucose (18 mM galactose) time point in NIK$^{-/-}$ GBM cells, DRP1 is strikingly absent from the mitochondria (Figure 9a). DRP1's inability to recruit at this 3-hour time point in NIK$^{-/-}$ GBM cells, combined with the finding that NIK

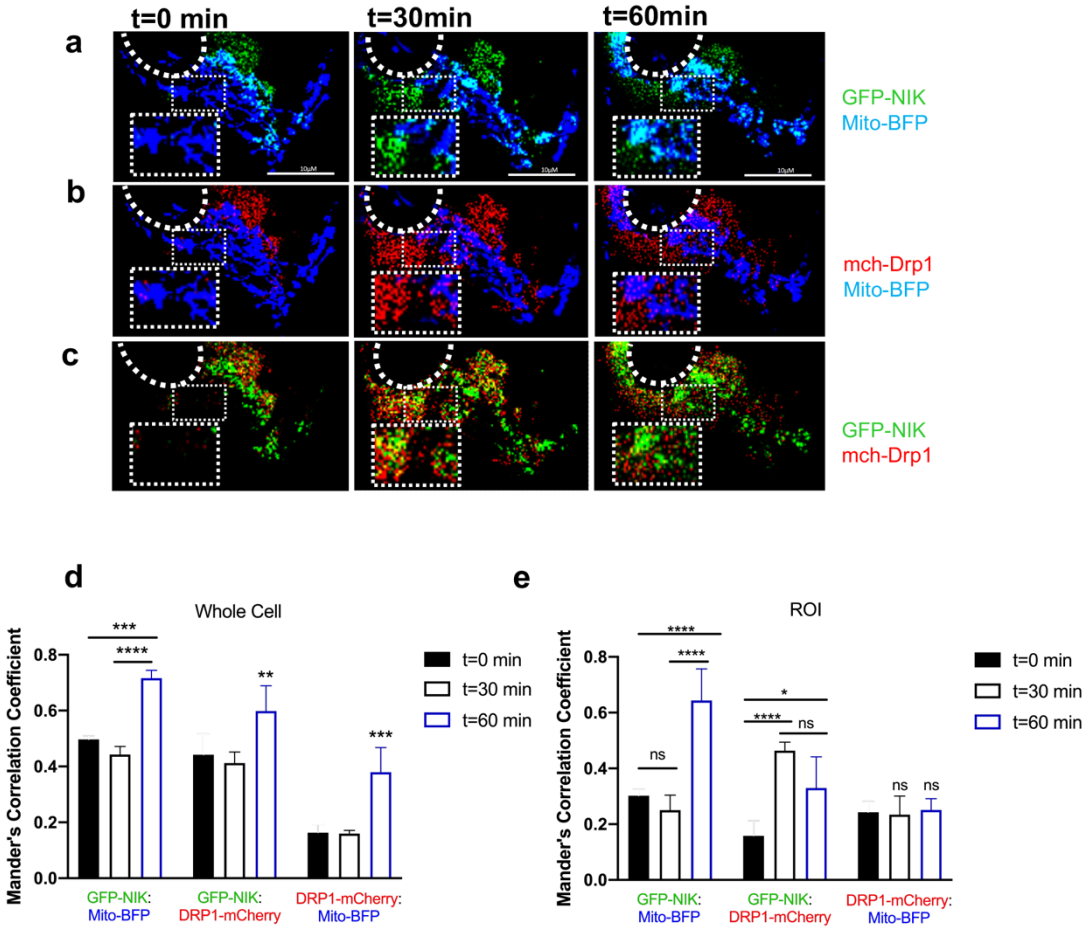

Figure 10. Metabolic shift to OXPHOS increases NIK and DRP1 recruitment in COS-7 cells

a-c, Representative live cell confocal imaging performed on COS-7 cells transfected with Mito-BFP, GFP-NIK, and mCherry-DRP1 (mchDrp1). Cells were imaged for an hour after a media switch that was absent of glucose and contained 25mM galactose. **d-e,** Mander's correlation coefficient (MOC) values for NIK (FITC) and mito-BFP (DAPI) (NIK:mitochondria), NIK (FITC) and DRP1(TRITC) (NIK:DRP1) and DRP1 (TRITC) and mito-BFP (DAPI) (DRP1:mitochondria) co-localization in the whole cell (d) and boxed ROI **(e).** Error bars indicate +/- SD of Mander's coefficient taken over 3 consecutive frames in image analyzed. Two-way ANOVA followed by Tukey post-hoc test ** indicates p<.01, *** indicates p<.001, **** indicates p<.0001.

recruitment peaks in 3 hours of nutrient stress, suggests that NIK is important maximal DRP1 recruitment and retention in GAL media. Single organelle analysis by flow cytometry confirmed that the percentage of DRP1 positive mitochondria in control, but

not NIK$^{-/-}$ GBM cells, increased upon switch from glucose to galactose media at 3 hours (Figure 9b). We further interrogated NIK and DRP1 accumulation at the mitochondria under forced metabolic switching to OXPHOS through the use of live cell confocal microscopy on COS-7 cells. We transfected COS7-cells with GFP-NIK, mito-BFP and mch-DRP1 and then shifted the cells form glucose to galactose. We found that NIK and DRP1 increased at the mitochondria over the course of an hour in galactose compared to glucose (Figure 10a-e). Taken together, these data demonstrate that glucose starvation and forced reliance on OXPHOS—even in the context of a noncancerous cell such as COS-7—induces mitochondria and NIK and DRP1 recruitment and NIK dependent DRP1 retention at the mitochondria.

3.4 NIK promotes cell survival by increasing mitochondrial spare respiratory capacity in response to metabolic shift to OXPHOS.

Our data suggests that NIK is important for the adaptive response of GBM cells to bioenergetic stress. In order to further interrogate NIK's role in mitochondria dynamics and metabolism, we utilized the Seahorse XFe96 Flux Analyzer to search for metabolic changes in GBM control and mutant cell lines in glucose and galactose media. Due to the widespread use of the Seahorse XFe96 Analyzer in this project, further discussion and introduction is warranted in regard to its use and how measurements are taken.

The Seahorse XF cell mitostress test utilizes three injections of mitochondria poisons to determine mitochondria ATP production, spare respiratory capacity, and

proton leak. First, measurements are made before injections of the mitochondria poisons. The oxygen consumption before injection of the first mitochondria poison, oligomycin, is termed basal respiration. Immediately following these measurements oligomycin—a complex V inhibitor—is injected and equilibrated with the cells. Since one mole of ATP is produced per mole of oxygen is consumed, mitochondria ATP production can be calculated by the drop in oxygen consumption from basal respiration to the oxygen consumption following addition of oligomycin.

Following the three measurements after addition of oligomycin, the ionophore FCCP is introduced to the GBM cells. FCCP permeabilizes the mitochondria membrane to protons and thereby disrupts the mitochondria membrane potential. The proton motive force, established by protons pumped into the inner membrane space by complexes I, III, and IV, is abolished. FCCP is also referred to as an uncoupler because it unlinks oxygen consumption from ATP production. As a response to FCCP, cells utilize as much oxygen as they can in a futile effort to reestablish the proton gradient. The difference between the basal respiration rate and the maximal respiration following FCCP is termed spare respiratory capacity (SRC). SRC is a measurement of how much ability to consume oxygen in case metabolic conditions demand it.

After these maximal respiration measurements are taken, a cocktail of rotenone and antimycin A are added which in effect completely shuts down mitochondria oxygen consumption. The difference in oxygen consumption immediately following oligomycin addition (complex V poisoning) and oxygen consumption after addition of rotenone/antimycin A is termed proton leak. It is a measurement of how efficiently the

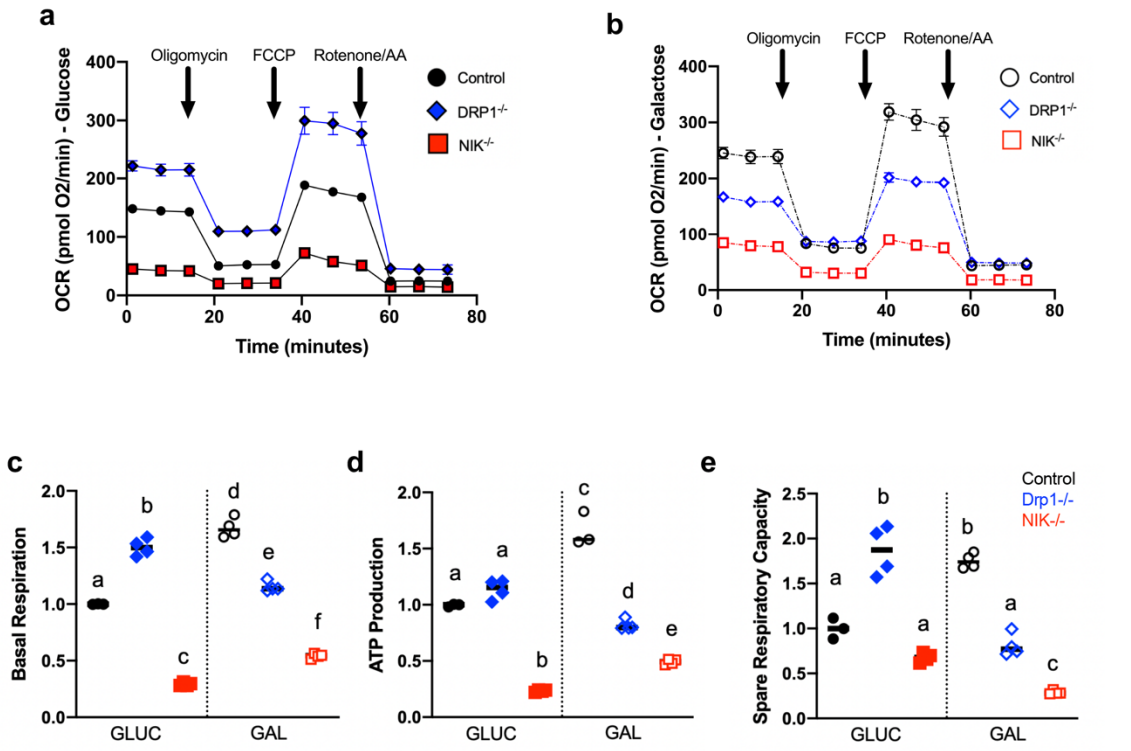

Figure 11. NIK increases mitochondrial spare respiratory capacity in response to forced reliance on OXPHOS

a-b, Oxygen Consumption Rate (OCR) was measured using the Seahorse Mito Stress test with Control cells (See Figure 2c), DRP1$^{-/-}$ and NIK$^{-/-}$ cells that were cultured in a, 18mM glucose (GLUC), or b, 18mM galactose (GAL) media. Data shown are the mean ± SD of ≥ 3 replicates for each cell type in each condition and are representative of at least 3 independent experiments. OCR values were normalized to cellular DNA content (DRAQ5 relative fluorescence units (RFUs)). **c-e**, Individual mitochondrial function parameters were calculated from the data shown in (**a**) and (**b**) and shown as fold change compared to control cells in GLUC. Data for control cells was taken from Fig 2c. **c,** Basal respiration. Different letters indicate statistical significance using One-Way ANOVA with Tukey post hoc test. All comparisons have $p<0.0001$ except "a vs. f" ($p=0.0169$) and "c vs. d" ($p=0.035$). **d,** ATP production. All statistical comparisons have $p<0.0001$ except "a vs d" ($p<.05$), "b vs e" ($p=.0009$). **e,** Spare respiratory capacity. All statistical comparisons have $p<0.0001$ except "a vs c" ($p<.05$).

mitochondria are utilizing oxygen to produce ATP. However, while proton leak is of critical importance to adipocyte function it is not widely discussed in terms of GBM metabolism and is not addressed further in this report.

In both 18 mM glucose and 18 mM galactose media, NIK$^{-/-}$ GBM cells

demonstrated impaired mitochondria metabolism. Basal respiration, mitochondrial ATP production, and as spare respiratory capacity were all impaired compared to control GBM cells in high glucose (18 mM) and galactose media (Figure 11a-e). DRP1$^{-/-}$ GBM cells, however, demonstrate significantly increased basal respiration and spare respiratory capacity compared to control GBM cells in high glucose (18 mM) media.

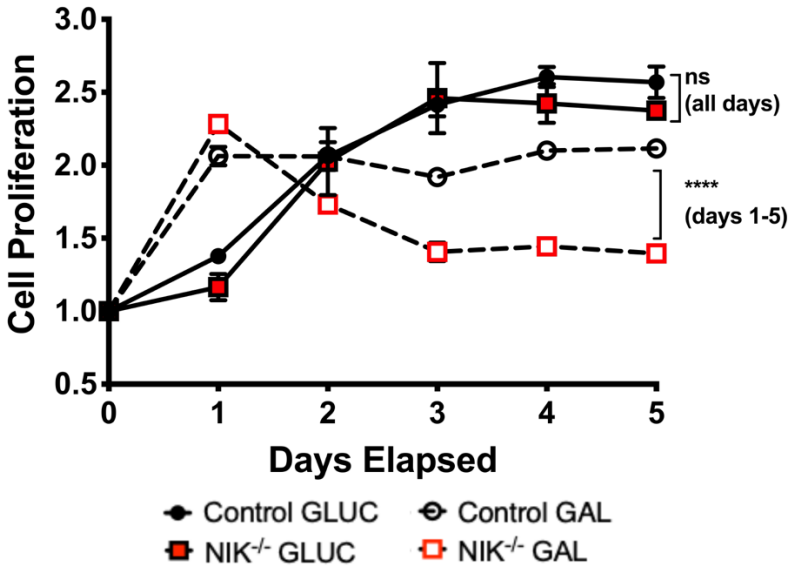

Figure 12. NIK promotes GBM cell survival in OXPHOS-promoting (GAL) media

Above: Representative MTS Proliferation assay. Control and NIK-/- cells were cultured in GLUC or GAL for the indicated times. Proliferation is represented as fold change compared to Day 0. Data are representative of 3 different experiments and are shown as mean ± SD (n=3) with Two-Way ANOVA followed by Tukey post-hoc test (****p<.0001).

This finding is consistent with other studies showing a link between mitochondria fusion and OXPHOS (Yao et al., 2019). However, in glucose starved media (18 mM galactose) DRP1$^{-/-}$ GBM cells—like NIK$^{-/-}$ GBM cells—exhibit impaired basal respiration, ATP

production, and spare respiratory capacity when compared to control GBM cells in galactose media (Figure 11b-e). This suggests that these GBM mutants are utterly lacking in metabolic reserves to cope with the bioenergetic stress associated with being cultured in glucose restricted (18 mM galactose) media. Indeed, it is the case that when NIK$^{-/-}$ GBM cells are switched from high glucose to galactose media their proliferation is significantly impaired compared to control cells. However, there is no significant

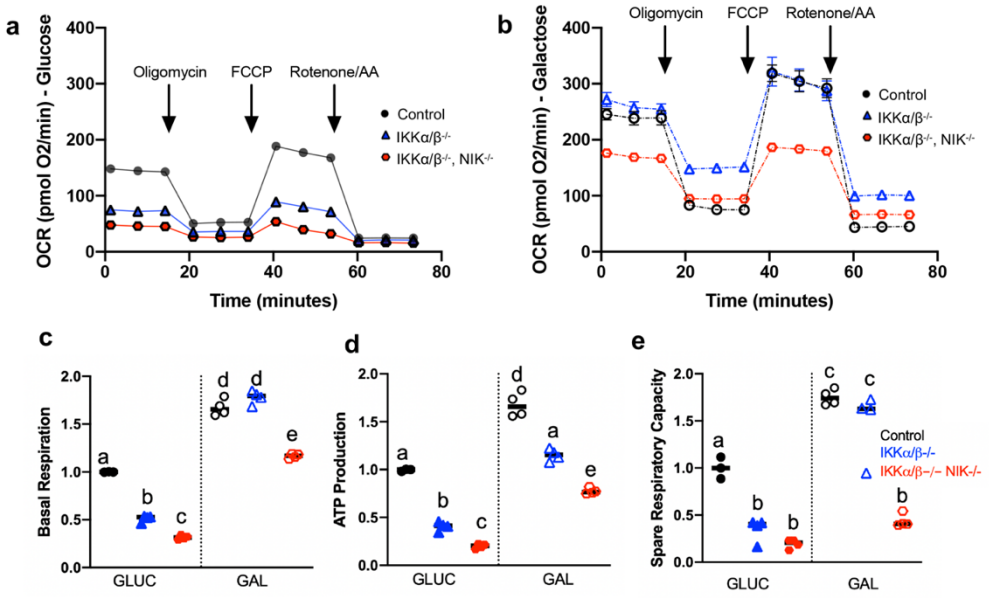

Figure 13. NIK regulation of mitochondrial metabolism is independent of IKK
a-b, Oxygen Consumption Rate (OCR) was measured using the Seahorse Mito Stress test with Control cells (see Figures 2b and 4a-b), IKKα/β$^{-/-}$ cells and IKKα/β$^{-/-}$, NIK$^{-/-}$ lines that were cultured in 18mM glucose (GLUC) (**a**) or 18mM galactose (GAL) media (**b**). Data shown are the mean± SD of ≥ 3 replicates for each cell type in each condition and are representative of at least 3 independent experiments. OCR values were normalized to cellular DNA content (DRAQ5 relative fluorescence units (RFUs)). **c-e,** Individual mitochondrial function parameters were calculated from the data shown in (**a**) and (**b**) and shown as fold change compared to control cells in GLUC. Data for control cells was taken from Fig 2c. **c,** Basal respiration. Different letters indicate statistical significance using One-Way ANOVA with Tukey post hoc test. All comparisons have p<0.0001 except "a vs e" (p=.0058), "b vs c" (p=.0005). **d**, ATP production. All statistical comparisons have p<0.0001 except "a vs e" (p<.01), and "b vs c" (p=.0040). **e,** Spare respiratory capacity. All statistical comparisons have p<0.0001 except "a vs b" (p=<.01), "a vs c" (p=<.05).

difference in proliferation between control and NIK$^{-/-}$ GBM cells in high glucose (Figure 12).

3.5 NIK regulation of mitochondrial oxidative metabolism and cell survival is independent of IKK and NF-κB.

Although NIK is well established as a positive regulator of the inhibitor of kB kinase (IKK) complex, which is required for activation of NF-κB signaling, IKK-independent functions for NIK have also been described. We next wished to deduce whether the metabolic effects of NIK that we observed were dependent or independent of IKK. We developed GBM cells the lacked IKKα and IKKβ (IKKαβ$^{-/-}$) as well as cells that lacked IKKα, IKKβ and NIK (IKKα/β$^{-/-}$ NIK$^{-/-}$) and returned to the Seahorse XF96e Flux Analyzer to monitor metabolic changes in these mutant cell lines.

Our results revealed that while both IKKαβ$^{-/-}$ and IKKα/β$^{-/-}$ NIK$^{-/-}$ GBM mutants exhibited decreased basal respiration, mitochondria ATP production, and spare respiratory capacity in high glucose media compared to control GBM cells (Figure 13a, c-e). However, IKKαβ$^{-/-}$ but not IKKα/β$^{-/-}$ NIK$^{-/-}$ GBM cells were able to remodel their metabolism when shifted to galactose media. IKKαβ$^{-/-}$ GBM cells were impaired in ATP production but not basal respiration or spare respiratory capacity compared to their control counterparts in galactose media (Figure 13b-e). Unlike the IKKαβ$^{-/-}$ double knockout GBM cells, IKKα/β$^{-/-}$ NIK$^{-/-}$ triple knockout GBM cells could not increase

basal respiration, mitochondria ATP production, or spare respiratory capacity when transitioned to galactose (Figure 13b-e).

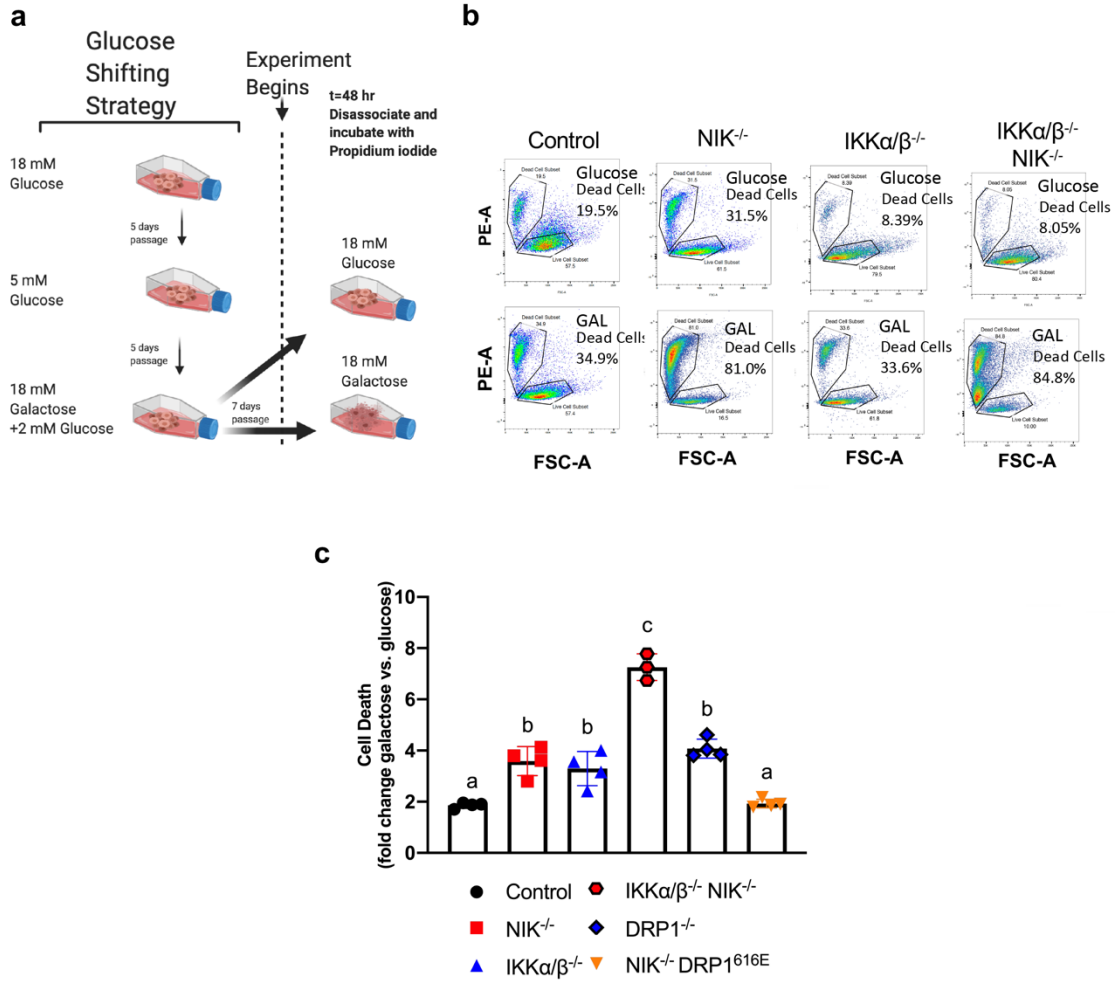

Figure 14. NIK regulation of cell survival upon shift to OXPHOS metabolism is independent of IKK and is restored by addition of active DRP1-S616E phosphomimetic

a, Schematic demonstrating the strategy employed to shift GBM cells to galactose media. The cells utilized for GLUC and GAL cell death data each come from the same flask 18 mM galactose + 2 mM glucose before propidium iodide staining and flow cytometry analysis. **b,** Representative Flow cytometry analysis of cell death using propidium iodide staining. Indicated BT25 GBM cells were grown for 48 hours in either 18 mM glucose (upper panels) or galactose media (lower panels). **c,** Fold change in cell death induced by shifting from GLUC to galactose media for 48 hours (% dead cells in galactose/%dead cells glucose). Different letters indicate statistical significance using One-Way ANOVA with Tukey post hoc test. For all comparisons $p<.01$. n=3-4 independent experiments, n ≥ 10,000 cells per condition. Error bars indicate mean +/- SD.

We next investigated whether NIK promoted cell survival in response to shifting cells from high glucose (18 mM) to glucose depleted media (18 mM galactose). Cells were gradually shifted from high glucose to galactose media over the course of several weeks before introducing the cells back to high glucose or galactose media for 48 hours (Figure 14a). At the 48-hour time point, cells were disassociated, stained with propidium iodide, and analyzed by flow cytometry (Figure 10a). Interestingly, when we used this strategy with control, $NIK^{-/-}$, $IKK\alpha\beta^{-/-}$, $IKK\alpha/\beta^{-/-}$ $NIK^{-/-}$ GBM cells we noted that $NIK^{-/-}$ and $IKK\alpha\beta^{-/-}$ cells exhibited more cell death in galactose than control GBM cells. Critically, we observed that $IKK\alpha/\beta^{-/-}$ $NIK^{-/-}$ GBM cells exhibited an additive cell death effect which was greater than $IKK\alpha/\beta^{-/-}$ or $NIK^{-/-}$ mutants alone (Figure 14b-c).

We built upon our observation of impaired mitochondria fission upon switch to galactose media by looking at cell death in DRP1 mutant constructs. We found that $DRP1^{-/-}$ GBM cells were similarly inept at withstanding metabolic stress as the $NIK^{-/-}$ GBM cells. To see if DRP1 could rescue the NIK-dependent protection from glucose-deprivation induced cell death, we performed gain-of function studies using a DRP1 mutant with a serine 616 glutamic acid (S616E) substitution in the absence of NIK. This construct mimics DRP1 phosphorylation and drives mitochondria fission. We found that overexpression of this constitutively active DRP1-S616E phosphomimetic in a $NIK^{-/-}$ GBM background restored glucose deprivation-induced cell death to levels comparable to control GBM cells (Figure 14c).

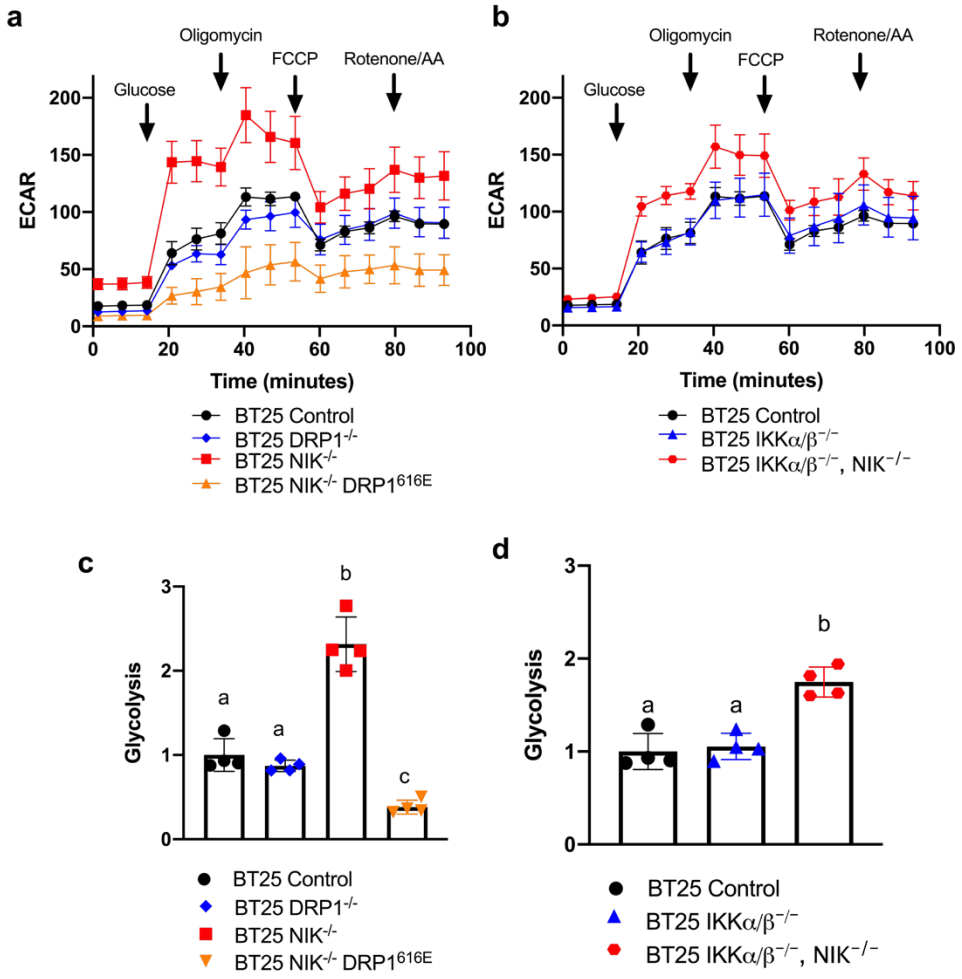

Figure 15. NIK depletion rewires GBM cells toward glycolysis independent of IKK.

a-b, ECAR measurements in BT25 cell lines for Seahorse glycolysis stress. Glycolysis is measured as the difference in basal ECAR in glucose free media from the peak ECAR immediately following 5 mM glucose injection. **c-d,** Representative graphs of glycolysis measurements for BT25 Control, DRP1$^{-/-}$, NIK$^{-/-}$, NIK$^{-/-}$ DRP1616E (**c**) and BT25 Control, IKKα/β$^{-/-}$, IKKα/β$^{-/-}$, NIK$^{-/-}$ cell lines (**d**). One-way ANOVA followed by Tukey-post hoc analysis. Different letters indicate statistical significance. a vs b $p<.0001$, a vs c $p<.001$, b vs c, $p<.0001$.

Seahorse XFe96 glycolytic stress test revealed that NIK depletion in GBM cells also resulted in an upregulation in glycolysis (Figure 15a-d). This increase in ECAR in

$NIK^{-/-}$ GBM cells upon injection with 5 mM glucose may have been in order to compensate for diminished mitochondria ATP production. It is also apparent that this upregulation in glycolysis, similar the impairments in mitochondria metabolism we observed, is independent of IKK. $IKK\alpha/\beta^{-/-}$ GBM cells do not exhibit upregulation of ECAR. Only when NIK was depleted in an $IKK\alpha/\beta^{-/-}$ GBM cell line ($IKK\alpha/\beta^{-/-}$ $NIK^{-/-}$) did ECAR significantly increase compared to control GBM cells (Figure 15 b and d). While DRP1 knockout did not significantly change ECAR levels, active phosphomimetic DRP1-S616E over expression in $NIK^{-/-}$ BT25 GBM cells reduced glycolysis to levels below the control GBM cell line (Figure 15a and c).

Collectively, these data suggest that NIK does have independent functions from IKK in protection from cell death in response to metabolic stress and that constitutively active DRP1 can respond to this metabolic stress even in the absence of NIK.

3.6 Constitutively active DRP1 rescues oxidative metabolism and tumorigenic potential in NIK-/- GBM cells.

To examine whether Drp1 could rescue the metabolic and tumorigenic potential in the absence of NIK, we returned again to the Seahorse XFe96 analyzer to analyze $NIK^{-/-}$ GBM cells stably overexpressing DRP1-S616E, as well as the corresponding inactive DRP1-S616A substitution, which is not phosphorylated and inhibits fission. We found basal respiration was restored in $NIK^{-/-}$ DRP1-S616E, but not $NIK^{-/-}$ DRP1-S616A

GBM cells to levels observed in control cells in both high glucose (18 mM) and OXPHOS-promoting media (18 mM galactose) (Figure 16a-b). Furthermore, while ATP

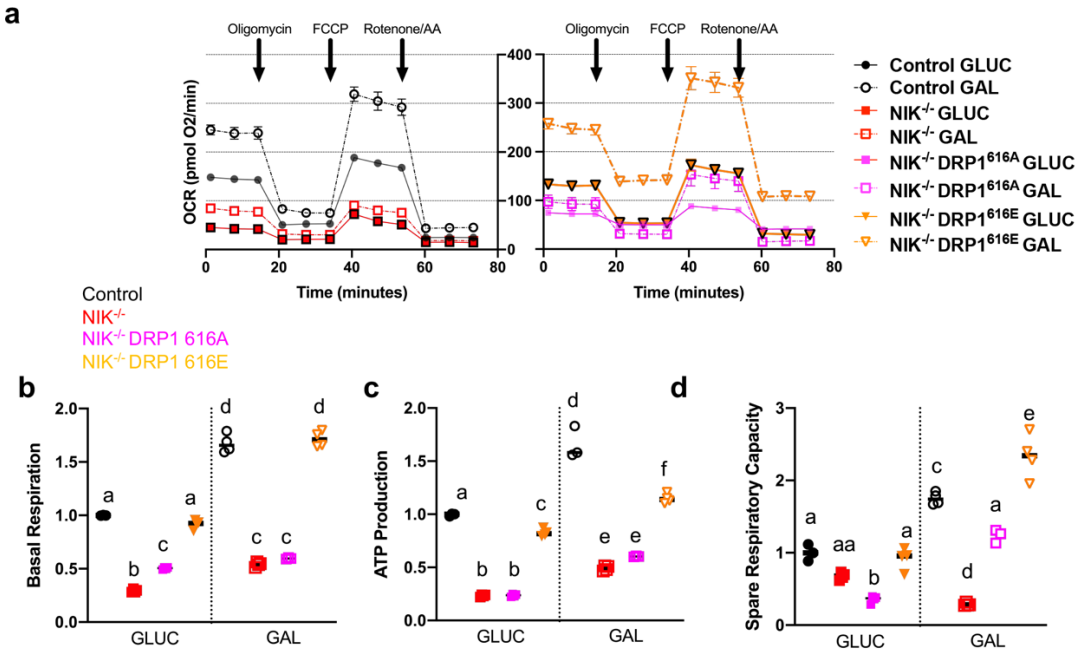

Figure 16. Constitutively active DRP1-S616E restores oxidative metabolism of NIK-deficient GBM cells.
a, Oxygen Consumption Rate was determined using the Seahorse Mito Stress test with Control and NIK$^{-/-}$ cells (see Figs. 7, 9), as well as NIK$^{-/-}$ cells ectopically expressing DRP1-616E that were cultured in 18mM glucose (GLUC) or 18mM galactose (GAL) media. Data depict the mean of ≥ 3 replicates per each cell type. **b-d,** Individual mitochondrial function parameters were calculated from the data shown in (**a**) and shown as fold change compared to control cells in GLUC. **b**, Basal respiration. Different letters indicate statistical significance using One-Way ANOVA with Tukey post hoc test. All comparisons have $p<0.0001$. **c,** ATP production. All statistical comparisons have $p<0.0001$ except "a vs f" ($p<.001$). **d,** Spare respiratory capacity. All statistical comparisons have $p<0.0001$ except "a vs aa" (ns), "aa vs b" ($p<.001$), "aa vs d" ($p<.05$) "a vs c" ($p<.001$), and "c vs e" ($p<.001$).

was slightly lowered in NIK$^{-/-}$ DRP1-S616E cells compared to control GBM cells, the ATP production was significantly higher than NIK$^{-/-}$ and NIK$^{-/-}$ DRP1-S616A cells in both glucose and galactose media (Figure 16a-d). Spare respiratory capacity was restored in NIK$^{-/-}$ DRP1-S616E cells to comparable levels seen in the control in glucose media (GLUC) and surpassed levels observed in control GBM cells in 18 mM galactose

media (Figure 16d). GBM cells deficient in NIK but overexpressing the DRP1-S616A inactive phosphomimetic construct exhibited decreased spare respiratory capacity in both high glucose (18 mM) and galactose media compared to their control counterparts (Figure 16d).

However, while spare respiratory capacity in NIK$^{-/-}$ DRP1-S616A cells was lower than NIK$^{-/-}$ GBM cells in high glucose, NIK-deficient GBM cells overexpressing the inactive phosphomimetic construct were able to increase their spare respiratory capacity compared to NIK$^{-/-}$ GBM cells in galactose. We did not uncover why exactly

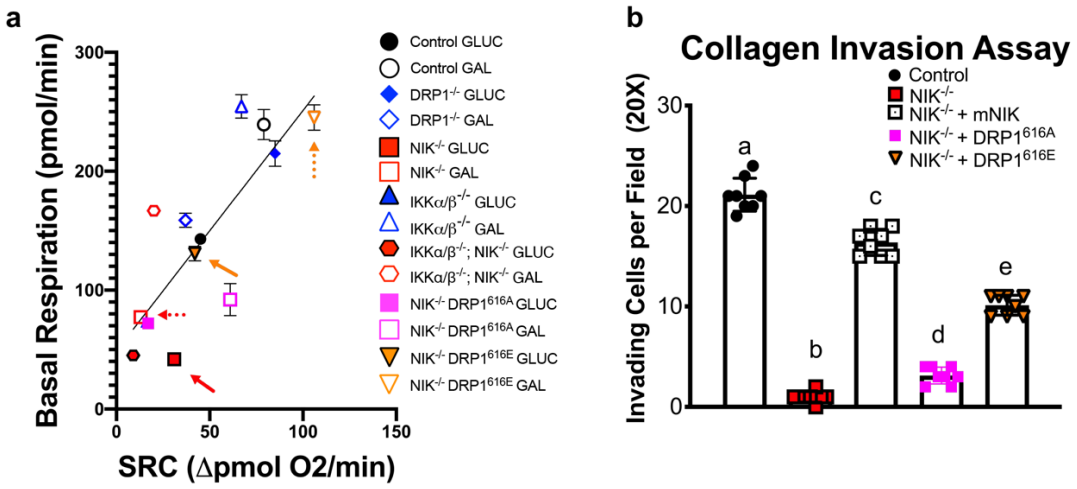

Figure 17. Constitutively active DRP1 rescues oxidative metabolism and invasion of NIK-deficient GBM cells.
a, Composite graph plotting basal respiration vs mean spare respiratory capacity (SRC) (n ≥ 3 replicates per each cell type). Solid arrows indicate glucose condition and dotted arrows indicate galactose condition for NIK$^{-/-}$ and NIK$^{-/-}$ DRP1^{616E} cell lines (red and orange respectively). **b,** Three-dimensional collagen invasion assay with indicated cell lines (mNIK indicates murine NIK), n=8 replicates. p<.0001 between all conditions a-e. Significance was determined by One-Way ANOVA followed by Tukey post hoc analysis.

the inactive phosphomimetic was able to increase SRC. However, it may be that the simple act of introducing more DRP1 to the cell was able to promote some minimal

DRP1 activity through other regulatory mechanisms aside from phosphorylation on S616 (Figueroa-Romero et al., 2009).

To gain an overall assessment of the oxidative metabolism and metabolic fitness across all the NIK$^{-/-}$, IKKα/β$^{-/-}$, and DRP1$^{-/-}$ mutants cell lines, we plotted the relationship between SRC and OCR. This analysis demonstrated that NIK$^{-/-}$, IKKα/β$^{-/-}$, and IKKα/β$^{-/-}$ NIK$^{-/-}$ triple knockout cells cultured in glucose and NIK$^{-/-}$ in galactose are least oxidative and have the least spare respiratory capacity. This is in contrast with DRP1$^{-/-}$ cells in glucose as well as control, IKKαβ$^{-/-}$, and NIK$^{-/-}$ +DRP1-S616E cells cultured in galactose, are the most oxidative and possessed the highest spare respiratory capacity (Figure 17a).

We next wished to determine whether forced activation of DRP1 could rescue the invasion defects that were previously characterized in NIK-deficient cancers. Three-dimensional (3D) collagen invasion assays clearly demonstrate that NIK was critical for GBM tumor invasion—as previously described. Strikingly, 3D collagen invasion assays also revealed that DRP1-S616E overexpression in NIK-deficient GBM cells were able to increase invasion compared to NIK$^{-/-}$ cells. Overexpression of DRP1-S616A in NIK$^{-/-}$ GBM cells, increased invasion compared to NIK$^{-/-}$ cells—similar to how NIK$^{-/-}$ DRP1-S616A GBM exhibited higher SRC compared to their NIK$^{-/-}$ parental cell line. However, the number of invading cells observed in NIK$^{-/-}$ DRP1-S616A is significantly reduced compared to the NIK$^{-/-}$ DRP1-S616E cell line (Figure 17b).

Next, we tested whether our findings in our *in vitro* 3D collagen invasion assays were translatable *in vivo*. To achieve this, we utilized an orthotopic xenograft model in which one million BT25 control, NIK$^{-/-}$, DRP1$^{-/-}$, NIK$^{-/-}$ +mNIK, NIK$^{-/-}$ DRP1-S616A, and NIK$^{-/-}$ DRP1-S616E cells stably expressing luciferase were implanted into the brains of CD1 null mice. We took weekly luminescence measurements to monitor the growth of the control and mutant constructs (Figure 18). While control GBM cells grew and formed tumors over the course of 28 days, NIK$^{-/-}$ and DRP1$^{-/-}$ cells regressed from their initial injection volume (Figure 19a) over the course of the first two weeks. From day 7

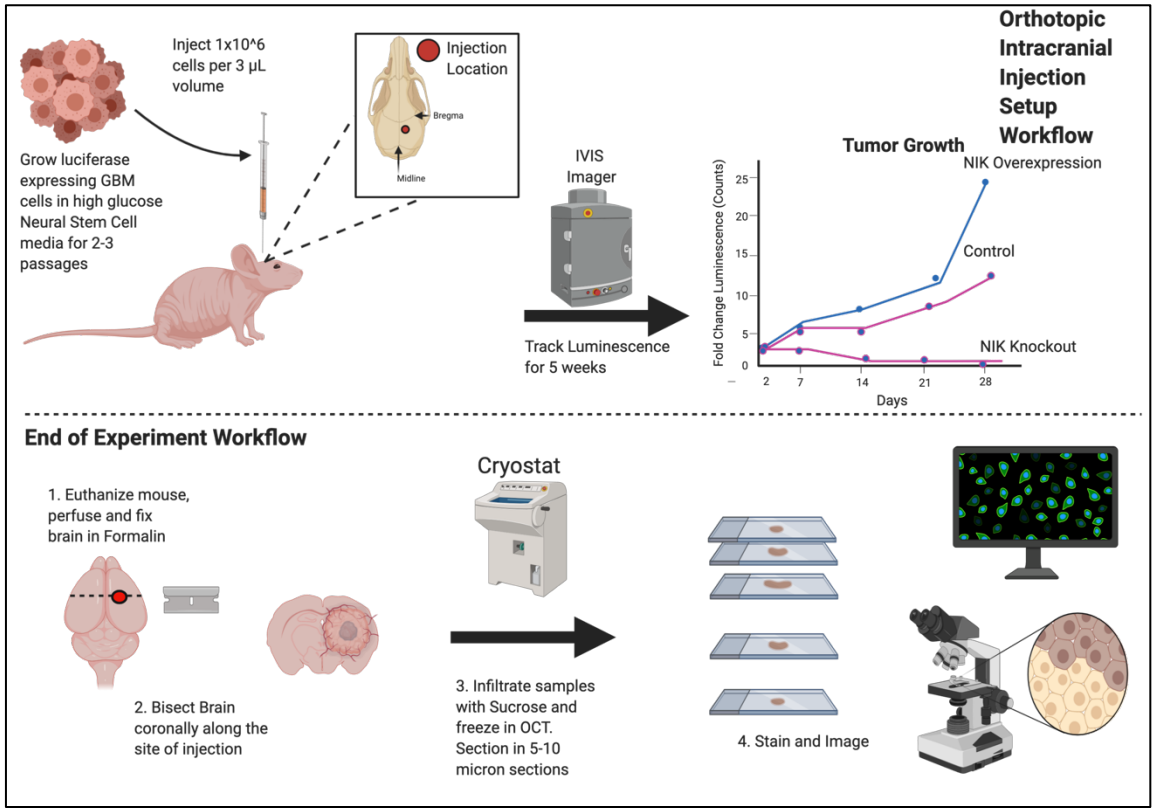

Figure 18. Workflow for orthotopic intracranial injections
Above: 1 x 10^6 GBM cells stably expressing luciferase were injected into CD1 null (nude) mice. Weekly luciferin injections were given to the mice and analyzed with the IVIS imager for 28 days (4 weeks). The mice were then euthanized, and their brains were fixed in 10% neutral buffered formalin, sectioned on cryostat, H&E stained and imaged.

onward, they demonstrated no observable growth (Figure 19b). Although no luminescence was detected in the NIK$^{-/-}$ injected mice after day 14 (Figure 19a), the histology for the brain tumors did reveal at least one cluster of NIK$^{-/-}$ tumor cells (Figure

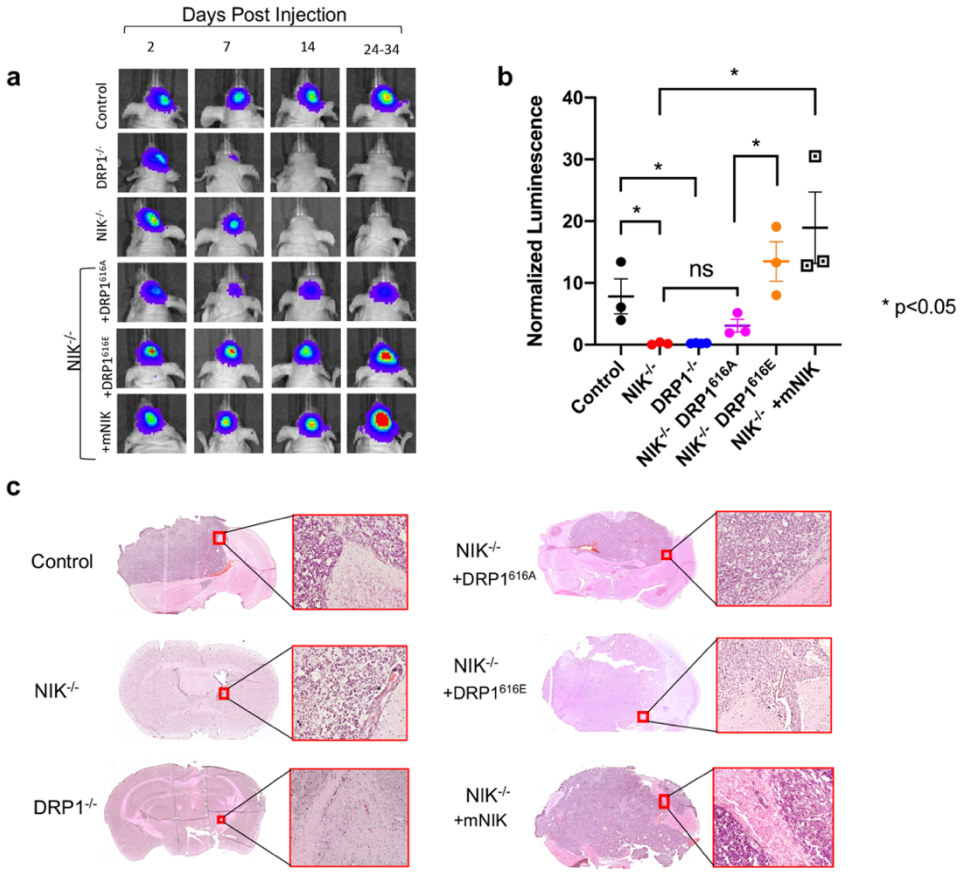

Figure 19. Constitutively active DRP1 restores tumorigenic potential in NIK-deficient GBM cells.

a, Representative cropped images from IVIS imaging showing luminescence of individual mice pictured here over the course of 35 days n ≥ 3 mice per cell type. Mice were imaged at regular intervals with the exception of the final endpoint since mice with large tumor growth required euthanasia at earlier timepoints. Mice harboring DRP1$^{-/-}$, NIK$^{-/-}$, and NIK$^{-/-}$ +DRP1^{616A} tumors were last imaged at day 35 and mice harboring NIK$^{-/-}$ +DRP1^{616E} and NIK$^{-/-}$ +DRP1^{616E} +mNIK tumors were last imaged at days 28 and 24, respectively. **b**, Graph depicting fold change luminescence on day 28 from fold change on day 7, with the exception of NIK$^{-/-}$ + mNIK which is fold change from day 21. **c,** Representative images of tumors and histology (pictured as enlargements of red box inset) in Control, NIK$^{-/-}$, DRP1$^{-/-}$, NIK$^{-/-}$ DRP1^{616A}, NIK$^{-/-}$ DRP1^{616E} and NIK$^{-/-}$ + mNIK.

19c). However, no tumor cells were detected in the histology for the DRP1$^{-/-}$ GBM-injected mice.

Mice injected with NIK$^{-/-}$ cells stably expressing murine NIK exhibited rapid tumor growth compared to control GBM cells—highlighting the importance of NIK to GBM tumorigenesis (Figure 13b-c). Strikingly, NIK$^{-/-}$ cells expressing DRP1-S616E but not S616A exhibited levels of tumor growth comparable to control GBM cells (Figure 19b-c). Taken together, these data highlight the importance of mitochondria fission to GBM growth and invasion and demonstrate NIK has important IKK independent roles in GBM metabolism that can be restored with constitutively active DRP1.

IV. RESULTS: PART II

4.1 Reactive oxygen species trigger NIK recruitment to the mitochondria

While we present strong data that demonstrates NIK moves to the mitochondria upon switch to OXPHOS-promoting (GAL) media, we cannot yet fully pinpoint the

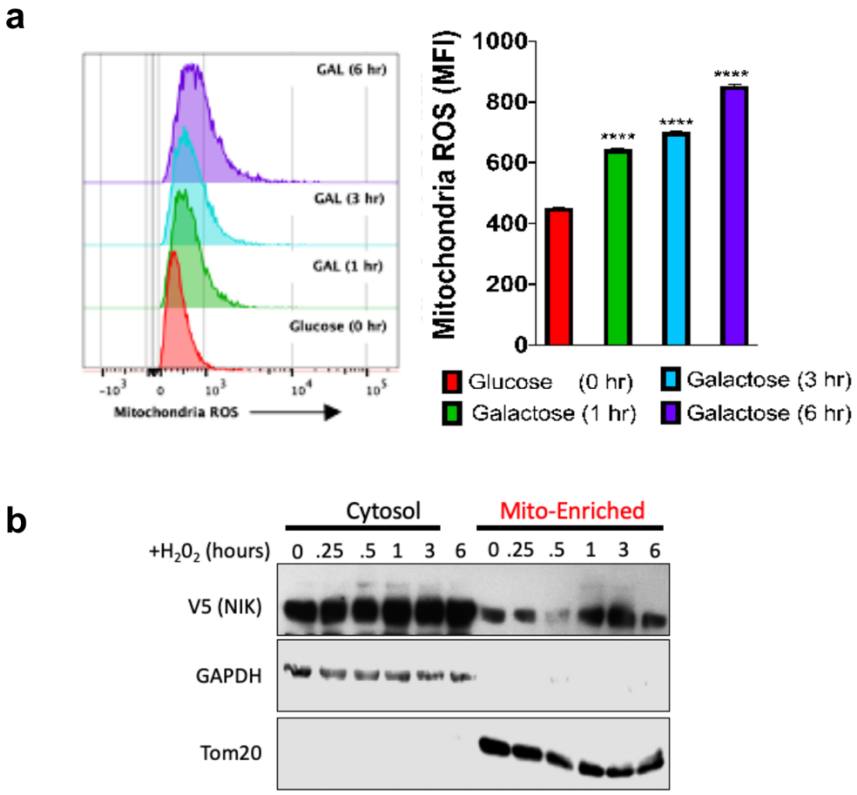

Figure 20. NIK accumulates at the mitochondria in response to exogenous ROS. **a,** Mitosox™ flow cytometry measurements of BT25 control GBM cells showing the increase in mitochondria superoxide upon the switch from glucose to galactose media over six hours. Statistics calculated based on MFI values +/- CV. One-way ANOVA followed by Tukey post-hoc analysis. $p<.0001$ for all comparisons, n=10,000 cells per condition. **b,** Representative immunoblot demonstrating NIK accumulation at the mitochondria upon addition of 250 µM H_2O_2 over the course of six hours.

exact trigger for this recruitment. This ambiguity the exact recruitment trigger is due to the fact that multiple cell stress/survival pathways are activated accompanying the forced

reliance on OXPHOS. Indeed, mitochondria superoxide production (Figure 20a), ER stress, and autophagy are all induced in glucose depleted (18 mM galactose) media.

Mitosox Red™, a superoxide specific dye that accumulates in the mitochondria matrix, was incubated with BT25 control cells in glucose and galactose for 1 hour, 3 hours, and 6 hours. This experiment revealed that GBM cells exhibit increased mitochondria ROS production over the course of our recruitment experiments (Figure 24a). Furthermore, NIK does indeed respond to exogenous ROS and is recruited to the mitochondria upon addition of H_2O_2 to the media (Figure 20b). The link between

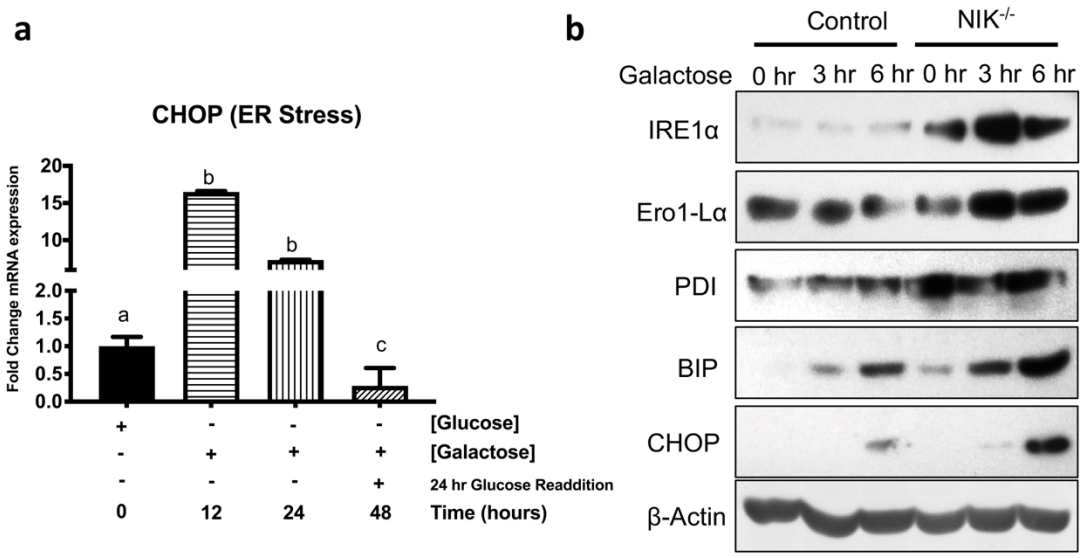

Figure 21. ER stress response is upregulated by glucose deprivation and increased in NIK$^{-/-}$ GBM cells
a, Representative RT-PCR demonstrating CHOP induction in BT25 GBM cells in 0, 12, and 24 hours 18 mM galactose and 24 hours 18 mM galactose + 24 hours 18 mM glucose media. **b,** Representative Immunoblot of ER stress/UPR pathway in BT25 control and NIK$^{-/-}$ cells with indicated antibodies.

mitochondria superoxide production in galactose media as well NIK recruitment to the mitochondria with exogenous ROS suggests that the two phenomena may be linked. However, future research into the mitochondria localization of NIK in response to

reactive oxygen species should look at a variety of types of ROS stimuli to determine if NIK responds to certain reactive oxygen species and not others.

4.2 Forced switch to OXPHOS is associated with ER stress

Additional stressors are interwoven with use of galactose media. C/EBP homologous protein (CHOP), a critical signaling transcription factor to respond to ER stress is increased upon glucose deprivation (18 mM galactose media) and is reversible by addition of glucose (Figure 21a). The principle reason for this increase in ER stress is that when glucose is unavailable in the cell, proteins can no longer be sufficiently glycosylated and the proteins misfold (Palorini et al., 2013). ER chaperones—such as BiP—are required to help stabilize these proteins. If the UPR is not alleviated in a given time, CHOP will eventually trigger apoptosis (Hu et al., 2018). We have found that under the same conditions and time points that trigger NIK recruitment to the mitochondria, ER stress is also increasing (Figure 21 a-b).

IRE1α is a transmembrane ER protein where it can act as a sensor for unfolded proteins. When activated through the UPR, IRE1α carries out RNA splicing and removes an intron from X-box binding protein 1 (XBP1) (Adams et al., 2019). Once the intron is removed it can be translated. XBP1 then upregulate ER chaperones, such as BiP (Chen et al., 2017), and endoplasmic reticulum associated degradation (ERAD) genes that alleviate the ER stress(Lee et al., 2003). Ero1-like protein alpha (Ero1-Lα) and protein-disulfide isomerase (PDI) work together through redox reactions to add disulfide bonds to proteins in the ER (Benham et al., 2013). If disulfide bonds fail to

form, proteins will become destabilized and the UPR will activate. If all safeguards for the unfolded protein response fails, CHOP will be upregulated several signaling pathways including XBP1—and will then lead to ER-induced mitochondria-dependent apoptosis pathway.

All of these proteins are of critical importance to the UPR pathway and all are upregulated in $NIK^{-/-}$ GBM cells compared to control (Figure 25b). The upregulation of UPR sensors such as IRE1 alpha may suggest increased sensitivity to unfolded proteins. This is supported by the increased expression in BiP—even in 18 mM glucose (0 hr GAL)—and the increase in CHOP expression at 3 hours GAL compared to control (Figure 25b). It may be the case, given the close and often intertwined relationship between the ER and mitochondria, that some portion of NIK may also move to the ER to dampen the stress response pathway, as to not overly sensitize the cells to ER-induced apoptosis. It also is plausible that NIK may be strictly mitochondria bound and can dampen the mitochondria-dependent apoptosis triggered by the ER by some means. Investigations into NIK's potential involvement in ER stress should be pursued.

4.3 pAMPK T172 is chronically elevated in $NIK^{-/-}$ GBM cells and $NIK^{-/-}$ mice and addition of amino acids alleviates this hyperactivation

Recent studies into AMPK have shown that it is of critical importance to cancer progression through the upregulation of and upregulation of catabolic pathways such as fatty acid oxidation (Eichner et al., 2019). AMPK's activity is inversely related to nutrient abundance. Under fed conditions, the gamma subunit of AMPK sterically

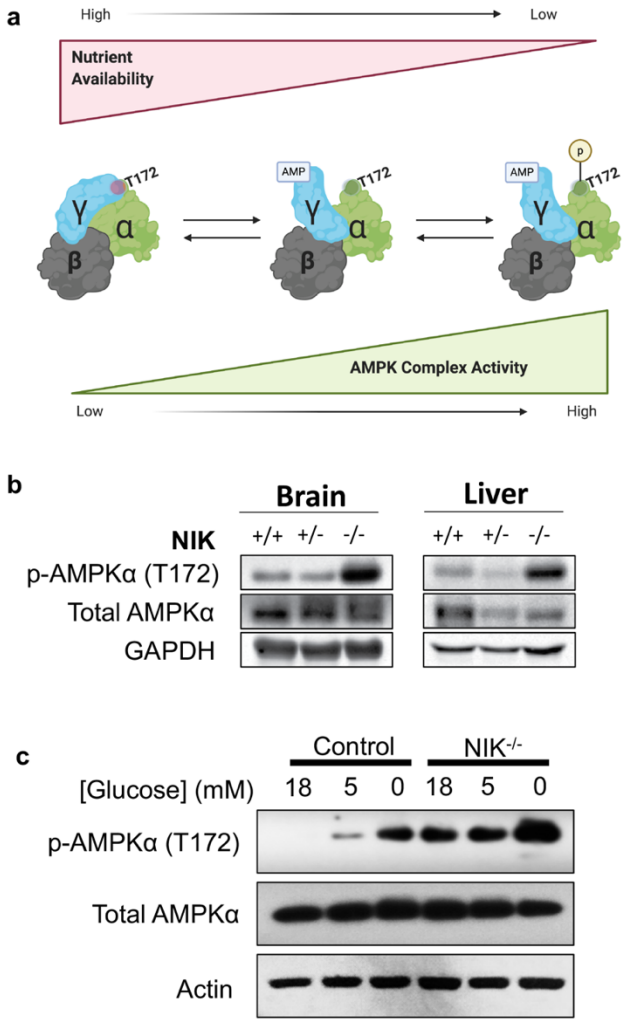

Figure 22. AMPK is hyperactivated/derepressed in NIK$^{-/-}$ GBM cells under high glucose and glucose depleted conditions

a, AMPK is a heterotrimeric protein composed of α,β, γ and gamma subunits. AMPK activity is controlled through phosphorylation on T172 of AMPKα. Under nutrient rich conditions. AMPKα T172 is sterically hindered by the γ subunit. As the cells are starved, AMP increases and binds to the subunit. This creates a conformational change and renders AMPKα T172 accessible to upstream kinases. **b**, Representative western blot of age and littermate matched NIK +/+, +/-, and -/- mice probed with indicated antibodies. **c**, Representative western blot of BT25 control and NIK$^{-/-}$ GBM cells grown in indicated media conditions for 24 hours.

hinders T172 on the alpha subunit. Upon fasting, ATP stores become depleted and the concentration of AMP rises in the cell. AMP then binds to the gamma subunit on AMPK which triggers a conformational change that allows access to T172 on the alpha

subunit (Figure 22a). Upstream kinases such as LKB1 or CAMKK2 can phosphorylate AMPK on the alpha subunit to activate this critical nutrient sensor.

We investigated AMPK activity in our cells and in our mice and have discovered that in a multitude of NIK-deficient cell lines and in NIK-deficient mice phospho-AMPKα T172 expression is increased (Figure 22b-c). The $NIK^{-/-}$ GBM cell lines are no different in this regard and demonstrate increased pAMPKα T172 expression as well. In BT25 GBM cells, pAMPKα T172 is upregulated—as expected given the understanding of classical AMPK activation (Figure 22a)—upon glucose depletion from 18 mM glucose to 5 mM glucose to 0 mM glucose (18 mM galactose). Strikingly, pAMPKα T172 is upregulated/derepressed in $NIK^{-/-}$ GBM cells even in high glucose media and as glucose levels drop it continues to increase (Figure 26c). This suggests that under steady state (fed) conditions NIK acts as a repressor of AMPK.

AMPK can promote glycolysis through PFK2 (Marsin et al., 2000), and also can promote OXPHOS through breakdown of non-glycolytic intermediates—such as through activation of fatty acid oxidation through acetyl-CoA carboxylase (ACC)(Hardie, 2011). Our findings of upregulated glycolysis in $NIK^{-/-}$ GBM cells are consistent with elevated AMPK activity in that regard. However, what is inconsistent with increased AMPK activity is that our $NIK^{-/-}$ GBM cells consistently had reduced OXPHOS metabolism. This may also indicate that NIK's important role in mitochondria dynamics upon metabolic shifting to OXPHOS is important for AMPK's

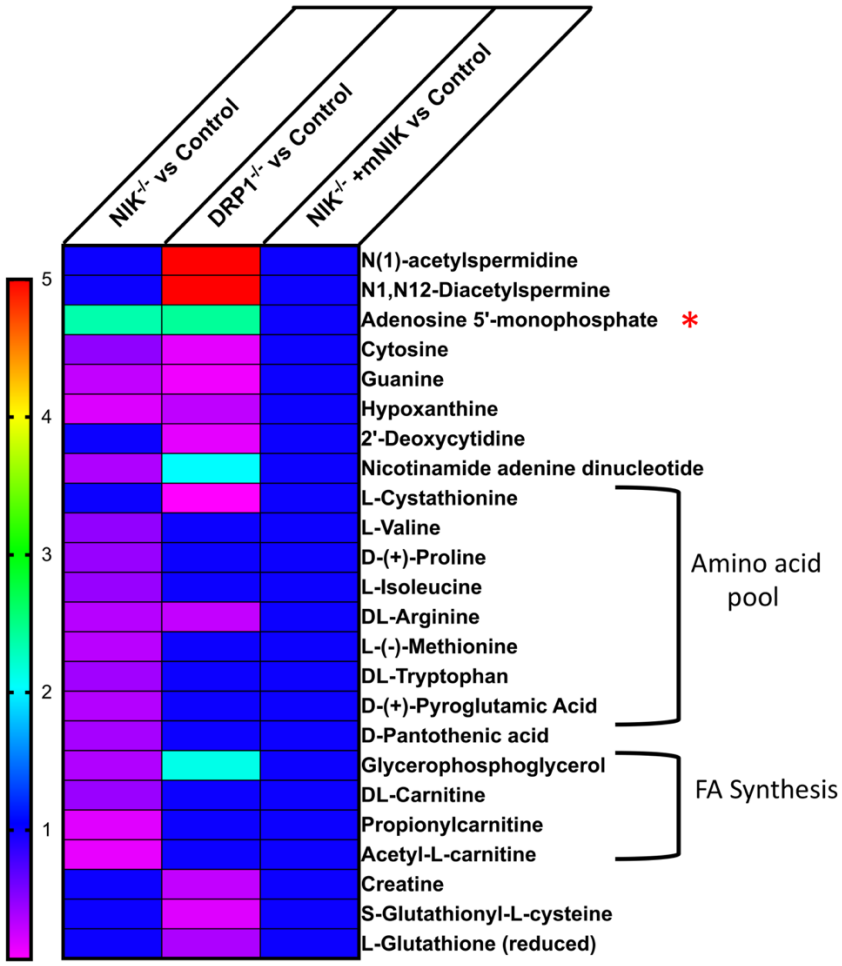

Figure 23. LC-MS metabolomics analysis reveals deficiencies in amino acid pool and fatty acid synthesis intermediates in NIK$^{-/-}$ GBM cells
Above: LC-MS positive phase metabolomics demonstrates that NIK$^{-/-}$ GBM cells are deficient in amino acids and amino acid intermediates. * is indicated AMP is elevated in both NIK$^{-/-}$ and DRP1$^{-/-}$ compared to control GBM cells. In each case the metabolite balance was restored upon stable expression mNIK in the NIK$^{-/-}$ GBM cell line (third column, blue indicates a fold change of 1 or no difference).

control of mitochondria metabolism and without NIK, AMPK cannot support mitochondrial energy production.

Consistent with pAMPKα T172 elevation in BT25 NIK$^{-/-}$ GBM cells, liquid-chromatography-mass spectrometry (LC-MS) metabolomics in high glucose media revealed that the AMP metabolite is elevated in NIK$^{-/-}$ as well as DRP1$^{-/-}$ mutants

compared to control (Figure 23). The elevation in AMP in these mitochondria fission deficient cell lines furthers support for fission in energy metabolism even under basal conditions. The elevation in AMP in the DRP1$^{-/-}$ in high glucose is curious since our Seahorse XFe96 mitostress analysis demonstrated that DRP1 deficient GBM cells had elevated mitochondrial ATP production in high glucose media. The deficiencies in energy product may be coming from elsewhere. In the case of the NIK$^{-/-}$ GBM mutant cell line, two other major clusters of metabolites are impacted: amino acids and their metabolic intermediates and metabolites involved in beta-oxidation of fatty acids.

Defects in both beta-oxidation of fatty acids as well a depleted amino acid pool can have significant impacts on mitochondria metabolism. Carnitine is a critical shuttle for beta-oxidation intermediates to the mitochondria (Longo et al., 2016) and complete oxidation of one palmitate molecule (fatty acid with 16 carbons) and subsequent metabolism by the mitochondria can generate a massive amount of energy for the cell (129 ATP). It is plausible that a defect in the fatty acid oxidation pathway could be attributable to some of the mitochondria energy production defects and this should be a further avenue of study in our lab.

The reduction in amino acids and fatty acid oxidation intermediates, as well as the AMP metabolite, suggest that the hyperactivation of pAMPKα T172 is primarily through defects in metabolic pathways and energy production. But the diminished amino acid pool under steady state (high glucose) conditions could also indicate that there may be a defect in nutrient recycling through autophagy.

CAMKK2 operates a specialized arm of the AMPK pathway. While the upstream kinase LKB1 is thought to be primarily responsible for AMPK activation under nutrient deprivation (Shaw et al., 2004), CAMKK2 phosphorylates AMPK when it senses calcium and amino acids (Figure 24a) and this amino acid sensing is independent of mTOR (Dalle Pezze et al., 2016). This activity through CAMKK2 drives

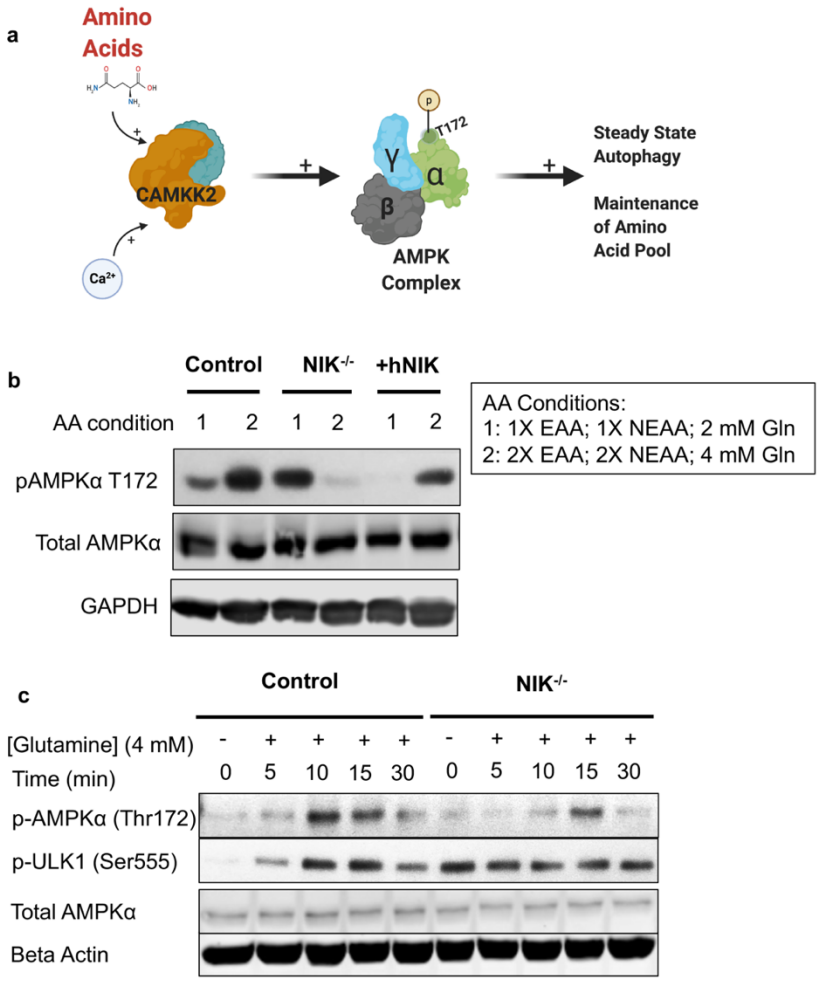

Figure 24. AMPK activation by amino acids is impaired in NIK$^{-/-}$ GBM cells
a, Schematic illustrating CAMKK2 control of AMPK activation through amino acids. **b**, Western blot of BT114 control, NIK$^{-/-}$, and hNIK overexpressing cells exposed to media with different amino acid concentrations for one hour and incubated with indicated antibodies. **c**, Western blot of BT116 control and NIK$^{-/-}$ GBM cells are grown in high glucose media and spiked with 4 mM glutamine at indicated time points and incubated with the indicated antibodies.

AMPK/ULK1-dependent autophagy under steady state/nutrient rich conditions to maintain the amino acid pool.

To test whether introduction of amino acids can modulate AMPK activity in our control, NIK$^{-/-}$, and NIK-overexpressing GBM cells, BT114 cells were supplemented with 18 mM glucose and 1X essential amino acids and nonessential amino acids +2 mM glutamine. Under this condition (AA condition 1, Figure 24b), the trends in amino AMPK activation are the same as they are in high glucose media—with NIK$^{-/-}$ GBM cells having the highest expression of pAMPKα T172 and NIK-overexpressing cells having the lowest. When the amino acid concentrations were spiked to 2-fold their typical concentration for one hour (AA condition 2, Figure 24b), pAMPKα T172 increased in control and NIK-overexpressing GBM cells but decreased in NIK$^{-/-}$ cells.

Our finding that amino acids can repress hyperactivity of AMPK in NIK-deficient GBM cells, while increasing AMPKα phosphorylation on T172 in control and NIK overexpressing cells is striking. But this experiment does not address whether amino acids excess in the media are bypassing metabolism deficiencies or if amino acid sensing is somehow hindered and AMPK activity cannot increase in response to amino acids in NIK$^{-/-}$ cells. To test whether the kinetics of AMPK's response to amino acids is altered in NIK$^{-/-}$ GBM cells we utilized BT116 control and NIK$^{-/-}$ GBM cells. We utilized this cell line because while pAMPKα T172 is elevated in the NIK-depleted BT116 cells, it is very subtle—which makes it easy to monitor upregulation of AMPK activity. When 4 mM of glutamine was spiked into high glucose media and monitored for 30 minutes, pAMPKα T172 was induced but delayed and less sustained compared to

the control GBM cells (Figure 24c). Downstream of AMPK, ULK1 phosphorylation on serine 555 was induced in control cells but was consistently elevated and unresponsive to amino acids in the NIK$^{-/-}$ GBM cells.

4.4 NIK binds to multiple ER, mitochondria, and Rab proteins and possesses several highly conserved LIR domains

To test what proteins NIK binds to at the mitochondria in galactose media that could drive its recruitment, we cultured BT25 GBM cells in glucose or galactose media for 3 hours and fractionated the cells into cytosol and mitochondria enriched (heavy membrane, HM) fractions. The mass spec analysis (Figure 25a) revealed that NIK associates with a variety of ribosomal protein subunits in both the cytosol and heavy membrane, suggesting that perhaps there is some ER associated-NIK protein. Pyruvate kinase, GAPDH, and fatty acid synthase all bound NIK in the cytosol fraction, and all have important roles in metabolism. Pyruvate kinase and GAPDH are both critical enzymes necessary for glycolysis (Bolaños et al., 2010), while fatty acid synthase is critical for fatty acid production in cells (Menendez and Lupu, 2007).

The mass spec analysis identified several mitochondria proteins that NIK interacted with including Tu translation elongation factor (mitochondrial, TUFM) as well as C1 Tetrahydrofolate Synthase (mitochondrial, MTHFD1L). TUFM promotes the GTP-dependent binding of aminoacyl-tRNA into the A site of mitoribosomes and acts a stress sensor in mitochondria (Wilkening et al., 2018). Interestingly, TUFM knockdown in human lung cancer reduced OXPHOS activity, increased glycolysis, and

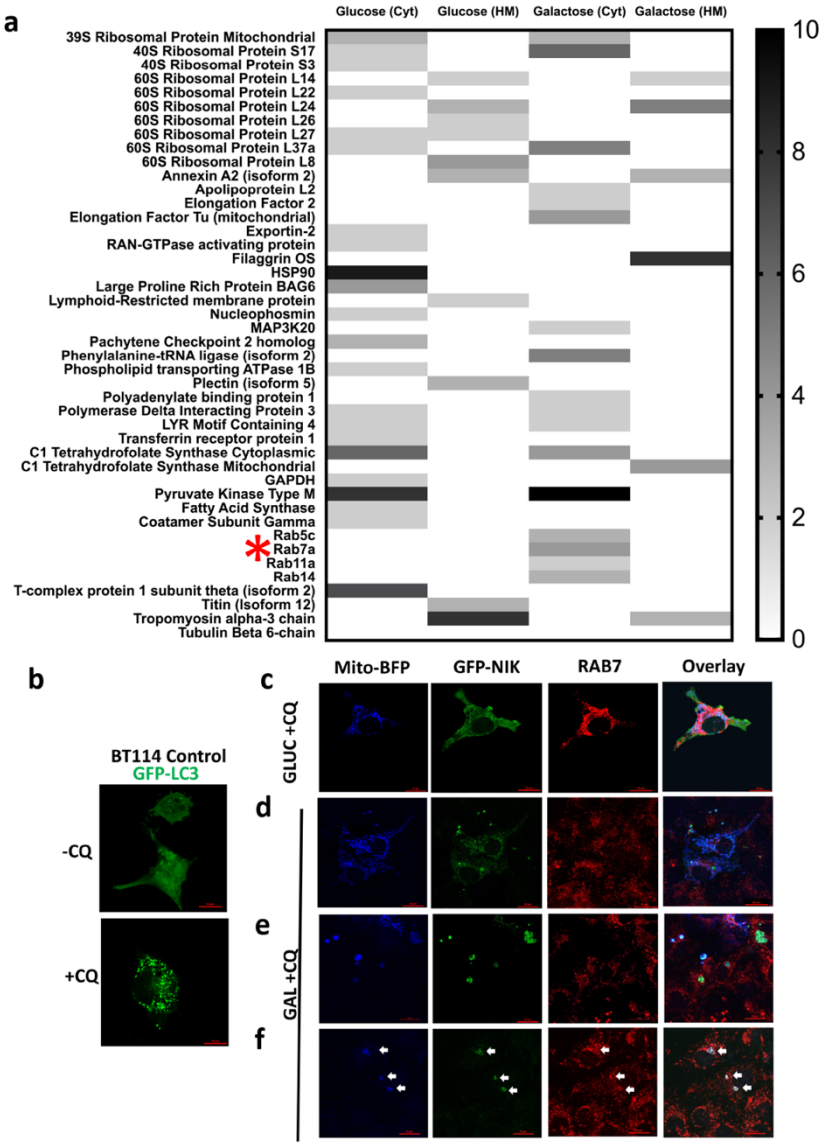

Figure 25. Mass spectroscopy and immunofluorescence analysis reveals NIK associates with Rab7 during metabolic stress

a, Heat map demonstrating peptide enrichment in a mass spec analysis of NIK-interacting proteins in glucose in galactose media at 3 hrs. Proteins are segregated by whether they bound NIK in glucose or galactose and whether they were bound in the heavy membrane or cytosol fraction. * indicates Rab7 binding **b**, BT114 control cells were transiently transfected with GFP-LC3 and then treated with 50 micromolar chloroquine (CQ) in galactose media for 12 hours. **c-d**, Immunofluorescence of BT114 cells transfected with mito-BFP and probed with the indicated antibodies after 24 hours in either glucose (**c**) or galactose (d-**f**) and treated with 50 micromolar chloroquine (CQ) for 12 hours.

increased phosphorylated AMPK T172 (He et al., 2006). Mitochondrial C1-

tetrahydrofolate synthase (MTHFD1L) is also an intriguing protein for NIK to bind,

since folate and one-carbon metabolism is critical for cancer cells (Koseki et al., 2018). However, both TUFM and MTHFD1L are located within the mitochondria. Given our data demonstrating NIK binds to the outer mitochondria membrane (Figure 5), it seems unlikely that these proteins would normally interact.

A particularly interesting cluster of proteins that the mass spec identified as NIK-interacting partners—specifically in galactose media in the mitochondria-enriched (HM) fraction—were the Rab proteins. The Rab family of proteins comprise the largest family of small GTP binding proteins and are responsible vesicle trafficking and vesicle targeting to membranes in the cell (Kelly et al., 2012). The mass spec identified Rab5, Rab7, Rab11, and Rab14. Rab5 associates with early endosomes and regulates their motility on microtubules (Nielsen et al., 1999). Rab5, along with Rab7, Rab11, and Rab14 are all implicated at different stages in autophagy (Ao et al., 2014; Mauvezin and Neufeld, 2017).

Rab7 is present on the outer membrane of late autophagosomes and promotes a crucial process in autophagy—the fusion of autophagosome to the lysosome for degradation (Tan and Tang, 2019). BT114 cells cultured in galactose media for 12 hours with addition of chloroquine—an antimalaria drug that is known to inhibit autophagosome/lysosome fusion (Mauthe et al., 2018). This treatment confirmed buildup of autophagosomes as indicated by GFP-LC3^{+} punctae (Figure 25b). To observe the interaction of Rab7 with NIK in GBM cells in vivo, we transfected BT114 control GBM cells with mito-BFP and GFP-NIK and cultured them in either glucose or galactose media and with chloroquine for 24 hours and probed with a Rab7 antibody

(Figure 25c-f). These confocal microscopy images (Figure 25c-f) reveal that NIK appears diffuse throughout the cytoplasm of the cell in glucose media with the addition of chloroquine (Figure 25c), but when the GBM cells are cultured in galactose media

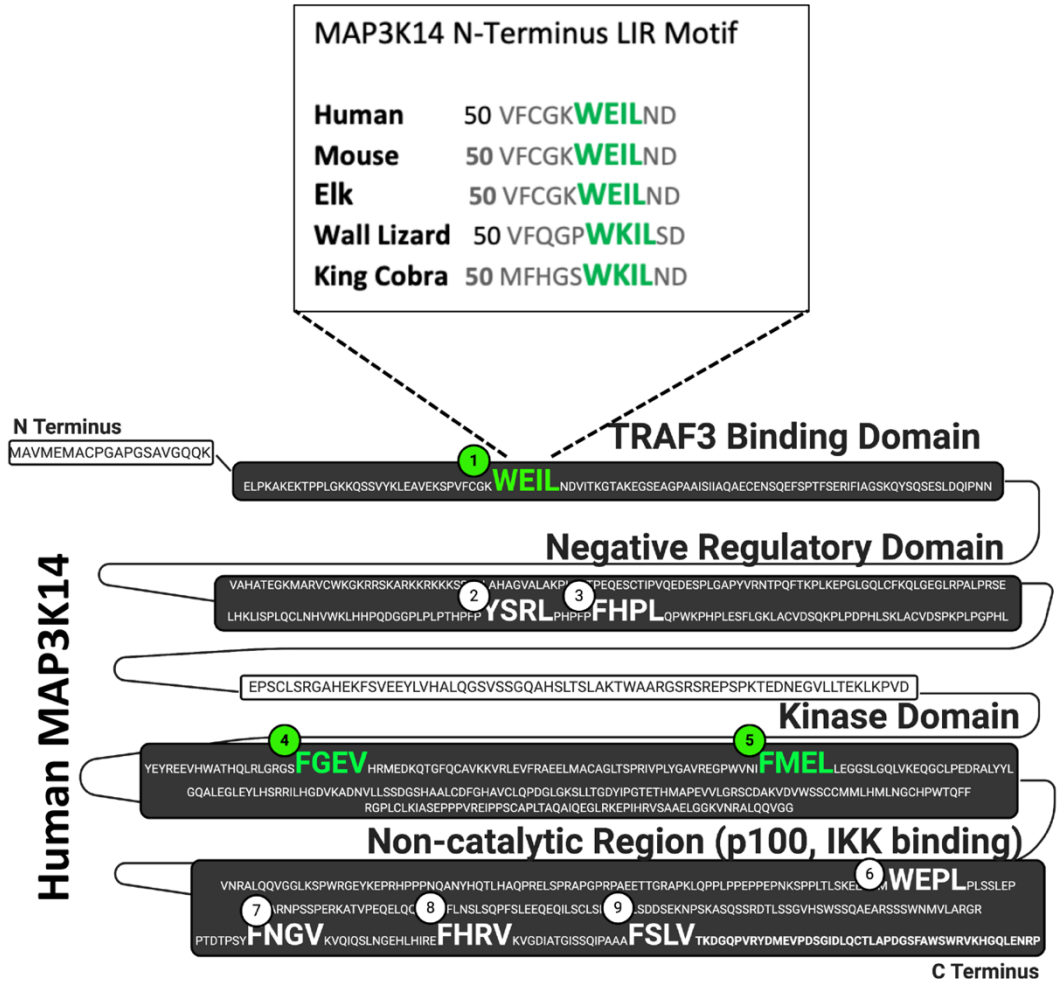

Figure 26. Conserved LC3 interacting region motifs are present in human MAP3K14

Above: Figure illustrates the positioning of the 9 LIR motifs (Y/W/F, X, X, I/L/V—where X is any amino acid) within the human NIK sequence. Of the 9 motifs present, three are conserved between 5 vertebrate species: human, mouse, elk, wall lizard, and king cobra. One of the conserved motifs is located at the N terminus in the TRAF3 binding domain. The remaining two conserved motifs are located in the kinase domain of NIK.

with chloroquine, GFP-NIK appears as punctae and colocalizes with Rab7 (Figure 25d-e and white arrows in 25f).

If NIK was involved in autophagosome formation or fusion of an autophagosome or mitophagosome (mitochondria contained in autophagosome) NIK would likely be required to bind to LC3—which is a critical for cargo recognition and incorporation of cargo into the autophagosome. LC3-interacting-region motifs (Y/W/F, X, X, I/L/V—where X is any amino acid) are required for cargo receptors to bind to LC3 (Birgisdottir et al., 2013).

To investigate whether NIK could direct binding of cargo to the autophagosome we searched the NIK protein sequence for LC3-interacting region domains (LIR domains). We have discovered that human NIK protein contains nine such motifs and that there are no fewer than three that are highly conserved among vertebrates (green highlighted motifs, Figure 25). One of these motifs is located at the N terminus in the TRAF3 binding domain of NIK (aa 55-58) and two are located in the kinase domain (aa 411-414; aa 468-471). Collectively, these data suggest that NIK associates with Rab7 late endosome/autophagosome vesicles under conditions of metabolic stress and NIK possesses the domains required to bind LC3 and direct the binding of cargo proteins to the autophagosome to undergo autophagy/mitophagy.

V. SUMMARY AND FUTURE DIRECTIONS

This study builds upon our previous report that a pool of NIK localizes to the mitochondria in unstimulated conditions where it promotes invasion and cell migration. Here we have demonstrated that NIK responds to glucose depletion and metabolic stress through increased recruitment to the outer mitochondria membrane where it promotes maximal recruitment of DRP1 to the mitochondria. Furthermore, this study establishes

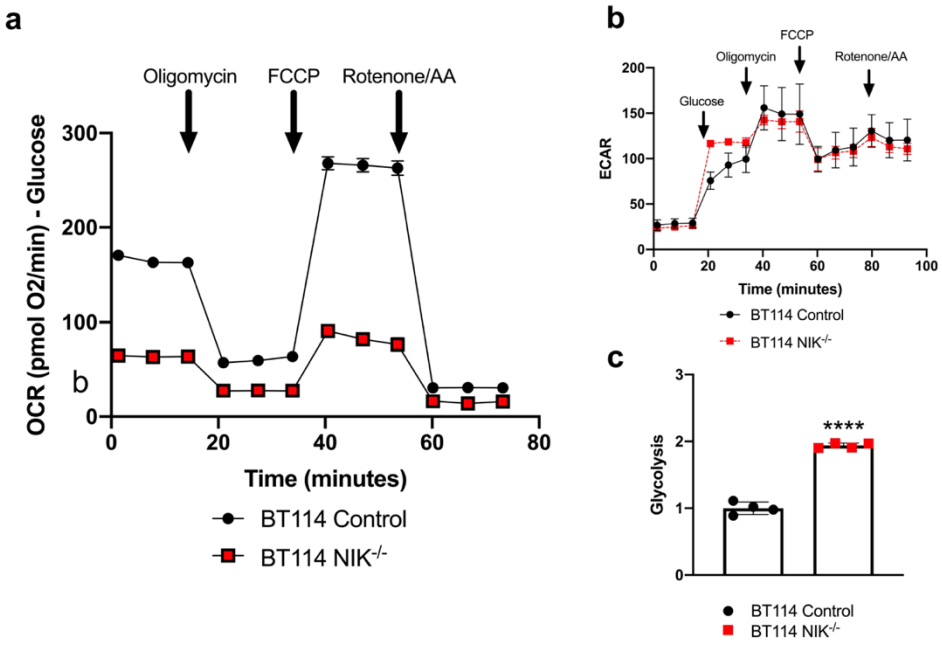

Figure 27. NIK depletion in BT114 GBM cells phenocopies metabolic deficits seen in BT25 GBM cells.
a, Representative Seahorse MitoStress plot showing the mean +/- SD values for BT114 control and NIK-/- cells (n=3 replicates per cell line). **b,** Representative graph of glycolysis measurements for BT114 control and NIK-/- GBM cell lines as measured by the Seahorse glycolysis stress test. **c,** ECAR measurements in BT1114 cell lines for Seahorse glycolysis stress test Student t-test, **** indicates p<.0001.

that NIK is an important regulator of basal respiration, mitochondrial ATP production as well as spare respiratory capacity in GBM cells. These NIK-dependent metabolic

phenotypes we observed in BT25 glioblastoma cells were also translatable to BT114 GBM cells as well (Figure 26a-c), suggesting that our observations are likely broadly translatable across glioblastoma cell types.

Our study also implies a role for OXPHOS and mitochondria dynamics in GBM progression. Consistent with our results, a review of RNAseq data from 8 human GBM

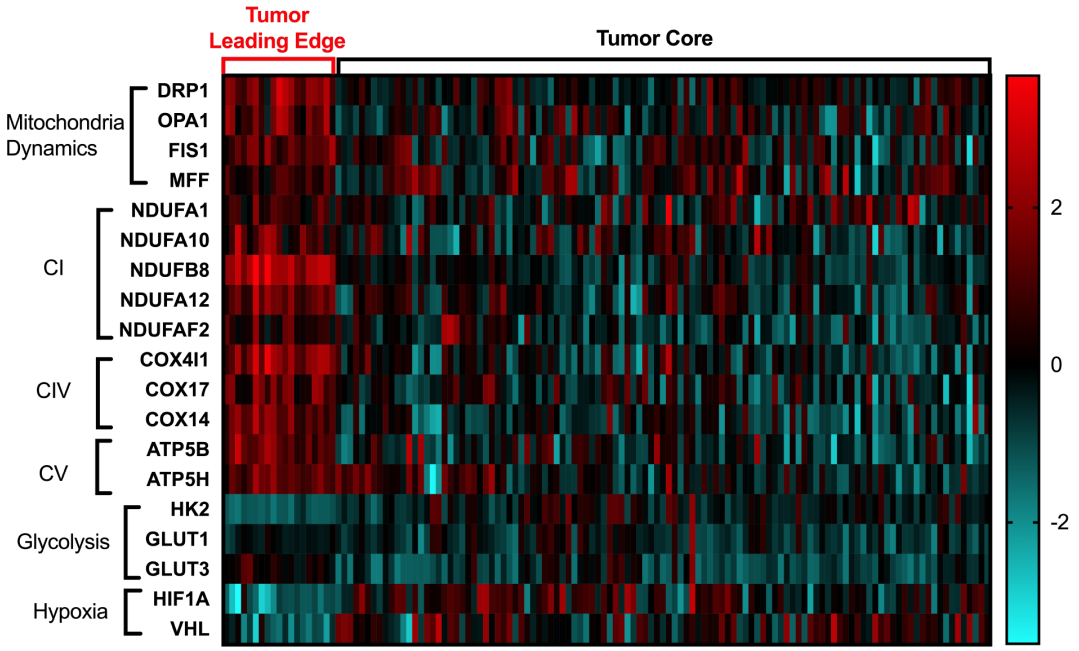

Figure 28. Mitochondrial dynamics and OXPHOS genes are upregulated at the leading edge of human GBM tumors.
Above: Heat map demonstrating genes essential for mitochondria dynamics, OXPHOS, glycolysis and hypoxia upregulated or downregulated at the tumor leading edge compared to the tumor core of 8 human GBM tumors. Data taken from IVY GAP database.

tumors on the IVYGAP database (Puchalski et al., 2018) revealed that many OXPHOS genes—particularly in complex I, IV, and V—are upregulated at the leading edge of the tumor during cancer progression. Critical mitochondria dynamics genes such as DRP1, Fis1, and MFF are likewise elevated at the leading edge, while genes regulating

glycolysis such as Hexokinase 2 as well as genes regulating hypoxia are upregulated at the tumor core (Figure 27). This data from patient GBM tumors suggest that our findings concerning the importance of mitochondria metabolism and OXPHOS may be translatable to the clinical setting, and that combinations of NIK inhibitors and metabolic therapies such as a low glucose (ketogenic) diet may be beneficial to GBM patients.

While it is true that multiple downstream proteins of the NF-κB signaling pathway have been found in mitochondria, such as IKK, our data provides evidence that $NIK^{-/-}$ control of mitochondria metabolism is independent of activity of these downstream components. Based on biochemical cell fractionation, single organelle analysis as well as live cell imaging and western blot, we propose that NIK is recruited to mitochondria upon forced OXPHOS shift/metabolic stress where it recruits and retains DRP1.

To recapitulate, $NIK^{-/-}$ GBM cells are impaired in basal respiration, mitochondria ATP production, and spare respiratory capacity in both high glucose (18 mM) and galactose media. BT25 $IKK\alpha/\beta^{-/-}$ cells do indeed have impaired basal respiration, mitochondria ATP production, and spare respiratory capacity in high glucose media. However, GBM cells deficient in IKKα/β components in galactose media can remodel their mitochondrial metabolism to increase basal respiration, ATP production, SRC, and to levels seen in the control. GBM cells lacking NIK and, critically, both IKKα/β and NIK (triple knockout) were unable to increase these metabolic parameters to the same extent as the $IKK\alpha/\beta^{-/-}$ GBM cells in forced OXPHOS conditions (Figure 11, Figure 13, Figure 17a).

Furthermore, while NIK$^{-/-}$ and IKKα/β$^{-/-}$ GBM cells died at higher rates when shifted to OXPHOS-promoting media, IKKα/β$^{-/-}$ NIK$^{-/-}$ (triple knockout) GBM cells

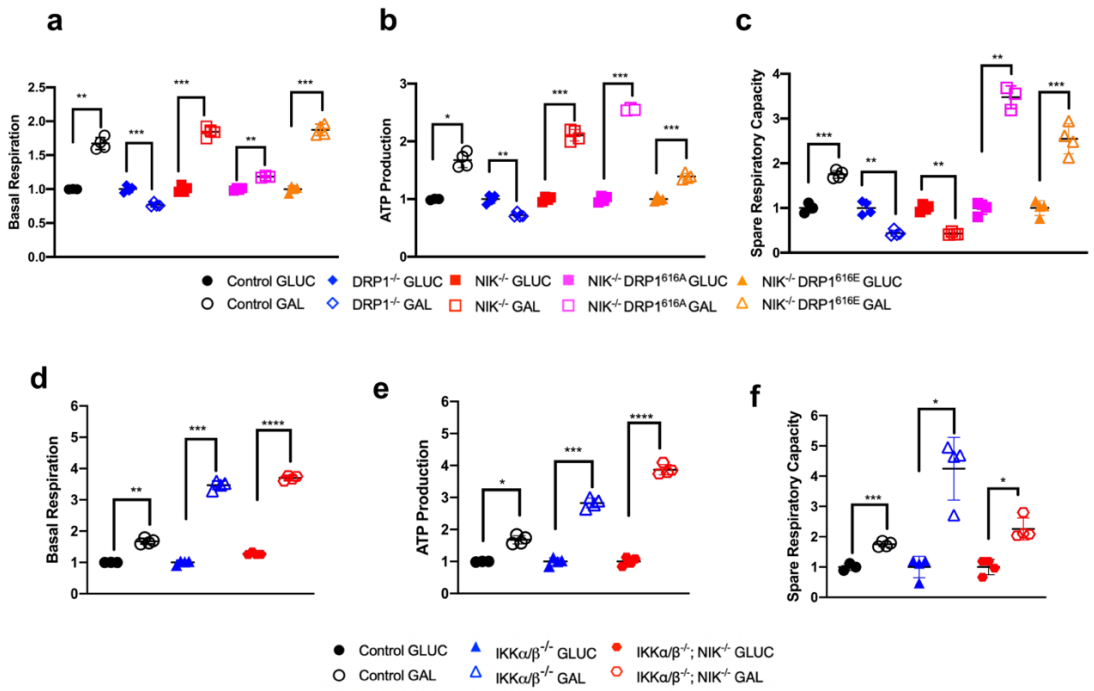

Figure 29. Galactose increases basal respiration, ATP production and spare respiratory capacity in GBM cells.
Data graphed here is the same as in Figures 7, 9, and 11 represented as fold change from each individual cell line's basal respiration, ATP production, or spare respiratory capacity in glucose. **a-f,** Increases in basal respiration (**a, d**), spare respiratory capacity (**b, e**) and ATP production **(c, f)** are observed in GBM cell lines indicated above except for the basal respiration, ATP production, and spare respiratory capacity of BT25 DRP1$^{-/-}$ cells and ATP production and spare respiratory capacity of BT25 NIK$^{-/-}$ cells. Paired t test, * indicates p<.05, ** indicates p<.01, *** indicates p<.001, **** indicates p<.0001.

exhibited an additive effect and their viability was lower than either knockout alone. NIK-depleted GBM cells transduced with constitutively active DRP1-S616E restores both viability and tumor growth potential *in vitro* (Figure 14) and *in vivo* (Figure 19). Though NIK-depleted cells exhibited impaired mitochondria impairment, they were able to increase glycolysis to compensate—which may suggest a Warburg shift of the cells to

aerobic glycolysis. Furthermore, this IKK-independent increase in glycolysis is likely the reason why we did not observe a significant difference in growth rate in high glucose media (Figure 12). Altogether, these data indicate that NIK has a unique role during periods of metabolic stress/glucose deprivation that does not phenocopy NIK-competent/IKK-deficient GBM cells under the same conditions.

It is also important to address that while NIK$^{-/-}$, DRP1$^{-/-}$, and IKKα/β$^{-/-}$ NIK$^{-/-}$ all demonstrated impaired mitochondrial metabolism compared to control GBM cells in

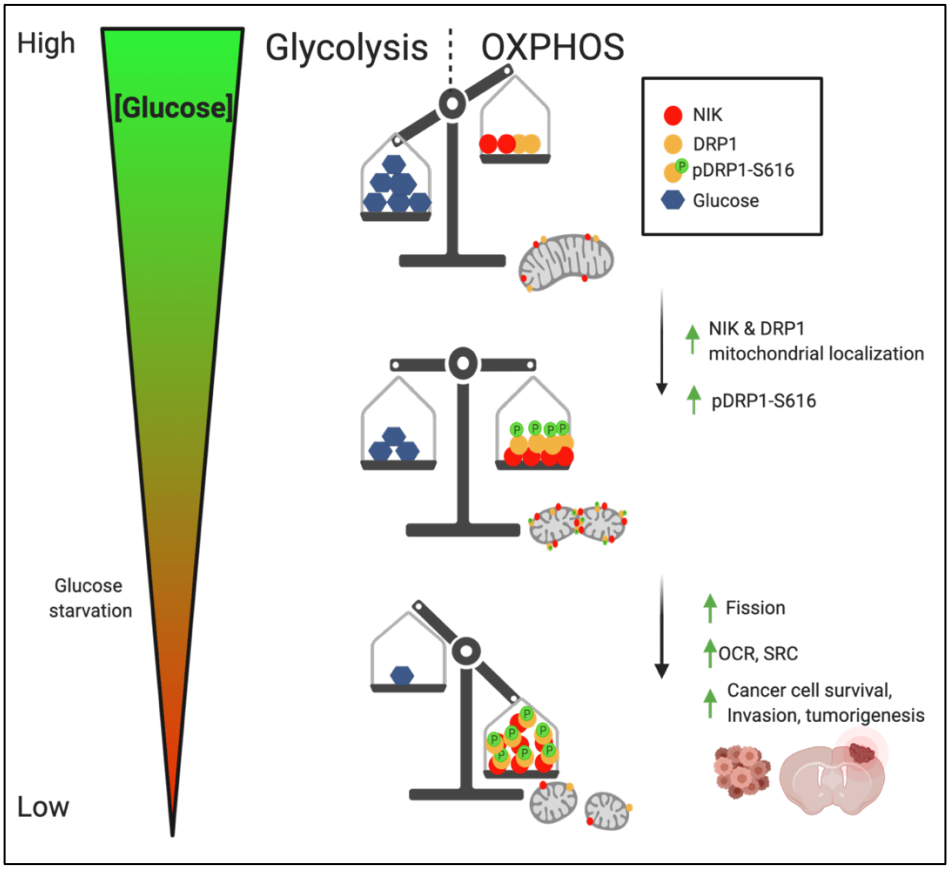

Figure 30. Model
Above: NIK accumulates at the mitochondria during glucose deprivation and bioenergetic stress. As GBM cells enter a glucose-poor environment, NIK is recruited to the mitochondria where it drives DRP1 fission, increased phosphorylation of DRP1 at serine 616 and mitochondria respiration. These bioenergetic and mitochondrial alterations work in concert to increase cancer cell survival, invasion, and tumorigenesis.

galactose, most cell lines were able to increase nearly every parameter of mitochondrial metabolism in galactose media compared to their own baseline in glucose (Figure 28). The exceptions to this trend were decreased basal respiration, mitochondria ATP production, and SRC for DRP1$^{-/-}$ GBM cells and decreased SRC for NIK$^{-/-}$ GBM cells in galactose compared to glucose.

Even so, the ability of a mutant GBM cell line to increase its mitochondrial metabolism in galactose from its glucose baseline was not prognostic for how well it would grow *in vivo*. The NIK$^{-/-}$ DRP1-S616A GBM cell line for example, displayed fold change increases of mitochondria ATP production and SRC that were greater than their NIK$^{-/-}$ DRP1-S616E counterparts (Figure 28 b-c). However, the NIK$^{-/-}$ DRP1-S616E GBM cells outpaced the NIK$^{-/-}$ DRP1-S616A cellular proliferation and tumor size in an *in vivo* orthotopic xenograft model (Figure 19). The parameter that tracks best as a predictor of how well a GBM cell will withstand the metabolic stress associated with the forced metabolic shift to galactose in cell survival assays *in vitro*, or how well the cells will proliferate in the harsh and chaotic tumor microenvironment of the brain *in vivo* is the spare respiratory capacity of the cell line in galactose media compared to control GBM cells (Compare SRC values for Control, NIK$^{-/-}$, DRP1$^{-/-}$ NIK$^{-/-}$ DRP1-S616E in GAL media in Figures 11, 13, and 16 to Figure 14, and 19 trends for survival and *in vivo* data).

To conclude, mitochondria undergo dynamic changes in response to bioenergetic stressors and nutrient availability. Our study is consistent with other reports that these stressors result in increased mitochondria fission and support a model (Figure 29) that

mitochondria fission and metabolic reprogramming under conditions of forced OXPHOS/nutrient stress is driven by NIK.

Cellular metabolism in response to mitochondria dynamics is still controversial. Some studies suggest that mitochondria fusion promotes oxidative phosphorylation while others demonstrate that increased DRP1 and mitochondria fission promotes OXPHOS (Mishra and Chan, 2016; Nagdas et al., 2019). These differences may be due to cell-context dependent effects as well as dependent on differences in source and quantity of sugar and amino acids the cells are being exposed to (Gomes et al., 2011; Nagdas et al., 2019; Shiratori et al., 2019). We believe that our study provides substantial evidence that increased DRP1 activation through phosphorylation at serine 616 and increased mitochondria fission enhances mitochondria metabolism in GBM.

We have found that NIK is a critical regulator of mitochondria fission and metabolic adaptation of glioblastoma cells and our findings suggest that a combinatorial approach of NIK inhibition and glucose restricted diet may be able to improve clinical outcomes in GBM.

Galactose media was utilized in this project because extensive research has demonstrated that galactose media increases dependence on oxidative phosphorylation in a wide variety of cell types (Aguer et al., 2011; Arroyo et al., 2016; Reitzer et al., 1979). However, switching from glycolysis to OXPHOS-promoting media also is associated with a variety of other stress pathways being induced aside from just oxidative phosphorylation.

What role NIK may have in autophagy is yet uncertain. The defects in the amino acid pool suggest a decrease in autophagy regulation in the NIK$^{-/-}$ glioblastoma cells. This finding would implicate NIK as an autophagy promoter; however, NIK also acts as a repressor of AMPK activation. Whether the repression of AMPK activity by NIK is direct, as is the case of some proteins like glycogen synthase kinase 3 (GSK3), remains to be determined (Suzuki et al., 2013).

Our data suggests there may be multiple metabolic defects that drive the decreased mitochondria metabolism in NIK$^{-/-}$ glioblastoma cells. First, the depletion of the amino acid pool and amino acid metabolic intermediates could impact OXPHOS which may also elevate AMP and increase AMPK activity. It is possible that spiking amino acids to extremely high levels allow the cells to cope with reduced amino acid availability. Secondly, it is possible that the reduction in amino acids is caused—paradoxically--by faulty sensing of amino acids in the environment and continuing maintenance of the amino acid pool through AMPK. Although pULK1 Ser555 is steadily elevated in the NIK$^{-/-}$ cells, what functions ULK1 is performing—or if it can perform them—is unknown and should be further explored.

NIK is recruited to the mitochondria under conditions of nutrient stress—under the same glucose-depleted conditions that would promote autophagy in the cell. Autophagosome formation, has been demonstrated to occur at mitochondria/ER contact sites (Hamasaki et al., 2013)—the very same sites that are known to be important for mitochondria fission. It is speculative, but not impossible to think that perhaps the metabolic deficits in the NIK$^{-/-}$ GBM cells are due to old, damaged mitochondria that are

not recycling properly. Mitophagy is a specialized form of directed autophagy that is performed primarily through the cargo receptors (such as BNIP3) on the mitochondria outer membrane (Pickles et al., 2018)—where we have demonstrated NIK is localizing. Our data mass spec data supports a potential direct role for NIK may have direct roles in autophagy through its binding to of late endosome/lysosome fusion protein Rab7 under conditions of metabolic stress (Figure 25). Furthermore, NIK contains three highly conserved LIR domains (Figure 26) that may allow it to interact with LC3 and bind autophagosomes directly.

Taken together, it may be that NIK is not just responding to nutrient stress but rather stress in general. Nutrient stress, ER stress, and oxidative stress seem to cause a response in the NIK protein in some manner. And all three of those stress response pathways can and do trigger autophagy (Altman and Rathmell, 2012; Kiffin et al., 2006; Yorimitsu et al., 2006). NIK may be driving mitochondria fission as some intermediary step in mitophagy where the mitochondria need to be partitioned into smaller bite-size chunks for the autophagosome/lysosome to devour, since it is known that DRP1-mediated fission is indeed important this process. Future studies should attempt to position NIK's role at the mitochondria in the context of a larger metabolic or stress response pathway—as it likely is part of one.

However, the fact that NIK has conserved LIR domains does not mean that these domains are only for directing cargo to the autophagosome. Recently, researchers demonstrated that non-canonical NF-κB signaling can be activated through NIK recruitment to $Rab5^{+}$ endosomes (Fang et al., 2019). This unique mechanism for NIK

stabilization and subsequent activation of non-canonical NF-κB signaling depends on Rab5 binding NIK and sequestering it away from the TRAF degradation complex (Fang et al., 2019).

The locations of the three conserved LIR domains in NIK (Figure 26) are in critical regulatory and catalytic regions of the NIK protein. One LIR domain is located in the TRAF3 binding domain and another two are located in the kinase domain. It may be that these domains are required as an additional mechanism to activate NIK under conditions of metabolic stress. It is purely hypothetical, but NIK loading onto autophagosomes may be a mechanism by which the TRAF3 binding domain is sterically blocked from interacting with the TRAF degradation complex. Further levels of regulation could occur through LC3 coated autophagosomes binding NIK at the kinase domain and either sterically blocking its activity or acting as a bridge to interact with other LC3 binding proteins.

There is a great deal of work and likely a great deal left to discover pertaining to NIK—a frustratingly elusive yet captivating protein—and its functions at the mitochondria in its response to metabolic stress.

REFERENCES

Adams, C.J., Kopp, M.C., Larburu, N., Nowak, P.R., and Ali, M.M.U. (2019). Structure and Molecular Mechanism of ER Stress Signaling by the Unfolded Protein Response Signal Activator IRE1. Front. Mol. Biosci. *6*, 11.

Aguer, C., Gambarotta, D., Mailloux, R.J., Moffat, C., Dent, R., McPherson, R., and Harper, M.-E. (2011). Galactose enhances oxidative metabolism and reveals mitochondrial dysfunction in human primary muscle cells. PloS One *6*, e28536.

Albensi, B.C. (2019). What Is Nuclear Factor Kappa B (NF-κB) Doing in and to the Mitochondrion? Front. Cell Dev. Biol. *7*, 154.

Altman, B.J., and Rathmell, J.C. (2012). Metabolic stress in autophagy and cell death pathways. Cold Spring Harb. Perspect. Biol. *4*, a008763.

Ao, X., Zou, L., and Wu, Y. (2014). Regulation of autophagy by the Rab GTPase network. Cell Death Differ. *21*, 348–358.

Arroyo, J.D., Jourdain, A.A., Calvo, S.E., Ballarano, C.A., Doench, J.G., Root, D.E., and Mootha, V.K. (2016). A Genome-wide CRISPR Death Screen Identifies Genes Essential for Oxidative Phosphorylation. Cell Metab. *24*, 875–885.

Ashton, T.M., McKenna, W.G., Kunz-Schughart, L.A., and Higgins, G.S. (2018). Oxidative Phosphorylation as an Emerging Target in Cancer Therapy. Clin. Cancer Res. Off. J. Am. Assoc. Cancer Res. *24*, 2482–2490.

Baldwin, A.S. (2001). Control of oncogenesis and cancer therapy resistance by the transcription factor NF-kappaB. J. Clin. Invest. *107*, 241–246.

Baltimore, D. (2009). Discovering NF-kappaB. Cold Spring Harb. Perspect. Biol. *1*, a000026.

Bayless, K.J., Kwak, H.-I., and Su, S.-C. (2009). Investigating endothelial invasion and sprouting behavior in three-dimensional collagen matrices. Nat. Protoc. *4*, 1888–1898.

Behnan, J., Finocchiaro, G., and Hanna, G. (2019). The landscape of the mesenchymal signature in brain tumours. Brain J. Neurol. *142*, 847–866.

Benham, A.M., van Lith, M., Sitia, R., and Braakman, I. (2013). Ero1-PDI interactions, the response to redox flux and the implications for disulfide bond formation in the mammalian endoplasmic reticulum. Philos. Trans. R. Soc. Lond. B. Biol. Sci. *368*, 20110403.

Bhutia, S.K., Mukhopadhyay, S., Sinha, N., Das, D.N., Panda, P.K., Patra, S.K., Maiti, T.K., Mandal, M., Dent, P., Wang, X.-Y., et al. (2013). Autophagy: cancer's friend or foe? Adv. Cancer Res. *118*, 61–95.

Birgisdottir, Å.B., Lamark, T., and Johansen, T. (2013). The LIR motif - crucial for selective autophagy. J. Cell Sci. *126*, 3237–3247.

Bister, K. (2015). Discovery of oncogenes: The advent of molecular cancer research. Proc. Natl. Acad. Sci. U. S. A. *112*, 15259–15260.

Bolaños, J.P., Almeida, A., and Moncada, S. (2010). Glycolysis: a bioenergetic or a survival pathway? Trends Biochem. Sci. *35*, 145–149.

Boutaffala, L., Bertrand, M.J.M., Remouchamps, C., Seleznik, G., Reisinger, F., Janas, M., Bénézech, C., Fernandes, M.T., Marchetti, S., Mair, F., et al. (2015). NIK promotes tissue destruction independently of the alternative NF-κB pathway through TNFR1/RIP1-induced apoptosis. Cell Death Differ. *22*, 2020–2033.

Brignall, R., Moody, A.T., Mathew, S., and Gaudet, S. (2019). Considering Abundance, Affinity, and Binding Site Availability in the NF-κB Target Selection Puzzle. Front. Immunol. *10*, 609.

Chae, Y.C., and Kim, J.H. (2018). Cancer stem cell metabolism: target for cancer therapy. BMB Rep. *51*, 319–326.

Chen, T.-H., Chiang, Y.-H., Hou, J.-N., Cheng, C.-C., Sofiyatun, E., Chiu, C.-H., and Chen, W.-J. (2017). XBP1-Mediated BiP/GRP78 Upregulation Copes with Oxidative Stress in Mosquito Cells during Dengue 2 Virus Infection. BioMed Res. Int. *2017*, 3519158.

Chhipa, R.R., Fan, Q., Anderson, J., Muraleedharan, R., Huang, Y., Ciraolo, G., Chen, X., Waclaw, R., Chow, L.M., Khuchua, Z., et al. (2018). AMP kinase promotes glioblastoma bioenergetics and tumour growth. Nat. Cell Biol. *20*, 823–835.

Dalle Pezze, P., Ruf, S., Sonntag, A.G., Langelaar-Makkinje, M., Hall, P., Heberle, A.M., Razquin Navas, P., van Eunen, K., Tölle, R.C., Schwarz, J.J., et al. (2016). A systems study reveals concurrent activation of AMPK and mTOR by amino acids. Nat. Commun. *7*, 13254.

Delgado-López, P.D., and Corrales-García, E.M. (2016). Survival in glioblastoma: a review on the impact of treatment modalities. Clin. Transl. Oncol. Off. Publ. Fed. Span. Oncol. Soc. Natl. Cancer Inst. Mex. *18*, 1062–1071.

Demchenko, Y.N., and Kuehl, W.M. (2010). A critical role for the NFkB pathway in multiple myeloma. Oncotarget *1*, 59–68.

Duran, C.L., Lee, D.W., Jung, J.-U., Ravi, S., Pogue, C.B., Toussaint, L.G., Bayless, K.J., and Sitcheran, R. (2016). NIK regulates MT1-MMP activity and promotes glioma cell invasion independently of the canonical NF-κB pathway. Oncogenesis *5*, e231.

Eichner, L.J., Brun, S.N., Herzig, S., Young, N.P., Curtis, S.D., Shackelford, D.B., Shokhirev, M.N., Leblanc, M., Vera, L.I., Hutchins, A., et al. (2019). Genetic Analysis Reveals AMPK Is Required to Support Tumor Growth in Murine Kras-Dependent Lung Cancer Models. Cell Metab. *29*, 285-302.e7.

Fang, C., Manes, T.D., Liu, L., Liu, K., Qin, L., Li, G., Tobiasova, Z., Kirkiles-Smith, N.C., Patel, M., Merola, J., et al. (2019). ZFYVE21 is a complement-induced Rab5 effector that activates non-canonical NF-κB via phosphoinosotide remodeling of endosomes. Nat. Commun. *10*, 2247.

Fedele, C., Tothill, R.W., and McArthur, G.A. (2014). Navigating the challenge of tumor heterogeneity in cancer therapy. Cancer Discov. *4*, 146–148.

Ferreira-da-Silva, A., Valacca, C., Rios, E., Pópulo, H., Soares, P., Sobrinho-Simões, M., Scorrano, L., Máximo, V., and Campello, S. (2015). Mitochondrial dynamics protein Drp1 is overexpressed in oncocytic thyroid tumors and regulates cancer cell migration. PLoS ONE *10*, e0122308.

Figueroa-Romero, C., Iñiguez-Lluhí, J.A., Stadler, J., Chang, C.-R., Arnoult, D., Keller, P.J., Hong, Y., Blackstone, C., and Feldman, E.L. (2009). SUMOylation of the mitochondrial fission protein Drp1 occurs at multiple nonconsensus sites within the B domain and is linked to its activity cycle. FASEB J. Off. Publ. Fed. Am. Soc. Exp. Biol. *23*, 3917–3927.

Friedman, J.R., Lackner, L.L., West, M., DiBenedetto, J.R., Nunnari, J., and Voeltz, G.K. (2011). ER tubules mark sites of mitochondrial division. Science *334*, 358–362.

Ge, Q.-L., Liu, S.-H., Ai, Z.-H., Tao, M.-F., Ma, L., Wen, S.-Y., Dai, M., Liu, F., Liu, H.-S., Jiang, R.-Z., et al. (2016). RelB/NF-κB links cell cycle transition and apoptosis to endometrioid adenocarcinoma tumorigenesis. Cell Death Dis. *7*, e2402.

Ghosh, S., and Hayden, M.S. (2012). Celebrating 25 years of NF-κB research. Immunol. Rev. *246*, 5–13.

Ghosh, S., May, M.J., and Kopp, E.B. (1998). NF-kappa B and Rel proteins: evolutionarily conserved mediators of immune responses. Annu. Rev. Immunol. *16*, 225–260.

Gloire, G., Legrand-Poels, S., and Piette, J. (2006). NF-kappaB activation by reactive oxygen species: fifteen years later. Biochem. Pharmacol. *72*, 1493–1505.

Gomes, L.C., Di Benedetto, G., and Scorrano, L. (2011). Essential amino acids and glutamine regulate induction of mitochondrial elongation during autophagy. Cell Cycle *10*, 2635–2639.

Gwinn, D.M., Shackelford, D.B., Egan, D.F., Mihaylova, M.M., Mery, A., Vasquez, D.S., Turk, B.E., and Shaw, R.J. (2008). AMPK phosphorylation of raptor mediates a metabolic checkpoint. Mol. Cell *30*, 214–226.

Hamasaki, M., Furuta, N., Matsuda, A., Nezu, A., Yamamoto, A., Fujita, N., Oomori, H., Noda, T., Haraguchi, T., Hiraoka, Y., et al. (2013). Autophagosomes form at ER-mitochondria contact sites. Nature *495*, 389–393.

Hardie, D.G. (2011). AMP-activated protein kinase: an energy sensor that regulates all aspects of cell function. Genes Dev. *25*, 1895–1908.

Hardie, D.G., and Hawley, S.A. (2001). AMP-activated protein kinase: the energy charge hypothesis revisited. BioEssays News Rev. Mol. Cell. Dev. Biol. *23*, 1112–1119.

Hawley, S.A., Boudeau, J., Reid, J.L., Mustard, K.J., Udd, L., Mäkelä, T.P., Alessi, D.R., and Hardie, D.G. (2003). Complexes between the LKB1 tumor suppressor, STRAD alpha/beta and MO25 alpha/beta are upstream kinases in the AMP-activated protein kinase cascade. J. Biol. *2*, 28.

He, J.Q., Zarnegar, B., Oganesyan, G., Saha, S.K., Yamazaki, S., Doyle, S.E., Dempsey, P.W., and Cheng, G. (2006). Rescue of TRAF3-null mice by p100 NF-kappa B deficiency. J. Exp. Med. *203*, 2413–2418.

Herzig, S., and Shaw, R.J. (2018). AMPK: guardian of metabolism and mitochondrial homeostasis. Nat. Rev. Mol. Cell Biol. *19*, 121–135.

Hu, H., Tian, M., Ding, C., and Yu, S. (2018). The C/EBP Homologous Protein (CHOP) Transcription Factor Functions in Endoplasmic Reticulum Stress-Induced Apoptosis and Microbial Infection. Front. Immunol. *9*, 3083.

Johnson, R.F., Witzel, I.-I., and Perkins, N.D. (2011). p53-dependent regulation of mitochondrial energy production by the RelA subunit of NF-κB. Cancer Res. *71*, 5588–5597.

Jones, R.G., and Thompson, C.B. (2009). Tumor suppressors and cell metabolism: a recipe for cancer growth. Genes Dev. *23*, 537–548.

Jung, J.-U., Ravi, S., Lee, D.W., McFadden, K., Kamradt, M.L., Toussaint, L.G., and Sitcheran, R. (2016). NIK/MAP3K14 Regulates Mitochondrial Dynamics and Trafficking to Promote Cell Invasion. Curr. Biol. CB *26*, 3288–3302.

Karin, M. (2006). Nuclear factor-kappaB in cancer development and progression. Nature *441*, 431–436.

Kashatus, J.A., Nascimento, A., Myers, L.J., Sher, A., Byrne, F.L., Hoehn, K.L., Counter, C.M., and Kashatus, D.F. (2015). Erk2 phosphorylation of Drp1 promotes mitochondrial fission and MAPK-driven tumor growth. Mol. Cell *57*, 537–551.

Keats, J.J., Fonseca, R., Chesi, M., Schop, R., Baker, A., Chng, W.-J., Van Wier, S., Tiedemann, R., Shi, C.-X., Sebag, M., et al. (2007). Promiscuous mutations activate the noncanonical NF-kappaB pathway in multiple myeloma. Cancer Cell *12*, 131–144.

Kelly, E.E., Horgan, C.P., Goud, B., and McCaffrey, M.W. (2012). The Rab family of proteins: 25 years on. Biochem. Soc. Trans. *40*, 1337–1347.

Kelly, J.J.P., Stechishin, O., Chojnacki, A., Lun, X., Sun, B., Senger, D.L., Forsyth, P., Auer, R.N., Dunn, J.F., Cairncross, J.G., et al. (2009). Proliferation of human glioblastoma stem cells occurs independently of exogenous mitogens. Stem Cells Dayt. Ohio *27*, 1722–1733.

Kiffin, R., Bandyopadhyay, U., and Cuervo, A.M. (2006). Oxidative stress and autophagy. Antioxid. Redox Signal. *8*, 152–162.

Kim, J., and DeBerardinis, R.J. (2019). Mechanisms and Implications of Metabolic Heterogeneity in Cancer. Cell Metab. *30*, 434–446.

Kodiha, M., Rassi, J.G., Brown, C.M., and Stochaj, U. (2007). Localization of AMP kinase is regulated by stress, cell density, and signaling through the MEK-->ERK1/2 pathway. Am. J. Physiol. Cell Physiol. *293*, C1427-1436.

Koseki, J., Konno, M., Asai, A., Colvin, H., Kawamoto, K., Nishida, N., Sakai, D., Kudo, T., Satoh, T., Doki, Y., et al. (2018). Enzymes of the one-carbon folate metabolism as anticancer targets predicted by survival rate analysis. Sci. Rep. *8*, 303.

Laforge, M., Rodrigues, V., Silvestre, R., Gautier, C., Weil, R., Corti, O., and Estaquier, J. (2016). NF-κB pathway controls mitochondrial dynamics. Cell Death Differ. *23*, 89–98.

Lee, A.-H., Iwakoshi, N.N., and Glimcher, L.H. (2003). XBP-1 regulates a subset of endoplasmic reticulum resident chaperone genes in the unfolded protein response. Mol. Cell. Biol. *23*, 7448–7459.

de Leon-Boenig, G., Bowman, K.K., Feng, J.A., Crawford, T., Everett, C., Franke, Y., Oh, A., Stanley, M., Staben, S.T., Starovasnik, M.A., et al. (2012). The crystal structure of the catalytic domain of the NF-κB inducing kinase reveals a narrow but flexible active site. Struct. Lond. Engl. 1993 *20*, 1704–1714.

Li, H., Mittal, A., Paul, P.K., Kumar, M., Srivastava, D.S., Tyagi, S.C., and Kumar, A. (2009). Tumor necrosis factor-related weak inducer of apoptosis augments matrix metalloproteinase 9 (MMP-9) production in skeletal muscle through the activation of nuclear factor-kappaB-inducing kinase and p38 mitogen-activated protein kinase: a potential role of MMP-9 in myopathy. J. Biol. Chem. *284*, 4439–4450.

Li, W., Saud, S.M., Young, M.R., Chen, G., and Hua, B. (2015). Targeting AMPK for cancer prevention and treatment. Oncotarget *6*, 7365–7378.

Liao, G., Zhang, M., Harhaj, E.W., and Sun, S.-C. (2004). Regulation of the NF-kappaB-inducing kinase by tumor necrosis factor receptor-associated factor 3-induced degradation. J. Biol. Chem. *279*, 26243–26250.

Liberti, M.V., and Locasale, J.W. (2016). The Warburg Effect: How Does it Benefit Cancer Cells? Trends Biochem. Sci. *41*, 211–218.

Liou, G.-Y., and Storz, P. (2010). Reactive oxygen species in cancer. Free Radic. Res. *44*, 479–496.

Liu, G.Y., and Sabatini, D.M. (2020). mTOR at the nexus of nutrition, growth, ageing and disease. Nat. Rev. Mol. Cell Biol. *21*, 183–203.

Liu, J., Sudom, A., Min, X., Cao, Z., Gao, X., Ayres, M., Lee, F., Cao, P., Johnstone, S., Plotnikova, O., et al. (2012). Structure of the nuclear factor κB-inducing kinase (NIK) kinase domain reveals a constitutively active conformation. J. Biol. Chem. *287*, 27326–27334.

Liu, J.-Q., Zhang, L., Yao, J., Yao, S., and Yuan, T. (2018). AMPK alleviates endoplasmic reticulum stress by inducing the ER-chaperone ORP150 via FOXO1 to protect human bronchial cells from apoptosis. Biochem. Biophys. Res. Commun. *497*, 564–570.

Longo, N., Frigeni, M., and Pasquali, M. (2016). Carnitine transport and fatty acid oxidation. Biochim. Biophys. Acta *1863*, 2422–2435.

Losón, O.C., Song, Z., Chen, H., and Chan, D.C. (2013). Fis1, Mff, MiD49, and MiD51 mediate Drp1 recruitment in mitochondrial fission. Mol. Biol. Cell *24*, 659–667.

Lu, J. (2019). The Warburg metabolism fuels tumor metastasis. Cancer Metastasis Rev. *38*, 157–164.

Marie, S.K.N., and Shinjo, S.M.O. (2011). Metabolism and brain cancer. Clin. Sao Paulo Braz. *66 Suppl 1*, 33–43.

Marsin, A.S., Bertrand, L., Rider, M.H., Deprez, J., Beauloye, C., Vincent, M.F., Van den Berghe, G., Carling, D., and Hue, L. (2000). Phosphorylation and activation of heart PFK-2 by AMPK has a role in the stimulation of glycolysis during ischaemia. Curr. Biol. CB *10*, 1247–1255.

Mauro, C., Leow, S.C., Anso, E., Rocha, S., Thotakura, A.K., Tornatore, L., Moretti, M., De Smaele, E., Beg, A.A., Tergaonkar, V., et al. (2011). NF-κB controls energy homeostasis and metabolic adaptation by upregulating mitochondrial respiration. Nat. Cell Biol. *13*, 1272–1279.

Mauthe, M., Orhon, I., Rocchi, C., Zhou, X., Luhr, M., Hijlkema, K.-J., Coppes, R.P., Engedal, N., Mari, M., and Reggiori, F. (2018). Chloroquine inhibits autophagic flux by decreasing autophagosome-lysosome fusion. Autophagy *14*, 1435–1455.

Mauvezin, C., and Neufeld, T.P. (2017). Autophagosomes take the Klp98-A train. Small GTPases *8*, 16–19.

McCool, K.W., and Miyamoto, S. (2012). DNA damage-dependent NF-κB activation: NEMO turns nuclear signaling inside out. Immunol. Rev. *246*, 311–326.

McCormick, E.M., Muraresku, C.C., and Falk, M.J. (2018). Mitochondrial Genomics: A complex field now coming of age. Curr. Genet. Med. Rep. *6*, 52–61.

Menendez, J.A., and Lupu, R. (2007). Fatty acid synthase and the lipogenic phenotype in cancer pathogenesis. Nat. Rev. Cancer *7*, 763–777.

Mishra, P., and Chan, D.C. (2016). Metabolic regulation of mitochondrial dynamics. J. Cell Biol. *212*, 379–387.

Miyawaki, S., Nakamura, Y., Suzuka, H., Koba, M., Yasumizu, R., Ikehara, S., and Shibata, Y. (1994). A new mutation, aly, that induces a generalized lack of lymph nodes accompanied by immunodeficiency in mice. Eur. J. Immunol. *24*, 429–434.

Nagdas, S., Kashatus, J.A., Nascimento, A., Hussain, S.S., Trainor, R.E., Pollock, S.R., Adair, S.J., Michaels, A.D., Sesaki, H., Stelow, E.B., et al. (2019). Drp1 Promotes KRas-Driven Metabolic Changes to Drive Pancreatic Tumor Growth. Cell Rep. *28*, 1845-1859.e5.

Newsholme, E.A., Crabtree, B., and Ardawi, M.S. (1985). The role of high rates of glycolysis and glutamine utilization in rapidly dividing cells. Biosci. Rep. *5*, 393–400.

Nielsen, E., Severin, F., Backer, J.M., Hyman, A.A., and Zerial, M. (1999). Rab5 regulates motility of early endosomes on microtubules. Nat. Cell Biol. *1*, 376–382.

Odqvist, L., Sánchez-Beato, M., Montes-Moreno, S., Martín-Sánchez, E., Pajares, R., Sánchez-Verde, L., Ortiz-Romero, P.L., Rodriguez, J., Rodríguez-Pinilla, S.M., Iniesta-Martínez, F., et al. (2013). NIK controls classical and alternative NF-κB activation and is necessary for the survival of human T-cell lymphoma cells. Clin. Cancer Res. Off. J. Am. Assoc. Cancer Res. *19*, 2319–2330.

Oeckinghaus, A., and Ghosh, S. (2009). The NF-kappaB family of transcription factors and its regulation. Cold Spring Harb. Perspect. Biol. *1*, a000034.

Otera, H., Wang, C., Cleland, M.M., Setoguchi, K., Yokota, S., Youle, R.J., and Mihara, K. (2010). Mff is an essential factor for mitochondrial recruitment of Drp1 during mitochondrial fission in mammalian cells. J. Cell Biol. *191*, 1141–1158.

Otto, A.M. (2016). Warburg effect(s)-a biographical sketch of Otto Warburg and his impacts on tumor metabolism. Cancer Metab. *4*, 5.

Palorini, R., Cammarata, F.P., Cammarata, F., Balestrieri, C., Monestiroli, A., Vasso, M., Gelfi, C., Alberghina, L., and Chiaradonna, F. (2013). Glucose starvation induces cell death in K-ras-transformed cells by interfering with the hexosamine biosynthesis pathway and activating the unfolded protein response. Cell Death Dis. *4*, e732.

Park, G.Y., Wang, X., Hu, N., Pedchenko, T.V., Blackwell, T.S., and Christman, J.W. (2006). NIK is involved in nucleosomal regulation by enhancing histone H3 phosphorylation by IKKalpha. J. Biol. Chem. *281*, 18684–18690.

Parzych, K.R., and Klionsky, D.J. (2014). An overview of autophagy: morphology, mechanism, and regulation. Antioxid. Redox Signal. *20*, 460–473.

Pavlova, N.N., and Thompson, C.B. (2016). The Emerging Hallmarks of Cancer Metabolism. Cell Metab. *23*, 27–47.

Pazarentzos, E., Mahul-Mellier, A.-L., Datler, C., Chaisaklert, W., Hwang, M.-S., Kroon, J., Qize, D., Osborne, F., Al-Rubaish, A., Al-Ali, A., et al. (2014). IκBα inhibits apoptosis at the outer mitochondrial membrane independently of NF-κB retention. EMBO J. *33*, 2814–2828.

Pham, L.V., Fu, L., Tamayo, A.T., Bueso-Ramos, C., Drakos, E., Vega, F., Medeiros, L.J., and Ford, R.J. (2011). Constitutive BR3 receptor signaling in diffuse, large B-cell lymphomas stabilizes nuclear factor-κB-inducing kinase while activating both canonical and alternative nuclear factor-κB pathways. Blood *117*, 200–210.

Phillips, H.S., Kharbanda, S., Chen, R., Forrest, W.F., Soriano, R.H., Wu, T.D., Misra, A., Nigro, J.M., Colman, H., Soroceanu, L., et al. (2006). Molecular subclasses of high-grade glioma predict prognosis, delineate a pattern of disease progression, and resemble stages in neurogenesis. Cancer Cell *9*, 157–173.

Pickles, S., Vigié, P., and Youle, R.J. (2018). Mitophagy and Quality Control Mechanisms in Mitochondrial Maintenance. Curr. Biol. CB *28*, R170–R185.

Prasad, S., Ravindran, J., and Aggarwal, B.B. (2010). NF-kappaB and cancer: how intimate is this relationship. Mol. Cell. Biochem. *336*, 25–37.

Puchalski, R.B., Shah, N., Miller, J., Dalley, R., Nomura, S.R., Yoon, J.-G., Smith, K.A., Lankerovich, M., Bertagnolli, D., Bickley, K., et al. (2018). An anatomic transcriptional atlas of human glioblastoma. Science *360*, 660–663.

Rabinovitch, R.C., Samborska, B., Faubert, B., Ma, E.H., Gravel, S.-P., Andrzejewski, S., Raissi, T.C., Pause, A., St-Pierre, J., and Jones, R.G. (2017). AMPK Maintains Cellular Metabolic Homeostasis through Regulation of Mitochondrial Reactive Oxygen Species. Cell Rep. *21*, 1–9.

Racioppi, L., and Means, A.R. (2012). Calcium/calmodulin-dependent protein kinase kinase 2: roles in signaling and pathophysiology. J. Biol. Chem. *287*, 31658–31665.

Rambold, A.S., Kostelecky, B., Elia, N., and Lippincott-Schwartz, J. (2011). Tubular network formation protects mitochondria from autophagosomal degradation during nutrient starvation. Proc. Natl. Acad. Sci. U. S. A. *108*, 10190–10195.

Rangaswami, H., Bulbule, A., and Kundu, G.C. (2006). Nuclear factor inducing kinase: a key regulator in osteopontin- induced MAPK/IkappaB kinase dependent NF-kappaB-mediated promatrix metalloproteinase-9 activation. Glycoconj. J. *23*, 221–232.

Raychaudhuri, B., Han, Y., Lu, T., and Vogelbaum, M.A. (2007). Aberrant constitutive activation of nuclear factor kappaB in glioblastoma multiforme drives invasive phenotype. J. Neurooncol. *85*, 39–47.

Rehman, J., Zhang, H.J., Toth, P.T., Zhang, Y., Marsboom, G., Hong, Z., Salgia, R., Husain, A.N., Wietholt, C., and Archer, S.L. (2012). Inhibition of mitochondrial fission prevents cell cycle progression in lung cancer. FASEB J. Off. Publ. Fed. Am. Soc. Exp. Biol. *26*, 2175–2186.

Reitzer, L.J., Wice, B.M., and Kennell, D. (1979). Evidence that glutamine, not sugar, is the major energy source for cultured HeLa cells. J. Biol. Chem. *254*, 2669–2676.

Saitoh, Y., Martínez Bruyn, V.J., Uota, S., Hasegawa, A., Yamamoto, N., Imoto, I., Inazawa, J., and Yamaoka, S. (2010). Overexpression of NF-κB inducing kinase underlies constitutive NF-κB activation in lung cancer cells. Lung Cancer Amst. Neth. *70*, 263–270.

Schneider, A., Kurz, S., Manske, K., Janas, M., Heikenwälder, M., Misgeld, T., Aichler, M., Weissmann, S.F., Zischka, H., Knolle, P., et al. (2019). Single organelle analysis to

characterize mitochondrial function and crosstalk during viral infection. Sci. Rep. *9*, 8492.

Schwarz, T.L. (2013). Mitochondrial trafficking in neurons. Cold Spring Harb. Perspect. Biol. *5*.

Scott, I., and Youle, R.J. (2010). Mitochondrial fission and fusion. Essays Biochem. *47*, 85–98.

Sen, R., and Baltimore, D. (1986). Inducibility of kappa immunoglobulin enhancer-binding protein Nf-kappa B by a posttranslational mechanism. Cell *47*, 921–928.

Shaw, R.J., Kosmatka, M., Bardeesy, N., Hurley, R.L., Witters, L.A., DePinho, R.A., and Cantley, L.C. (2004). The tumor suppressor LKB1 kinase directly activates AMP-activated kinase and regulates apoptosis in response to energy stress. Proc. Natl. Acad. Sci. U. S. A. *101*, 3329–3335.

Sheng, L., Zhou, Y., Chen, Z., Ren, D., Cho, K.W., Jiang, L., Shen, H., Sasaki, Y., and Rui, L. (2012). NF-κB–inducing kinase (NIK) promotes hyperglycemia and glucose intolerance in obesity by augmenting glucagon action. Nat. Med. *18*, 943–949.

Sheridan, C., Delivani, P., Cullen, S.P., and Martin, S.J. (2008). Bax- or Bak-induced mitochondrial fission can be uncoupled from cytochrome C release. Mol. Cell *31*, 570–585.

Shinkura, R., Kitada, K., Matsuda, F., Tashiro, K., Ikuta, K., Suzuki, M., Kogishi, K., Serikawa, T., and Honjo, T. (1999). Alymphoplasia is caused by a point mutation in the mouse gene encoding Nf-kappa b-inducing kinase. Nat. Genet. *22*, 74–77.

Shintaku, J., Peterson, J.M., Talbert, E.E., Gu, J.-M., Ladner, K.J., Williams, D.R., Mousavi, K., Wang, R., Sartorelli, V., and Guttridge, D.C. (2016). MyoD Regulates Skeletal Muscle Oxidative Metabolism Cooperatively with Alternative NF-κB. Cell Rep. *17*, 514–526.

Shiratori, R., Furuichi, K., Yamaguchi, M., Miyazaki, N., Aoki, H., Chibana, H., Ito, K., and Aoki, S. (2019). Glycolytic suppression dramatically changes the intracellular metabolic profile of multiple cancer cell lines in a mitochondrial metabolism-dependent manner. Sci. Rep. *9*, 18699.

Sun, S.-C. (2011). Non-canonical NF-κB signaling pathway. Cell Res. *21*, 71–85.

Sun, S.-C. (2017). The non-canonical NF-κB pathway in immunity and inflammation. Nat. Rev. Immunol. *17*, 545–558.

Suzuki, T., Bridges, D., Nakada, D., Skiniotis, G., Morrison, S.J., Lin, J.D., Saltiel, A.R., and Inoki, K. (2013). Inhibition of AMPK catabolic action by GSK3. Mol. Cell *50*, 407–419.

Tan, E.H.N., and Tang, B.L. (2019). Rab7a and Mitophagosome Formation. Cells *8*.

Tao, Z., and Ghosh, G. (2012). Understanding NIK Regulation from Its Structure. Structure *20*, 1615–1617.

Tegowski, M., and Baldwin, A. (2018). Noncanonical NF-κB in Cancer. Biomedicines *6*.

Thu, Y.M., and Richmond, A. (2010). NF-κB inducing kinase: a key regulator in the immune system and in cancer. Cytokine Growth Factor Rev. *21*, 213–226.

Tian, W., Li, W., Chen, Y., Yan, Z., Huang, X., Zhuang, H., Zhong, W., Chen, Y., Wu, W., Lin, C., et al. (2015). Phosphorylation of ULK1 by AMPK regulates translocation of ULK1 to mitochondria and mitophagy. FEBS Lett. *589*, 1847–1854.

Tilokani, L., Nagashima, S., Paupe, V., and Prudent, J. (2018). Mitochondrial dynamics: overview of molecular mechanisms. Essays Biochem. *62*, 341–360.

Toyama, E.Q., Herzig, S., Courchet, J., Lewis, T.L., Losón, O.C., Hellberg, K., Young, N.P., Chen, H., Polleux, F., Chan, D.C., et al. (2016). Metabolism. AMP-activated protein kinase mediates mitochondrial fission in response to energy stress. Science *351*, 275–281.

Uno, M., Saitoh, Y., Mochida, K., Tsuruyama, E., Kiyono, T., Imoto, I., Inazawa, J., Yuasa, Y., Kubota, T., and Yamaoka, S. (2014). NF-κB inducing kinase, a central signaling component of the non-canonical pathway of NF-κB, contributes to ovarian cancer progression. PloS One *9*, e88347.

Verhaak, R.G.W., Hoadley, K.A., Purdom, E., Wang, V., Qi, Y., Wilkerson, M.D., Miller, C.R., Ding, L., Golub, T., Mesirov, J.P., et al. (2010). Integrated genomic analysis identifies clinically relevant subtypes of glioblastoma characterized by abnormalities in PDGFRA, IDH1, EGFR, and NF1. Cancer Cell *17*, 98–110.

Vigneswaran, K., Neill, S., and Hadjipanayis, C.G. (2015). Beyond the World Health Organization grading of infiltrating gliomas: advances in the molecular genetics of glioma classification. Ann. Transl. Med. *3*, 95.

Wallach, D., and Kovalenko, A. (2008). Self-termination of the terminator. Nat. Immunol. *9*, 1325–1327.

Wertz, I.E., and Dixit, V.M. (2010). Signaling to NF-kappaB: regulation by ubiquitination. Cold Spring Harb. Perspect. Biol. *2*, a003350.

White, E., and DiPaola, R.S. (2009). The double-edged sword of autophagy modulation in cancer. Clin. Cancer Res. Off. J. Am. Assoc. Cancer Res. *15*, 5308–5316.

Wilkening, A., Rüb, C., Sylvester, M., and Voos, W. (2018). Analysis of heat-induced protein aggregation in human mitochondria (Cell Biology).

Willems, P.H.G.M., Rossignol, R., Dieteren, C.E.J., Murphy, M.P., and Koopman, W.J.H. (2015). Redox Homeostasis and Mitochondrial Dynamics. Cell Metab. *22*, 207–218.

Xiao, G., and Sun, S.C. (2000). Negative regulation of the nuclear factor kappa B-inducing kinase by a cis-acting domain. J. Biol. Chem. *275*, 21081–21085.

Xiao, G., Harhaj, E.W., and Sun, S.C. (2001). NF-kappaB-inducing kinase regulates the processing of NF-kappaB2 p100. Mol. Cell *7*, 401–409.

Xie, Q., Wu, Q., Horbinski, C.M., Flavahan, W.A., Yang, K., Zhou, W., Dombrowski, S.M., Huang, Z., Fang, X., Shi, Y., et al. (2015). Mitochondrial control by DRP1 in brain tumor initiating cells. Nat. Neurosci. *18*, 501–510.

Yang, X.-D., and Sun, S.-C. (2015). Targeting signaling factors for degradation, an emerging mechanism for TRAF functions. Immunol. Rev. *266*, 56–71.

Yao, C.-H., Wang, R., Wang, Y., Kung, C.-P., Weber, J.D., and Patti, G.J. (2019). Mitochondrial fusion supports increased oxidative phosphorylation during cell proliferation. ELife *8*.

Yorimitsu, T., Nair, U., Yang, Z., and Klionsky, D.J. (2006). Endoplasmic reticulum stress triggers autophagy. J. Biol. Chem. *281*, 30299–30304.

Zamanian-Daryoush, M., Mogensen, T.H., DiDonato, J.A., and Williams, B.R. (2000). NF-kappaB activation by double-stranded-RNA-activated protein kinase (PKR) is mediated through NF-kappaB-inducing kinase and IkappaB kinase. Mol. Cell. Biol. *20*, 1278–1290.

Zanotto-Filho, A., Gonçalves, R.M., Klafke, K., de Souza, P.O., Dillenburg, F.C., Carro, L., Gelain, D.P., and Moreira, J.C.F. (2017). Inflammatory landscape of human brain tumors reveals an NFκB dependent cytokine pathway associated with mesenchymal glioblastoma. Cancer Lett. *390*, 176–187.

Zhang, C.-S., and Lin, S.-C. (2016). AMPK Promotes Autophagy by Facilitating Mitochondrial Fission. Cell Metab. *23*, 399–401.

Zhang, P., Xia, Q., Liu, L., Li, S., and Dong, L. (2020). Current Opinion on Molecular Characterization for GBM Classification in Guiding Clinical Diagnosis, Prognosis, and Therapy. Front. Mol. Biosci. *7*, 562798.

Zhang, Q., Lenardo, M.J., and Baltimore, D. (2017). 30 Years of NF-κB: A Blossoming of Relevance to Human Pathobiology. Cell *168*, 37–57.

Zhao, J., Zhang, J., Yu, M., Xie, Y., Huang, Y., Wolff, D.W., Abel, P.W., and Tu, Y. (2013). Mitochondrial dynamics regulates migration and invasion of breast cancer cells. Oncogene *32*, 4814–4824.

Zhao, R.-Z., Jiang, S., Zhang, L., and Yu, Z.-B. (2019). Mitochondrial electron transport chain, ROS generation and uncoupling (Review). Int. J. Mol. Med. *44*, 3–15.